Functional analysis of the latrophilin homolog *dCirl* in *Drosophila melanogaster*

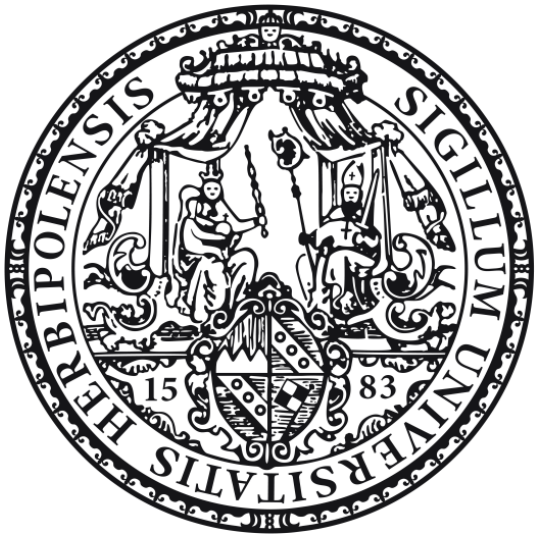

Dissertation zur Erlangung des

naturwissenschaftlichen Doktorgrades

der Julius-Maximilians-Universität Würzburg

vorgelegt von

Jennifer Gehring

aus Würzburg

Physiologisches Institut – Lehrstuhl für Physiologie

Schwerpunkt Neurophysiologie

Würzburg, 2014

Eingereicht am: ……

Mitglieder der Promotionskommission:

Vorsitzender: ……

Gutachter: Prof. Dr. Manfred Heckmann

Gutachter: Prof. Dr. Christian Stigloher

Tag des Promotionskolloquiums: ……...

Doktorurkunde ausgehändigt am: .....

Erklärung

Ich versichere hiermit, dass ich die vorliegende Dissertation mit dem Titel “Functional analysis of the latrophilin homolog *dCirl* in *Drosophila melanogaster*” eigenständig angefertigt und mich dabei keiner anderen als der von mir angegebenen Quellen und Hilfsmittel bedient habe. Die Dissertation wurde in der jetzigen oder einer ähnlichen Form noch bei keiner anderen Hochschule eingereicht.

Würzburg, 2014 _____

Jennifer Gehring

Contents

1. Summary

Latrophilin, alternatively named calcium-independent receptor of α-latrotoxin (CIRL), resembles a prototype of the adhesion class G-protein coupled receptors (GPCRs). Initially identified as a high-affinity receptor for α-latrotoxin, a component of the black widow spider, latrophilins are now associated with various distinct functions, such as synaptic exocytosis, tissue polarity and fertility (Tobaben et al., 2002; Langenhan et al., 2009; Promel et al., 2012). Despite these exploratory efforts the precise subcellular localisation as well as the endogenous ligand of CIRL still remains elusive. In this work genetic experiments, imaging approaches and behavioural studies have been used to unravel the localisation and physiological function of the latrophilin homolog *dCirl* in *Drosophila melanogaster*. Containing only one latrophilin homolog together with its genetic accessibility and well-established transgenic approaches, *Drosophila* seemed an ideally suited model organism. The present study showed that *dCirl* is widely expressed in the larval central nervous system including moto- and sensory neurons. Further, this work revealed that removal of the latrophilin homolog does not greatly affect synaptic transmission but it seems that aspects of the postsynaptic structural layout are controlled by dCIRL in the fruit fly. Additionally, *dCirl* expression at the transcriptional level was confirmed in larval and adult chordotonal organs, specialised mechanosensors implicated in proprioception (Eberl, 1999). Expression of dCIRL at the protein level could not yet been confirmed in moto- and sensory neurons likely due to low endogenous expression. However, behavioural studies using *dCirl* knockout mutant larvae indicated a putative mechanosensory function of dCIRL regarding touch sensitivity and locomotion behaviour.

The second part of this thesis presents a strategy to examine interactions between several presynaptic proteins in living cells. The attempt described in this work is based on the discovery that GFP when split into two non-fluorescent fragments can form a fluorescent complex. The association of the fragments can be facilitated by fusing them to two proteins that interact with each other. Therefore, the split GFP method enables direct visualization of synaptic protein interactions in living cells. In initial experiments I could show that full length reporter protein fusions with n-Synaptobrevin (n-Syb), Synaptotagmin (Syt) and Syntaxin (Syx) allow expression in *Drosophila* and confirmed that fusion to either end of each synaptic protein did not

impair expression or influence the viability of transgenic flies. Further, transgenes containing protein fusions of Syx, Syt, and n-Syb with split GFP fragments were established in previous studies (Gehring, 2010). The present work characterises the interaction of these protein fusions during different stages of synaptic vesicle turnover at active zones such as synaptic vesicle docking at the presynaptic membrane and vesicle fusion. These results suggest that the spGFP assay seems only partly suitable for resolving fast and transient protein-protein interactions at larval *Drosophila* active zones *in vivo*.

1. Zusammenfassung

Latrophilin, auch als Calcium-unabhängiger Rezeptor für α-Latrotoxin (CIRL) bezeichnet, repräsentiert einen Prototyp der Adhäsions G-Protein gekoppelten Rezeptorklasse. Ursprünglich als hoch-affiner Rezeptor für α-Latrotoxin entdeckt, werden Latrophiline heute mit zahlreichen verschiedenen Funktionen, wie synaptischer Exozytose, Gewebepolarität und Fertilität assoziiert (Tobaben et al., 2002; Langenhan et al., 2009; Promel et al., 2012). Trotz dieser Fortschritte sind die genaue subzelluläre Lokalisation sowie der endogene Ligand noch weitgehend unbekannt. Diese Studie verwendet genetische Ansätze, bildgebende Verfahren und Verhaltensstudien, um die Lokalisation und physiologische Funktion des Latrophilinhomologs *dCirl* in *Drosophila melanogaster* aufzuklären. Die Tatsache, dass *Drosophila* nur ein einziges Latrophilin Homolog besitzt, zusammen mit den genetischen Möglichkeiten und den sehr gut etablierten transgenen Methoden, machen die Fruchtfliege zu einem idealen Modellorganismus. Die erhobenen Daten belegen, dass *dCirl* verstärkt im larvalen Nervensystem, einschließlich motorischer und sensorischer Neurone, exprimiert wird. Weiterhin konnte gezeigt werden, dass in *dCirl* Knockout-Mutanten die basale synaptische Transmission unverändert ist, vermutlich aber Teile der postsynaptischen Struktur durch dCIRL in der Fruchtfliege kontrolliert werden. Zusätzlich konnte nachgewiesen werden, dass *dCirl* auf Transkriptionsebene in den larvalen und adulten Chordotonalorganen exprimiert wird, spezifische Mechanosensoren, die an der Propriozeption beteiligt sind (Eberl, 1999). Die Expression von dCIRL auf Proteinebene in motorischen und sensorischen Neuronen konnte aufgrund niedriger endogener Expressionslevel noch nicht

verifiziert werden. Allerdings deuten Verhaltensstudien, die Berührungsempfindlichkeit und Lokomotion untersuchen, auf eine mögliche mechanosensorische Funktion von dCIRL in den Larven von *Drosophila* hin.

Der zweite Teil dieser Arbeit zeigt eine Strategie auf, die es ermöglicht, das Zusammenspiel verschiedener präsynaptischer Proteine *in vivo* zu untersuchen. Die hier beschriebene Methode basiert auf der Entdeckung, dass sich zwei nicht-fluoreszierende Fragmente des grün leuchtenden Proteins (GFP), zu einem fluoreszierenden Komplex zusammenlagern können. Diese geteilten GFP-Fragmente (split-GFPs) werden mit zwei unterschiedlichen Proteinen fusioniert, die miteinander interagieren. Die split-GFP Methode ermöglicht so eine direkte Visualisierung von Protein-Protein-Interaktionen in lebenden Zellen. In ersten Experimenten konnte ich zeigen, dass Synaptobrevin (n-Syb), Synaptotagmin (Syt) und Syntaxin (Syx), die mit vollständigen Fluorophoren markiert wurden, für die Expression in Drosophila geeignet sind und bestätigen, dass sowohl die N-terminale als auch die C-terminale Proteinfusion möglich ist. Zudem konnte durch diese Versuche die Überlebensfähigkeit der transgenen Fliegen überprüft werden. In vorangegangenen Studien wurden Transgene hergestellt, die Proteinfusionen von n-Syb, Syt und Syx mit split-GFP Fragmenten enthalten (Gehring, 2010). Die vorliegende Arbeit charakterisiert die Wechselwirkung dieser Proteinfusionen während unterschiedlicher Stufen der synaptischen Vesikelfreisetzung an der aktiven Zone, wie beispielsweise dem Vesikel-docking an der präsynaptischen Membran und der Vesikelfusion. Die Ergebnisse dieser Studie deuten darauf hin, dass die split-GFP Technik nur bedingt geeignet ist um schnelle und transiente Protein-Protein Interaktionen an der larvalen aktiven Zone von Drosophila *in vivo* darzustellen.

2. Introduction

2.1 Adhesion class G-protein coupled receptors

G-protein coupled receptors (GPCRs) are essential for intra- and intercellular communication which is of enormous importance for the function of organisms (Aust, 2010). GPCRs are one of the largest protein families in the mammalian genome (Bjarnadottir et al., 2004). Consisting of seven-transmembrane (7TM) spanning domains GPCRs transduce extracellular received signals across the cell-membrane activating signal transduction pathways inside the cell and finally cellular responses (Pierce et al., 2002). Ligands binding and activating these receptors are manifold and range from light-sensitive compounds, calcium, pheromones, hormones and odorants to neurotransmitters amongst others (Bockaert and Pin, 1999). This underlines the implication of GPCRs in a plethora of physiological functions making them an excellent target for pharmaceutical drugs (Flower, 1999).

The GPCR superfamily is subdivided into five major classes: Glutamate, Rhodopsin, Adhesion, Frizzeled/taste2 and Secretin (Fig. 1) (Fredriksson et al., 2003). Although building the second largest group adhesion-GPCRs (aGPCRs) are poorly understood concerning their physiological function. This arises partly from the fact that a majority of aGPCRs are orphan receptors with unknown endogenous ligands. Notwithstanding the uncertainty of agonistic or antagonistic interactors of aGPCRs, many of their structural features have been well characterised over the years.

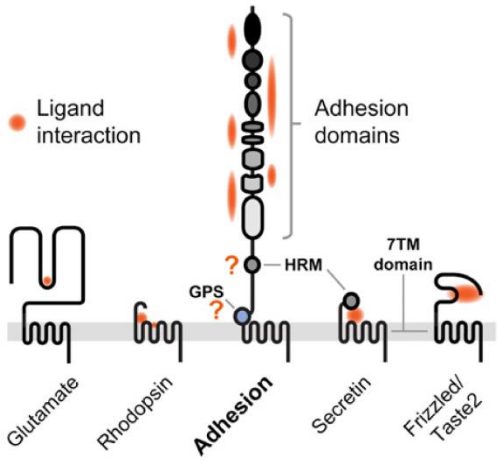

Fig. 1 The superfamily of G-protein coupled receptors (GPCRs),

GPCRs can be found in five 7TM receptor families, termed Glutamate, Rhodopsin, Adhesion, Frizzled/Taste2 and Secretin. Indicated in orange are confirmed and putative (indicated by question marks) sites of ligand interaction.

All adhesion-GPCRs are heterodimers consisting of a long extracellular adhesion subunit and GPCR-like transmembrane spanning regions. In humans there are 33 adhesion class receptors grouped into nine different families according to the sequence similarity of their 7TM domains and N-terminal domain architecture (Lagerstrom and Schioth, 2008) (Fig. 2). A further characteristic of aGPCRs is the GPCR proteolysis site (GPS) located close to the 7TM domain (Fig. 2). The GPS (~40 amino acids) is part of the much larger GPCR autoproteolysis inducing (GAIN) domain consisting of approximately 320 amino acid residues (Arac et al., 2012). Deletion experiments demonstrated that the entire GAIN domain is both required and sufficient for autoproteolysis (Arac et al., 2012). However, the self-cleavage occurs at the GPS and happens post-transcriptionally in the endoplasmatic reticulum (Krasnoperov et al., 2002). Upon autoproteolysis the GAIN domain prevents dissociation of the cleaved fragments by forming a tightly associated heterodimer of the cleavage fragments instead (Arac et al., 2012). The GAIN domain is conserved in all adhesion-GPCRs throughout vertebrates and invertebrates (except GPR123, not containing extracellular domains at all) as well as in human polycystic kidney disease (PKD) proteins and the sea urchin sperm receptors (Hughes et al., 1999; Ponting et al., 1999). These results suggest that the GAIN domain possesses an essential role in the function of all adhesion-GPCRs.

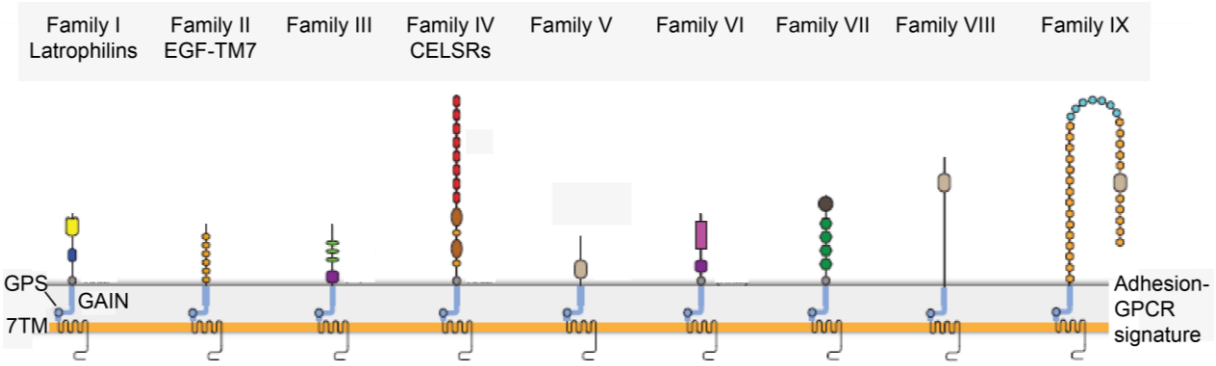

Fig. 2 Overview of Adhesion-GPCR families.

Adhesion-GPCRs can be subdivided into nine distinct families with 33 homologs in mammalian genomes. Categorisation is based on their extracellular folds and sequence similarities of 7TM domains. Note that families I and IV are also present in invertebrates (adapted from Langenhan et al., 2013).

2.1.1 Latrophilin – a prototype of adhesion-GPCRs

Besides the cadherin-like *flamingo/starry night* (FMI) and its mammalian homolog (CELSR) the lectin-like latrophilins (LPHN) are highly conserved adhesion-GPCRs across all phyla (Nordstrom et al., 2009). This makes LPHN an ideal prototype for the aGPCR class. The mammalian genomes contain three latrophilin homologs (*Lphn1-3*), *C. elegans* possesses two homologs (*lat-1* and *lat-2*), and only one homolog exists in *Drosophila melanogaster* (*dCirl*) (Fig. 3).

2.1.2 Structural characteristics of latrophilin

The primary structure of LPHN comprises an extracellular domain, followed by a 7TM and an intracellular cytoplasmic tail. Cleavage at the extracellular GPS motif, the hallmark of all adhesion-GPCRs (Bjarnadottir et al., 2004), produces heterodimers composed of an extracellular adhesion-subunit (120 kDa) and a GPCR-like domain with 7TM helices (85 kDa) (Krasnoperov et al., 1997).

The extracellular protein architecture of LPHN is characterised by a rhamnose-binding lectin (RBL) domain (Fig. 3). The RBL domain is located in the long extracellular multidomain region (Vakonakis et al., 2008) that also comprises a hormone-binding site and additionally an olfactomedin-like domain in mammals. Like the GAIN domain the RBL motif is also present in extracellular segments of PKD proteins (Li et al., 2003). However, carbohydrates are unlikely to be the endogenous ligands of this domain because rhamnose is not normally found in animals (Tymiak et al., 1993). Langenhan et al. (2009) demonstrated that the extracellular RBL domain is required for proper LAT-1 function in *C. elegans*. This observation strengthened the idea that the RBL domain interacts with the extracellular matrix, other cells, or unknown ligands. The RBL domain is followed by an olfactomedin domain, a glycoprotein of the extracellular matrix of the olfactory epithelium (Fig. 3). Interestingly, this domain is only present in vertebrate orthologues of latrophilin and thus presumably acquired during early evolution. Over the years other proteins containing an olfactomedin domain have been associated with cell-cell interaction, neurogenesis, cell cycle regulation and dorso-ventral patterning amongst others (Tomarev and Nakaya, 2009). The hormone receptor motif (HRM) is located downstream of the olfactomedin domain and is implicated in ligand binding and present in all LPHN homologs (Fig. 3). The GAIN domain holding the GPS motif is the defining feature of the adhesion-GPCRs (Fig. 3). This motif contains the site of

posttranslational cleavage splitting LPHN into two non-covalently bound subunits whereby the GPS motif itself becomes unequally divided between the N-terminal and C-terminal fragments (Krasnoperov et al., 1997). The latter consists of 7TM helices and exhibits little similarities with known domains except for proline-rich proteins due to several proline clusters. The cytoplasmic tail is the least conserved domain among LPHNs (Silva and Ushkaryov, 2010). Together these structural features point to the functional characteristics of LPHN producing an “outside-in” signal via the transmembrane domain structure upon extracellular interaction (Langenhan et al., 2009).

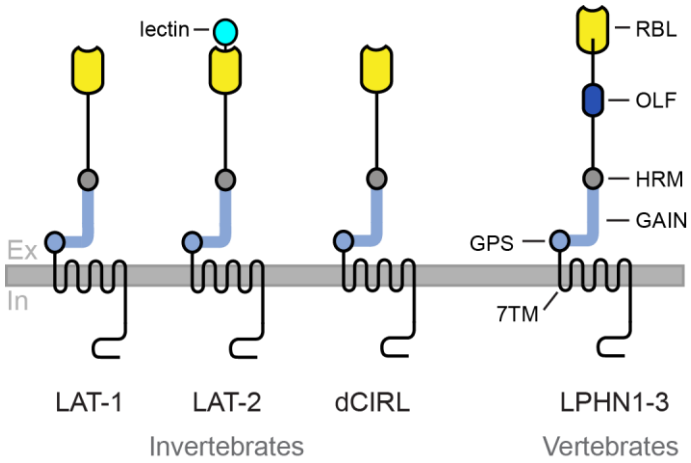

Fig. 3 Conservation of LPHN from invertebrates to vertebrates.

Schematic depiction of the conserved protein architecture of the adhesion-GPCR LPHN: C.elegans: LAT-1, LAT-2; *D. melanogaster*: dCIRL *Homo sapiens*: LPHN1-3. RBL: rhamnose-binding lectin, OLF: olfactomedin, HRM: hormone-binding motif, GAIN: GPCR autoproteolsyis inducing domain, GPS; GPCR proteolysis site, 7TM: seven-transmembrane domain (Langenhan et al., 2009).

2.1.3 Functional characteristics of latrophilin

Functional information about latrophilins is rather restricted. The mammalian LAT-1 homolog was originally described as cellular receptors for α-latrotoxin, a component of the black widow spider venom (Davletov et al., 1996; Krasnoperov et al., 1996). Upon the action of α-latrotoxin massive exocytosis of intracellular vesicles in neurons and other sensory cells occurs (Lang et al., 1998). Interestingly, binding of LPHNs to α-latrotoxin functions both in the presence and in the absence of Ca^{2+}, which gave LPHNs the alternative name Ca^{2+}-independent receptors of latrotoxin (CIRL) (Krasnoperov et al., 1997). Further, this denomination resulted in differentiation to another latrotoxin receptor, neurexin a neuronal cell surface protein binding α-latrotoxin merely dependent on extracellular Ca^{2+} (Ushkaryov et al., 1992).

Despite the utility of α-latrotoxin in the discovery of LPHN it is a rather disadvantageous tool for the functional investigation of this adhesion-receptor class because of its multifaceted actions. Upon binding to any receptor α-latrotoxin inserts into the plasma membrane and induces stable pore formation resulting in facilitation of synaptic vesicle exocytosis (Sudhof, 2001). There exist various models about the incorporation of LPHN in this process. By studies using a toxin mutant termed α-LTX^{N4C} incapable of inducing pore formation, Ichtchenko et al. (1998) confirmed that binding of α-latrotoxin to LAT-1 does not directly cause transmitter release. However, findings by Capogna et al. (2003) implicate LPHN as the main α-latrotoxin receptor transducing release of neurotransmitter. Studies by Volynski et al. (2003) on chromafine cells, rat hippocampal neurons and synaptosomes as well as mouse NMJs underline the LPHN-transduced α-latrotoxin exocytotic effect. This model suggests that LPHNs might be involved in modulating synaptic function. Other data obtained from the nematode *C. elegans* point towards a role of LPHNs in morphogenesis and tissue polarity (Langenhan et al., 2009). This model implies that LPHNs modulate neuronal development which seems consistent with findings of another adhesion-GPCR class, cadherin-like *flamingo/starry night* (FMI) and its vertebrate homologs (CELSR), which have been shown to be essential in planar cell polarity and neuronal development (Hadjantonakis et al., 1998; Usui et al., 1999). Additional data from *C. elegans* claim a role of LPHN in reproduction confirmed by loss of fertility in *lat-1* mutants (Promel et al., 2012). Other findings from zebrafish show that loss of *lphn3.1* function, one of the zebrafish orthologs of *LPHN3*, affects dopaminergic system development and causes a hyperactive/impulsive motor behaviour, which is linked to attention-deficit/hyperactivity disorder (ADHD) (Lange et al., 2012). Although these findings are not mutually exclusive the actual functional role of LPHN signalling in neurons still remains elusive.

2.1.4 Mammalian latrophilin homologs

Besides LPHN1 two additional homologs, termed LPHN2 and LPHN3, exist in vertebrates (Matsushita et al., 1999). Murine LPHN1 and LPHN3 are enriched in the brain, whereas LPHN2 is ubiquitously expressed in all tissues (Sugita et al., 1998; Matsushita et al., 1999). To date no specific antibody is available to reveal the cellular and subcellular localisation of LPHNs. Beyond the lack of knowledge of the endogenous ligand this complicates the effort to unravel their physiological function. LPHN1 knockout mouse models showed that LPHN1 is neither necessary for the

viability and activity of neurons nor for the survival of the organism itself indicating that the two other homologs are able to compensate for loss of LPHN1 function (Tobaben et al., 2002). However, all three LPHNs are alternatively spliced indicating high degree of specialisation and hence distinct functions (Matsushita et al., 1999). Recent studies claimed a direct interaction between neurexins lacking an insert in splice site 4 and LPHN1, both receptors for α-latrotoxin producing a stable intercellular adhesion complex (Boucard et al., 2012). Unfortunately, due to the lack of avid antibodies the endogenous localisation of these proteins remains unknown. The same is true for the physiological function of the Neurexin-LPHN1 complex. However, current experiments using affinity chromatography revealed a possible natural ligand for LPHN1 termed Lasso (LPH1-associated synaptic surface organizer) (Silva et al., 2011). Lasso is a splice variant of teneurin-2, a brain-specific cell surface glycoprotein involved in neuronal pathfinding and synaptogenesis (Oohashi et al., 1999; Tucker et al., 2007). Cell culture studies suggest that LPHN1 located presynaptically interacts with postsynaptic Lasso, building a transsynaptic protein pair presumably involved in synaptic function (Silva et al., 2011). Recent findings from O'Sullivan et al. (2012) identified fibronectin leucin-rich repeat transmembrane (FLRT) proteins as an endogenous ligand for LPHNs. They substantiated an interaction between FLRT3 and LPHN3 functioning as a synaptic ligand-receptor pair that regulates excitatory synapse number. These observations suggest that LPHN3 and its ligand FLRT3 are important for the development of glutamatergic synapse development (O'Sullivan et al., 2012). Together, these data propose that LPHNs might be presynaptic components that interact with different postsynaptic ligands, such as teneurins or FLRTs and thus modulate synaptic function.

2.1.5 Latrophilin in *C. elegans*

The orthologues of mammalian latrophilins in the nematode *C. elegans* are encoded by two genes: *lat-1* and *lat-2* (Fig. 3). Studies revealed that toxic effects of the venom of the black widow spider are mediated by the LAT-1 homolog, but not by LAT-2 (Mee et al., 2004). Further results obtained from *lat-1* knockout models suggest a physiological role of LAT-1 in facilitating neurotransmitter release (Willson et al., 2004). In addition, loss of function mutations indicated a different role for LAT-1 in *C. elegans* development. Due to defects in anterior-posterior polarity nearly all homozygous *lat-1* animals arrest in the first larval stage of development (Langenhan

et al., 2009). Progeny of crosses between homozygous escapers and heterozygous individuals, not showing any phenotype, revealed maternal-effect lethality suggesting that maternal *lat-1* is required for embryonic development. Rescue experiments revealed that LAT-1 function is dependent on the presence of the RBL motif indicating a possible protein-protein interaction via this domain. Further observations using loss-of-function mutations in *lat-1* suggest that LAT-1 is implied in cell migration and polarity of cell division during worm embryogenesis. However, the fact that these processes are rather delayed than blocked entirely indicates that LAT-1 acts in parallel with other signaling cascades, e.g. components of the *wnt* pathway (Langenhan et al., 2009). Besides functioning in development further studies suggest that LAT-1 is also required for reproduction confirmed by loss of fertility in *lat-1* mutants (Promel et al., 2012). Both phenotypes can be rescued by transgenes carrying wild-type *lat-1*. On the contrary, constructs expressing a truncation in LAT-1 causing either the lack of the 7TM domain or the intracellular C-terminal fragment are able to compensate for the fertility defect in *lat-1* mutants, but fail to rescue the tissue polarity phenotype (Promel et al., 2012). These results indicate different functions of LAT-1 domains and uncover 7TM-dependent and 7TM-independent components of the LAT phenotype in *C. elegans*.

2.2 *Drosophila melanogaster*

Drosophila melanogaster, commonly known as the fruit fly, has been used as a model organism for nearly a century and has advanced to become one of the most powerful and valuable organisms in scientific research.

2.2.1 Strength of the fruit fly as a model organism

The fly genome, which was completely sequenced thirteen years ago (Adams et al., 2000), consists of 165Mbp distributed over four chromosome pairs. Despite its relatively small genome size, most Drosophila genes (approximately 14.000) are largely evolutionary conserved in vertebrates. Due to this, insights gathered from the fly model are helpful in understanding similar phenomena in higher species.

However, one of the main advantages of working with *Drosophila* is its short generation time of about ten days at 25 °C, the easy and robust handling and especially its genetic accessibility (Fig. 4). Compared to vertebrates, gene

redundancy hardly plays a role which facilitates fast and straightforward establishment and application of various transgenic and knockout strategies. Additionally, the well-established UAS/GAL4 system allows tissue specific and temporally defined expression of a gene of interest (Brand and Perrimon, 1993) compared with a wide variety of approved driver lines (Sanyal 2009, for example in *Drosophila* motoneurons). I focused mainly on larval *Drosophila* combining the advantages of the genetic toolkit with a relative simple system due to lower cell numbers in comparison to the adult fly. Morphologically, most developmental stages are easily accessible with a huge variety of physiological, histological and microscopical techniques allowing numerous approaches that address questions regarding genetics, neurobiology, and developmental biology.

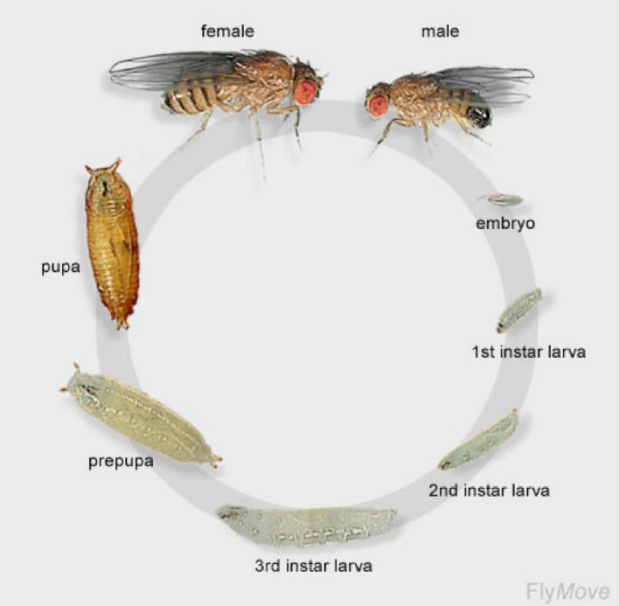

Fig. 4 *Drosophila* life cycle.

The eggs of *Drosophila* are about 0.5 mm long and the embryo hatches about 24h after egg laying (at 25°C). The resulting larvae grow for about four days while molting twice, at about 24h and 48h after hatching. Then the larvae encapsulate in the puparium and undergo a four-day-long metamorphosis after which the adult flies eclose (Weigmann et al., 2003).

2.2.2 Mechanosensation in *Drosophila*

In order to respond to mechanical stimuli it is essential that mechanical inputs are transduced into neuronal impulses, a process called mechanosensation. Along with the sense of touch, mechanosensation incorporates hearing and proprioception. In contrast to other senses like sight, taste and smell, mechanical sensations are rather poorly understood concerning their molecular basis. *Drosophila* providing the

advantages of a sequenced genome allied with powerful genetic techniques, and the ability to conduct electrophysiological recording from mechanoreceptor neurons is well-suited to make a significant contribution to this field.

Two main classes of mechanosensory organs are found in *Drosophila*: type I mechanoreceptors, which have monodendritic, ciliated neurons and are associated with specialized accessory cells. In contrast, type II mechanoreceptors have multiple non-ciliated dendrites and lack accessory cells (Eberl, 1999). Type II neurons, also known as multidendritic (MD) neurons, are differentiated into tracheal dendrite (td) neurons, bipolar dendrite (bd) neurons, and dendritic arborization (da) neurons (Bodmer and Jan, 1987). Type I mechanosensory organs are further subdivided into two distinct types: external sense organs and chordotonal organs (Keil, 1997) (Fig. 5B, C). External sense organs, such as sensory bristles, are cuticular structures being deformed or deflected by airflow, touch or proprioceptive stimulation.

Proprioception is defined as the ability to sense the relative position or motion of parts of the body by responding to stimuli arising within the body. In the fruit fly and other insects proprioception is provided by specialised type I mechanosensory organs termed chordotonal organs (chos). Chos represent a distinct version of type I sensory neurons as they are internal sense organs, lying under the cuticle, being stretched upon flexion of the joint between two segments (Eberl, 1999). The core of each cho is a sensory unit composed of a neuron and a scolopale cell. The latter represents a spindle-shaped cage that encloses an extracellular cavity, into which the ciliary outer segment extends. The neuron is suspended via its support cells between two points of epidermis allowing detection of relative movement for reception of stretching, vibration or both (Fig. 5C) (Jarman et al., 1993). By displacement of the epidermal attachment the sensory unit is stretched resulting in opening of specific channels, referred to as transient receptor potential vanilloid (TRPV) channels, at the outer segment of the dendrite (Gong et al., 2004). This elicits a signal that is then transferred to the locomotor central pattern generator circuit in the central nervous system. However, even in the absence of peripheral input the central pattern generator elicits movement but fine-tuning of motility results from sensory feedback providing additional behaviourally relevant information to the animal (Suster and Bate, 2002). Findings by Caldwell et al. (2003) suggest that chos

provide major feedback to locomotor central pattern generator generating rhythmic peristalsis and thus mediate touch sensitivity in *Drosophila* larvae.

Unlike external sense organs, that are located on the cuticule, chos are typically organised in arrays and found internally near the joints of adult fly legs, wings and halteres (Fig. 5A) (Eberl, 1999; Jarman, 2002). Additionally, a relatively large number of cho arrays forms the Johnston´s organ within in the antenna (Fig. 5A). This structure is adapted to detect sound transduced via vibration of the antennal capsule and is essential to discriminate species-specific courtship songs (Eberl, 1999).

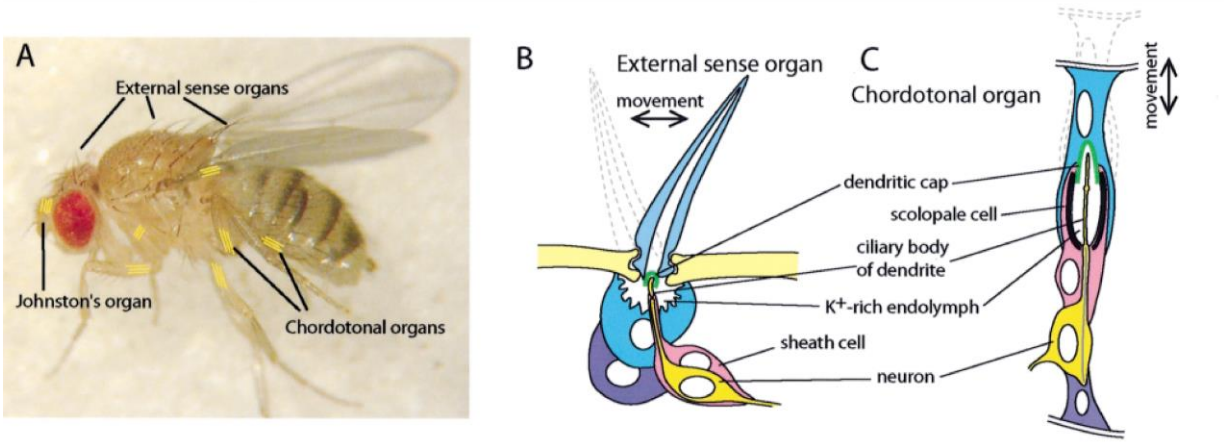

Fig. 5 Mechanoreceptive sense organs in *Drosophila*.

Depicted are the external sense organs (sensory bristles) as well as the Johnston´s organ, the auditory organ and the localisation of some internal chordotonal organs of the adult fly (A). Cartoon of an external sense organ (B) and a chordotonal organ (C) indicating structural features and emphasising their similarities (Jarman, 2002).

2.2.3 The *Drosophila* neuromuscular junction

The neuromuscular junction (NMJ) of *Drosophila* is particularly suited for the study of molecular and cellular mechanisms of neurotransmission and synaptic development. Basic features of the glutamatergic *Drosophila* synapse concerning its synaptic function and the majority of synapse-associated proteins are evolutionary conserved with mammalian excitatory CNS synapses.

2.2.3.1 Structural organisation of the *Drosophila* NMJ

The NMJ of the fruit fly encompasses a segmentally stereotypic pattern of 30 abdominal muscle fibers within each hemisegment demonstrating a bilateral symmetry (Fig. 6) (Bate et al., 1999). The muscles are innervated by a set of 36 motoneurons which emerge from the ventral ganglion and are generated during

embryogenesis (Landgraf and Thor, 2006). The axons terminate on their target muscle branching into presynaptic boutons (Fig. 6) that are surrounded by the subsynaptic reticulum (SSR). The SSR is a membrane-layered structure derived from the muscle cell membrane (Atwood et al., 1993). The postsynaptic membrane further carries the postsynaptic receptors.

Presynaptic boutons are categorised into four distinct groups according to their morphology, position and neurotransmitter identity (Johansen et al., 1989; Jia et al., 1993): Type Ib (big) boutons, present on all muscle cells, have large (3-6 µm in diameter) round terminals and are glutamatergic with a pronounced SSR. Type Is (small) boutons are present on almost all muscle fibers and have smaller (2-4 µm in diameter) glutamatergic terminals with a less noticeable SSR. By contrast, type II boutons are very small endings (1-2 µm) present on most muscle fibers and contain octopamine in addition to glutamate (Monastirioti et al., 1995). Finally, type III peptidergic terminals are medium sized (3-4 µm), oval shaped and are found solely on longitudinal muscle number 12 (Gorczyca et al., 1993).

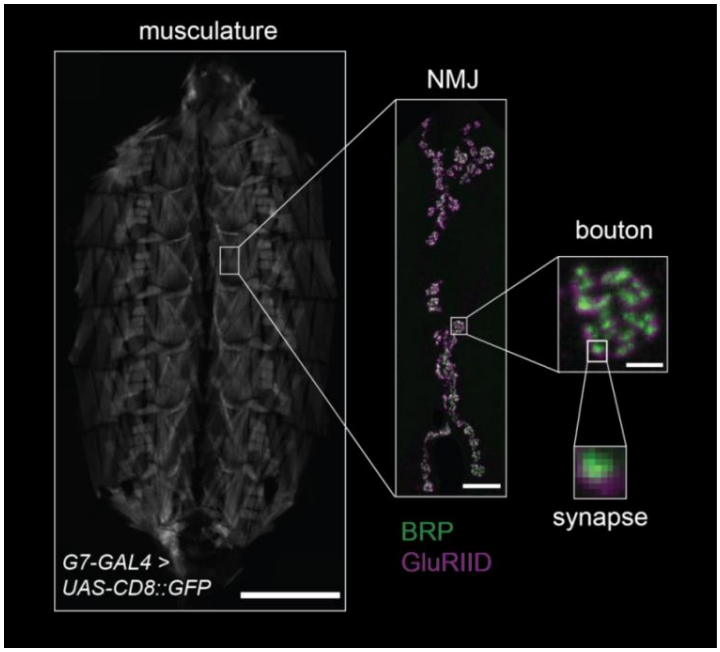

Fig. 6 Overview of the larval *Drosophila* NMJ.

Illustration of the *Drosophila* larva from the musculature to the NMJ to a bouton to a single synapse, depicting the main structural features of this model system. Shown is a an overview of the musculature of a *G7-GAL4* (muscle specific driver line) driven *UAS-CD8::GFP* larva as well as a wild-type larval NMJ of muscle 6/7 double-labeled for the presynaptic active zone marker *bruchpilot* (BRP; green) and postsynaptic glutamate receptor subunit IID (GluRIID; magenta). Scale bars = 1 mm, 50 µm and 2.5 µm.

2.2.3.2 Molecular organisation of the NMJ

Within the synapse, the release of neurotransmitter is restricted to specialized presynaptic membrane compartments called active zones (AZ). At these electron-dense specializations, synaptic vesicle exocytosis proceeds in a temporally and spatially highly coordinated fashion. The AZs of most *Drosophila* synapses contain T-shaped structures at the electron microscopic level (Fig. 7) (Atwood et al., 1993; Zhai and Bellen, 2004) and have been shown to be important for synaptic transmission, particularly Ca^{2+}-channel clustering and coordinated vesicle release (Kittel et al. 2006). Bruchpilot (BRP), a homolog to mammalian ELKS/CAST/ERC was identified as a direct T-bar component at the AZ (Wagh et al., 2006; Fouquet et al., 2009). At synapses lacking BRP, T-bars are absent, clustering of presynaptic Ca^{2+}-channels is defective, evoked excitatory junctional current (eEJC) amplitudes are decreased, and short-term plasticity is altered (Atwood, 2006; Kittel et al., 2006). This demonstrates that BRP is a main organiser of presynaptic AZs.

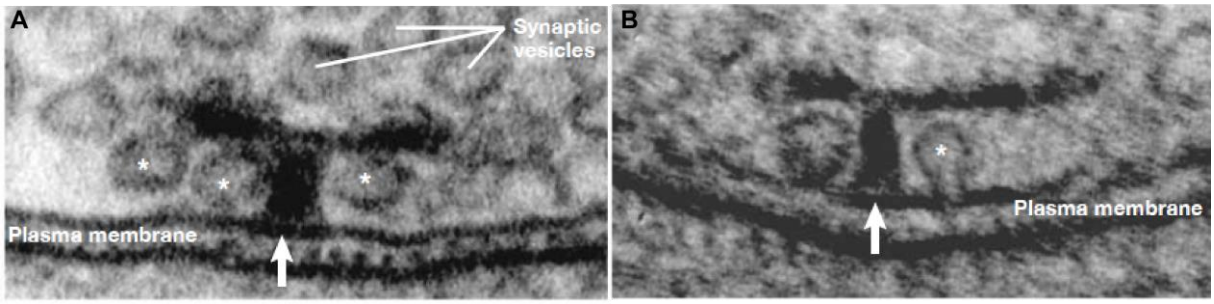

Fig. 7 Electron micrograph of the *Drosophila* NMJ.

Electron micrograph showing an electron dense T-bar (white arrow) with synaptic vesicles (asterisk) close to the AZ membrane (A). Putative fusion of synaptic vesicle (asterisk) with the presynaptic plasma membrane nearby a T-bar (arrow) release site (B) (Rohrbough and Broadie, 2005).

AZ proteins show a high degree of homologies, e.g. voltage-gated Ca^{2+} channels, CAST, Neurexins and Neuroligins as well as SNARE proteins (soluble *N*-ethylmaleimide sensitive factor attachment receptors). The perisynaptic region surrounding individual synapses harbours adhesion proteins like Fascilin II (FasII). Fas II is related to vertebrate NCAMs (neuronal cell adhesion molecules) and linked to synaptic stabilisation and growth (Schuster et al., 1996). The postsynaptic density (PSD) juxtaposed to the AZ provides the clustering of glutamate receptors, voltage-gated ion channels, scaffolding and regulatory molecules (Qin et al., 2005; Prokop and Meinertzhagen, 2006). Beneath the PSD the muscle membrane is highly convoluted forming the subsynaptic reticulum (SSR). Various scaffolding and

adhesion proteins like Discs-large (DLG), which might function in the structural organisation and signalling mechanisms of cell adhesion molecules and ion channels, are found at the SRR membrane (Thomas et al., 1997).

2.2.3.3 Mechanism of synaptic vesicle exocytosis

In order for a synaptic vesicle to release its neurotransmitter into the synaptic cleft it must undergo exocytosis. Upon arrival of an action potential exocytosis and recycling of synaptic vesicles define how much transmitter is released. This requires a complex protein machinery interacting in a highly coordinated fashion. Synaptic vesicles undergo several steps before the final fusion event. First, filled vesicles translocate to and dock at the AZ where they undergo a priming reaction which makes them competent for Ca^{2+}-triggered fusion pore opening before they are finally triggered for membrane fusion (Sudhof, 2004). Synaptic AZs contain proteins which are referred to as t-SNAREs (target-SNARE) that interact with specific proteins on the synaptic vesicle, called v-SNAREs (vesicle-SNARE) (Richmond and Broadie, 2002). The structural hallmark of SNARE proteins, the SNARE motif, is a homologous 70 amino acid residue sequence. The interaction of four SNARE motifs forming a four-helical bundle results in the formation of a core complex, which brings the membrane sheets on which the SNAREs reside in close proximity, thereby initiating membrane fusion (Sudhof, 2004). Like at most synapses including the *Drosophila* NMJ exocytosis is mainly mediated by three proteins: the v-SNARE Synaptobrevin and the t-SNAREs Syntaxin-1A and SNAP-25 on the presynaptic membrane (Sollner et al., 1993). The complex is thought to be primed by the protein Unc13 which was initially isolated from *C.elegans* and is homologous to mammalian Munc13-1 (Richmond et al., 1999). The binding of Ca^{2+} to Synaptotagmin, a synaptic vesicle protein which interacts with Syntaxin, seems to cause intertwined α-helical bundles within the SNARE complex to contract, causing the two lipid bilayers to mix (Weber et al., 1998). This results in a fusion pore causing the release of transmitter into the synaptic cleft. After fusion the SNARE complex has to disassemble and rewind a process that occurs via ATP-dependent hydrolysis, in order to prepare for subsequent rounds of exocytosis (Sollner et al., 1993). After fusion-pore opening, synaptic vesicles undergo endocytosis and recycle via several routes: local reuse (kiss-and-stay), fast recycling without an endosomal intermediate (kiss-and-run), or clathrin-mediated endocytosis with recycling via endosomes (reviewed in Sudhof, 2004).

2.3 Reconstitution of split GFP fragments

2.3.1 GRASP – GFP reconstitution across synaptic partners

A comparatively novel method, termed GFP reconstitution across synaptic partners (GRASP), enables mapping of cell contacts, such as synaptic partners *in vivo* (Feinberg et al., 2008). Initially the idea is based on reconstitution of a fluorescent protein previously split into two polypeptides (Fig. 8). Although it was known that GFP still yields a fluorescent product if interrupted at several positions (Abedi et al. 1998; Baird et al. 1999), Ghosh et al. (2000) first demonstrated that other division sites disable the flourophore's photo center thereby enabling the study of intracellular protein-protein interaction in living cells using the split-GFP method. Cabantous et al. (2005) engineered soluble, self-associating GFP fragments to overcome folding problems. One fragment, split GFP 1-10 (spGFP1-10), includes ten of the elven strands of the GFP beta-barrel and consists of 214 residues. The second fragment split GFP11 (spGFP11) contains the 16 C-terminal residues of GFP and builds the 11th strand of the beta-barrel structure of GFP. The split GFP fragments are non-fluorescent but assemble into a fluorescent form when the two fragments meet (Fig. 8). So far, GRASP has been used effectively to map connectivity between synapses in the nematode (Feinberg et al., 2008) and the fruit fly (Gordon and Scott, 2009; Gong et al., 2010). Thus, they applied spGFP fragments as transmembrane proximity detectors demonstrating extracellular membrane-membrane interactions via a set of suitable spGFP fusion proteins.

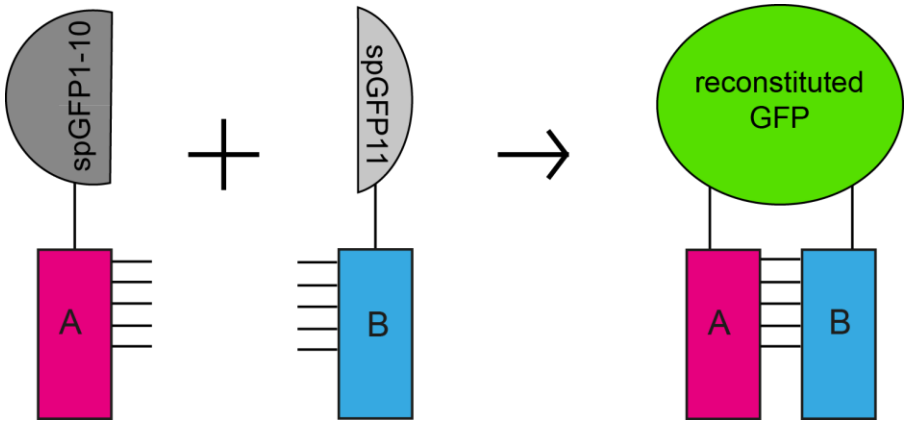

Fig. 8 Schematic diagram representing the principle of the split GFP (spGFP) assay.

Two fragments of the green fluorescent protein (GFP), termed spGFP1-10 and spGFP11are fused to two putative interaction partners (A and B). An interaction between the proteins A and B facilitates assembling of the non-fluorescent spGFP fragments into a fully functional reconstituted GFP.

2.3.2 Analysing intracellular membrane protein interactions with split GFP fragments

At present, no appropriate method is available to capture the transient and fast interactions of presynaptic proteins residing on the vesicle and presynaptic membrane. To date, the methods used to study protein dynamics and interactions at the synapse are primarily electrophysiological or optical tools. Mainly two principle techniques are utilised to visualise protein interactions in living cells: Fluorescence resonance energy transfer (FRET) and bimolecular fluorescence complementation (BiFC). The latter relies on the interplay between two putative interaction partners, covalently linked to complementary fragments of a reporter protein, such as YFP (Hu et al., 2006). In contrast FRET is based on the measurement between two molecules labeled with two different fluorophores by the transfer of energy from the excited donor to the acceptor (Clegg, 1995). Both assays are adapted for investigation of protein interactions in living cells, however the main compromise between both approaches is one of sensitivity versus dynamics (Kerppola, 2006a). Because of its stable protein complementation, the BiFC assay is typically more sensitive than FRET. Instead of producing changes in an already existing fluorescence signal, as it is the case with FRET, BiFC produces new functions (Kerppola, 2006a). However, the strength of the FRET approach is the instantaneous real-time monitoring of protein interactions. This allows the detection of proteins that associate only for short time (Fan et al., 2008). BiFC on the other hand requires time for fluorophore activation that proceeds through an autocatalytic cyclisation reaction occurring after the protein has been folded correctly (Kerppola, 2006b). In addition, FRET produces background fluorescence by excitation of the acceptor fluorophore making it difficult to detect weak protein interactions using FRET. Consequently, FRET requires higher levels of protein expression in order to produce detectable change in fluorescence intensities. Further, FRET quantification asks for specialised equipment, such as irreversible photo-bleaching, to maintain fluorescence over time (Hu et al., 2006). By contrast, BiFC is not in need for special tools, as visualisation is possible with a fluorescence microscope and appropriate objectives for monitoring protein interactions *in vivo* (Kerppola, 2006b).

In order to analyse intracellular membrane protein interactions in *Drosophila* the split-GFP method was applied in terms of coincidence detection upon direct protein-protein interaction, an attempt already started during my diploma thesis. To enlighten

the essential steps of transmitter release presynaptic proteins were fused with spGFP fragments to detect their interactions *in vivo* during synaptic exocytosis. In addition to Bruchpilot (BRP) three synaptic proteins, which are important for synaptic exocytosis: the Ca^{2+}-sensor Synaptotagmin (Syt), the t-SNARE Syntaxin-1A (Syx) and the v-SNARE n-Synaptobrevin (n-Syb) were used in this study. Initial experiments showed that full length reporter protein fusions with n-Syb, Syt and Syx allow expression in *Drosophila* and confirmed that fusion to either end of each synaptic protein did not impair expression and moreover not influence the viability of transgenic flies. Further, transgenes containing protein fusions of Syx, Syt, and n-Syb with split GFP fragments were established in previous studies (Gehring, 2010).

2.4 Study objectives

The first and major part of this thesis addresses the localisation and functional analysis of the fly LPHN homolog dCIRL. Several data previously indicated that LPHNs might be involved in regulating synaptic function and thus directly or indirectly modulate transmitter release (Ichtchenko et al., 1998; Sudhof, 2001; Capogna et al., 2003). Other results from the nematode *C.elegans* suggest that LPHNs are implicated in neuronal development and tissue polarity (Langenhan et al., 2009). Although these findings are not mutually exclusive the actual functional role of LPHN in neurons remains blurry. By using a *dCirl* knockout mutant fly, generated previously by Fischer (2011), this study aimed to clarify the physiological function of dCIRL in the fruit fly *Drosophila*. Additionally, by using genomic tagging of dCIRL as well as *dCirl* promoter-driven expression of GFP the expression pattern of dCIRL in adult flies and larvae was analysed. Further, behavioural studies were performed to relate the localisation and structure of dCIRL to its physiological function in the larval fruit fly.

The second part of this thesis investigates protein-protein interactions at the active zone of the larval *Drosophila* NMJ using a modified form of the spGFP system developed by the Hamilton, Regan, Kerppola, Gosh, Chalfie, Shen and Bargmann labs. The attempt takes advantage of the principle of coincidence detection upon direct protein interactions when protein fusions with different spGFP components encounter each other. To shed light on the essential steps of transmitter release we set out to bestow key presynaptic proteins with spGFP fragments to detect their

interactions *in vivo* during distinct steps of synaptic exocytosis. The results from spGFP studies might reveal to what extent this method is suitable for resolving the extremely fast and transient processes at active zones. In my diploma thesis I already described the development of a generic set of plasmids for expression of spGFP-tagged proteins in *Drosophila*. Now, this work presents the initial characterisation of spGFP complementation of different synaptic protein homologs from *Drosophila* fused to spGFP fragments.

3. Materials and Methods

3.1 Molecular biology

3.1.1 Material

All chemicals were, if not stated otherwise, purchased from Roth (Karlsruhe), Sigma (Diesenhofen) or Merck (Darmstadt). T4 DNA ligase and T4 polynucleotide kinase were purchased from Roche (Mannheim). Various restriction endonucleases were obtained from New England Biolabs (Frankfurt). Gateway® enzyme mix used for LR- and BP-reaction was purchased from Invitrogen (Karlsruhe). Unless stated elsewhere all molecular biology kits for DNA extraction and purification were obtained from Qiagen (Hilden) or Macherey-Nagel (Düren). Chemically competent *E. coli* cells were produced in the lab with standard procedures. All PCRs were performed with the Thermocycler T3, T3000 or UNOII (Biometra, Göttingen). Oligonucleotides were obtained from MWG-Biotech (Ebersberg, Germany) and dissolved in dH_2O at a concentration of 20 pmol/µl.

3.1.2 Transgene construction

Construction of *dCirl* transgenes

The *dCirl* targeting construct pTL161 was built by initially amplifying the 3.5 kb 3´ homology arm with primers tl_53F and tl_54R and insertion into the plasmid pGX-attP via *Nsi*I and *Avr*II restriction sites (Huang et al., 2009). Amplification of the 5.0 kb 5´ homology arm was performed using primers tl_51F and tl_52R containing *Not*I and *Kpn*I sites followed by insertion into pGX-attP-3´arm plasmid.

The *dCirl*^{RFP} construct pTL391 was produced by amplification of an 10.8 kb fragment of the genomic dCirl locus (primers tl_299F and tl_300R) and insertion into the phiC31-integration vector pGE-attB-GMR (Huang et al., 2009) via *Not*I and *Asc*I sites (=pTL370). After opening this vector at a single *Aat*II site, a 0.7 kb *mRFP* fragment amplified from the *Drosophila* Gateway© destination vector pTWR (primers tl_332F and tl_338R) was inserted in-frame.

The *dCirl*^{Flag} construct pTL393 was produced similarly: Following amplification of 0.1 kb 3xFLAG sequence from Gateway© destination vector pTWF (primers tl_337F and tl_338R) the plasmid was inserted into pTL370 via a single *Nhe*I site.

The genomic DNA template for the PCR-based homology arm and locus amplification of the DNA was the BAC clone #BACR21H10 (#RP98-21H10) from BacPac repository (Children´s Hospital Oakland Research Institute). Dr. T. Murphy (Carnegie Institution of Washington, Baltimore) provided the pTWR and pTWF vectors for cloning.

The *dCirl::spGFP1-10* construct pTL426 was designed by amplification of a 0.7 kb fragment from the pJG3 vector (see J. Gehring, 2010) using the primers tl_377F and tl_378R and insertion into pTL370 via a single *Aat*II site. Amplification of a 0.7 kb fragment from pTL149 (see J. Gehring, 2010) using the primers jg_45F and jg_46R and cloning into the ptW-attB vector via *EcoR*I and *Nhe*I led to the spGFP11::RFP construct pJG55.

For PCR-amplification the AccuStar high-fidelity proof-reading DNA polymerase (Eurogentec, Cologne, Germany) was used and each PCR-amplified region of the constructs was completely sequenced (MWG-Biotech, Ebersberg, Germany). The following primers, restriction sites indicated in bold letters, were used for transgene construction:

Name	Sequence 5`-3`
tl_51F	atagtttaGCGGCCGCtgtggaatccgcagcactacgacta
tl_52R	cggGGTACCtattgataaatacaaacatatttaact
tl_53F	ccaATGCATtcctcgtaagctaagtgctatgca
tl_54R	aatgcaCCTAGGcatcttaacggagctcacgagctgt
tl_299F	atagtttaGCGGCCGCagtaatttgtcttcgatgtatgcat
tl_300R	aGGCGCGCCatttaaagccatttttgaaagcaaa
tl_332F	atcggaGACGTCtagctgctgcagctGCCtcctccgaggacgtgatcaag
tl_333R	atcggaGACGTCcagccgctgcagcggcgccggtggagtggcggccctc
tl_337F	ctaGCTAGCgctgcggctgcagctgactacaaagaccatgacggtga
tl_338R	ctaGCTAGCcgctgcagcagccttgtcatcgtcatccttgtaat
tl_377F	atcggaGACGTCtagctgctgcagcttccaaaggagaagaactgtttaccggcgt
tl_378R	atcggaGACGTCcagccgctgcagctgttccttttttcatttggatctttgctcag
jg_45F	cGAATTCcaacatgcgtgaccacatggtccttcatgagtatgtaaatgctgctgggattacagctg ctgcagctgcggtaaccggtatggcctcctccgaggacgtcatca
jg_46R	gagggccgccactccaccggcgcctagGCTAGCtac

3.1.3 Ends-out targeting of *dCirl*

The ends-out strategy via homologous recombination consists of three major steps: Targeting, screening for incorrectly or non-targeted recombinants and confirming targeting to the correct chromosome location. Ends-out targeting of *dCirl* was performed by R. Fischer (2011) according to Huang et al. (2008) with the fly strains used therein.

3.1.4 Reverse Transcription PCR

cDNA synthesis was performed using total RNA from *Drosophila melanogaster* larvae and was directly reverse-transcribed with Superscript® II RT (Invitrogen, Karlsruhe, Germany). The following primers were used for PCR-amplification on transcribed cDNA libraries:

Name	Sequence 5`-3`
tl_5F	tcatcagggagcgcagcgtggtgca
tl_6R	atgctggtatagatcgaggtgcgcg
tl_444F	gttgcaaccacctgacaaactttgc

3.1.5 dCIRL antibody production

BioGenes (Berlin, Germany) produced a polyclonal antiserum against the synthetic peptide, which corresponds to amino acid 365-379 of dCIRL (CVLMKRIPDSGYDEY).

3.1.6 Western Blot

For each lane in Western Blots five larval heads (*dCirl*^{RFP} and *dCirl*^{Flag}) or larval filets (*dCirl*^{KO} null confirmation and DLG intensity) were homogenized in 15 µl 5x Laemmli sample buffer on ice. The sample was heated to 70°C for 5 min and centrifuged for 2 min before electrophoresis. Proteins were separated in a 12.5% SDS-PAGE gel and transferred to a polyvinylidene diflouride membrane (Hybond P, Amersham). 5% milk powder in 1x TBST was used as blocking solution. Immunoreactions were accomplished with the following antisera at 4°C overnight: polyclonal rabbit-anti-dCirl 1:500, polyclonal rabbit-anti-RFP (antibodies-online GmbH, Germany; #ABIN129578) 1:500, monoclonal mouse-anti-FLAG M2 (Sigma-Aldrich, Taufkirchen, Germany; #F3165) 1:1000. Following washing, membranes were incubated for 1 hr at room temperature with horseradish-peroxidase-conjugated goat-anti-rabbit (1:2000) or

goat-anti-mouse secondary antisera (1:5000; both Sigma-Aldrich), respectively, and washed again according to standard protocols. Visualization was achieved by an enhanced chemiluminescence (ECL) detection system (Thermo Scientific, Illinois, USA) according to manufacturer´s specifications.

3.2 *Drosophila melanogaster*

3.2.1 Fly rearing

Fly strains were kept in small acrylic glass vials (Klühspies, Retzstadt, Germany) containing cultivation medium (1l H20, 4,5 g Agar, 20 g beet syrup, 72,2 g malt, 16,3 g yeast, 9 g soy flour, 72,2 g corn flour, 1,45 g nipagine, 5,7 g propionic acid). *Drosophila* stocks were reared at either 18 °C or 25 °C and transferred to fresh vials after 12-14 days at 25 °C and after 3-4 weeks at 18 °C.

3.2.2 Transgenesis

Drosophila germ line transformation was performed by BestGene Inc (California, USA) using either P-element transformation ((Rubin and Spradling, 1983), *spGFP* constructs, except *spGFP11::RFP* and *dCirl::spGFP1-10*) or PhiC31 integrase-mediated transgenesis systems ((Groth et al., 2004), *dCirl* constructs).

3.2.3 Transgenic lines used in thesis

Transgenic animals were established in the following genetic backgrounds:

Lab name	Genetic background
dCirl	
LAT01	w^{1118};+; *P{pTL161 [dCirl targeting vector]*w^{+}*/TM3 (Sb)}*
LAT26	w^{1118}; *Cirl*$^{108/11A}${attP+ loxP +}$^{w-}$/CyO GFPw^{-};
LAT47	w^{1118}; *Cirl*$^{108/11A}${attP+ loxP-mW-loxP}$^{w+}$*/CyOGFP*w^{-} *; +*
LAT52	w^{1118}; *Df(2R)Exel8047/CyOGFP* w^{-}*; +*
LAT54	w^{1118}; *dCirl*^{KO} attP loxP-w^{+}-loxP;;
LAT56	w^{1118}; *dCirl*^{KO} *attP{dCirl::rfp* w^{+}*} loxP;; +*
LAT67	w^{1118}; *dCirl*^{KO} *attP{dCirl::flag* w^{+}*} loxP;; +*
LAT60	w^{1118}; *dCirl*^{KO} *attP{dCirl::spGFP1-10* w^{+}*} loxP;; +*
LAT79	w^{1118}; *Cirl*$^{108/11A}$ *{attP+ loxP+}*$^{w-}$ *att{Cirl*$^{w+}$*}; CyO*
LAT91	w^{1118}; *dCirl*^{KO} *ok6-GAL4*w^{+}*/CyOGFP*w^{-}*;+*

LAT109	*w^{1118}; dCirl^{KO}/CyoGFPw^{-};Act-5C-GAL4w^{+}/TM6B, Tb*
LAT110	*w^{1118}; dCirl^{KO}/CyoGFPw^{-};elav-GAL4w^{+}/TM6B, Tb*
LAT111	*w^{1118}; dCirl^{KO}/CyoGFPw^{-}; 20xUAS-dCirl::Flag w^{+}/TM6B, Tb*
LAT113	*w^{1118};dCirl^{KO}/CyOGFPw^{-};P{y$^{+t7.7}$w^{+mC}=20XUAS-IVS-mCD8::GFP}attP2/TM6B, Tb*
LAT114	*w^{1118};dCirl^{KO}21-7-GAL4/CyOGFPw^{-};+*
LAT116	*w^{1118};dCirl^{KO}/CyOGFPw^{-}; iav- GAL4w^{+}/TM6B, Tb*
LAT117	*w^{1118} 5-40-GAL4; dCirl^{KO}/CyOGFPw^{-};+*
split-GFP	
GR48	*w^{1118}; P{UAS::spGFP1-10::Syx w^{+}}/CyO; +*
GR60	*w^{1118}; +; P{UAS::nSyb::spGFP11 w^{+}}/TM3(Sb)*
GR65	*w^{1118}; +; P{UAS::Syx::spGFP1-10 w^{+}}/TM3(Sb)*
GR69	*w^{1118}; +; P{UAS::Syx::spGFP11 w^{+}}/TM3(Sb)*
GR80	*w^{1118}; P{UAS::spGFP1-10::Syt w^{+}}/CyO; +*
GR89	*w^{1118}; +; P{UAS::Syt::spGFP11 w^{+}}/TM3 (Sb)*
GR108	*w^{1118}; P{UAS::Syb::spGFP1-10 w^{+}}/CyO; +*
GR145	*w^{1118}; +; P{UAS::spGFP11::RFP w^{+}}/TM3(Sb)*

The following strains were obtained from the Bloomington Stock Center (Bloomington, USA):

Stock no.	Genetic background
BL#766	*y^{1} w^{67c23} P{y^{+}Cre}1b; sna^{Sco}/CyO;;*
BL#7863	*w^{1118}; Df(2R)Exel8047/CyO*
BL#25679	*y1 w^{-}/Dp(2;Y)^{G}, P{w$^{[+mC]}$=hs-hid}^{Y}; ; P{ry$^{+t7.2}$=70FLP}^{23} P{v$^{+t1.8}$=70I-SceI}^{4A}/TM3 P{w^{+mC}=hs-hid}^{14}, Sb^{1};*
BL#26259	*w^{-}; Pin^{1}/CyO; P{?GawB}$^{221w-}$;*

3.3 Immunohistochemistry

3.3.1 Materials

Hemolymph-like saline solution (HL-3) without $CaCl_2$ was used for all dissections: NaCl 70 mM, KCl 5 mM (high potassium: KCl 90mM), $MgCl_2$ 5 mM, $NaHCO_3$ 10 mM,

trehalose 5 mM, sucrose 115 mM, HEPES 5 mM, ad 500 ml H2O, pH adjusted to 7,2. Afterwards preparations were fixed in 4% paraformaldehyde (PFA): 2g PFA ad 18 ml H2O (58 °C), 1 N NaOH, 25 ml 0,15 M KH2PO4, 6 ml 0,15 M NaHPO4 , pH adjusted to 7,4. Split-GFP constructs were fixed in methanol (Merck). For NMJ staining procedures PBS with 0.05 % Triton TX100 was used (PBS 10x: 74 g NaCl, 12.46 g Na2HPO4 x 2 H2O, 4.14 g NaH2PO4 x H2O, add 1 l H2O, pH 7,4). VNC were stained using PBS with 0.1% Triton TX100.

3.3.2 Larval body wall preparation

Wandering third instar larvae were put on rubber pad, covered with a drop of ice-cold HL-3 solution and fixed with fine insect pins (0.1 x 10 mm, FST, Heidelberg, Germany). Using dissection spring scissors (FST, Heidelberg, Germany) the larvae were cut open dorsally along the midline from the anterior to the posterior end. After stretching and pinning down the epidermis with two pins on each side, the fat body was removed carefully with fine forceps (FST, Heidelberg, Germany) to expose the muscles and nervous system of the ventral inner side of the animal.

3.3.3 Fixation and staining procedures

The dissected samples were fixed either for ten minutes in 4% PFA at room temperature or for five minutes in 98% methanol on ice (for splitGFPs). After 30 minutes of blocking with PBT containing 5% goat serum (NGS), the PBT/NGS mixture was refreshed, primary antibodies were added, and the dissections were incubated at 4 °C overnight. The next day samples were rinsed two times shortly and three times for 20 minutes with PBT, following application of fluorescence-labeled secondary antibodies for two hours at room temperature. Samples were washed again and incubated for at least 30 minutes at 4 °C in Vectashield mounting medium (Vector Laboratories, California, USA). Finally, fillets were embedded in mounting medium on an object slide, the dorsal side facing up, covered with a cover slip and sealed with nail polish.

To prevent inter-experimental variations, all genotypes with appropriate controls per experiment were incubated and stained in the same tube.

Antibody	Species	Dilution	Reference	Antigen
nc82	mouse	1:250	Prof. Erich Buchner (Uni Würzburg)	Bruchpilot
anti-GFP	rabbit	1:500	Invitrogen (Karlsruhe, Germany)	GFP
anti-GFP	mouse	1:500	Sigma-Aldrich (St. Louis, USA)	GFP
anti-RFP	rabbit	1:250	antikoerper-online.de (Aachen, Germany)	RFP
anti-GluRIID	rabbit	1:500	Prof. Stefan Sigrist (FU Berlin)	GluRIID
anti-FLAG	mouse	1:500	Sigma-Aldrich (St. Louis, USA)	FLAG
anti-DLG	mouse	1:500	Developmental Studies Hybridoma Bank (Iowa, USA)	Discs-large
anti-MIP	mouse	1:500	Prof. Christian Wegener (University of Würzburg)	MIP
anti-Futsch	mouse	1:250	Developmental Studies Hybridoma Bank (Iowa, USA)	Futsch
anti-Spectrin	mouse	1:250	Developmental Studies Hybridoma Bank (Iowa, USA)	Spectrin
anti-Fasciclin II	mouse	1:250	Developmental Studies Hybridoma Bank (Iowa, USA)	Fasciclin II
anti-integrin betaPS	mouse	1:100	Developmental Studies Hybridoma Bank (Iowa, USA)	Integrin betaPS
Alexa 488	rabbit	1:250	Invitrogen (Karlsruhe, Germany)	-
Alexa 488	mouse	1:250	Invitrogen (Karlsruhe, Germany)	-
HRP-Cy3	goat	1:250	Dianova (Hamburg, Germany)	HRP

3.4 Image acquisition

3.4.1 Confocal microscopy

Confocal images were acquired with a line scanning confocal LSM 5 system (Zeiss, Germany), while using a 63x/1,25 oil immersion objective for NMJ recordings, a 40x/1.30 oil immersion objective was applied for VNC recordings with a 1.3x magnification, respectively. Confocal settings were chosen to obtain a pixel size of 100 nm. For the resolution on the Z-axis an interval of 0.4 µm (NMJ recordings) and 2 µm (VNC recordings) between each slide was set up. The pinhole ranged between 0.8 to 1.5 airy units, depending on signal strength. Alexa 488 was excited using the

488 nm Argon laser line, while Cy3 was excited with a 543 nm HeNe laser. To achieve comparable results within the experimental group, laser power and image settings were kept identical for each channel.

3.4.2 Image processing

Confocal stacks were processed using MacBiophotonics ImageJ version 1.43u (http://www.macbiophotonics.ca/imagej/). Background subtraction and removal of non-synaptic material was performed manually, but macros were utilised to automate quantifications. Graphics and image annotation was processed with Adobe Illustrator CS5 (Adobe Systems, San Jose, USA). Statistical analysis were performed with Prism 5 (GraphPad Software, La Jolla, USA) using the nonparametric Mann Whitney test. The data are reported as mean ± s.e.m, n indicates the sample number, and *p* denotes the significance: * $p<0.05$, ** $p<0.01$, *** $p<0.001$.

3.5 Larval behavioural studies

3.5.1 Survival analysis

Larvae missing *dCirl* were tested for developmental dysfunction by analysing their survival rate. Following genotypes were counted over 16 days past fertilization (d.p.f.): *dCirl*^{KO}*/CyoGFPw*$^{-}$, *dCirl*^{KO}*/Df* and +/ *CyoGFPw*$^{-}$ at 1st larval stadium (two d.p.f.), 3rd larval stadium (seven d.p.f.), pupal state (eleven d.p.f.) and adult flies (16 d.p.f.). Three different vials per genotype were added, averaged and normalized to 100%. The data are stated as mean ± s.e.m, averaged sample number is indicated by n and significant differences are denominated by *p*: * $p<0.05$, ** $p<0.01$, *** $p<0.001$ for all larval behavioural studies.

3.5.2 Wandering behaviour

Third-instar larvae raised at 25 °C were put in a drop of water in the middle of an agar plate (1% agarose) with 14 cm in diameter and immediately video recorded. Up to five larvae at once were recorded continuously for at least two minutes. Larval images were frame-sized and crawling distance was analyzed using ImageJ software. Behavioural data were statistically analysed as described in 3.4.2.

3.5.3 Touch sensitivity assay

External touch sensitivity was tested on single third-instar larvae, raised at 25 °C. During linear locomotion in a Petri dish (5 cm in diameter) the larvae were gently

touched with tip of a von Frey filament (0.3 mN) on their anterior thoracic segments (Kernan et al., 1994). A score system as described by Caldwell et al. (2003) was applied: A score of 0 obtained those larvae not responding to touch. If the larvae stopped or hesitated they were scored as 1, while those that retracted briefly but continued crawling forward were scored 2. Larvae that retracted and turned away from the stimulus < 90° gained a score of 3, and those retracted and turned away > 90° yield a score of 4. Each larva was gently touched during linear locomotion and scored four times. The values were summed up to attain possible scores from 0 to 16 per larva.

4. Results

4.1 Functional characterisation of *dCirl*

To date, rather little is known about the function of the single latrophilin homolog *dCirl* in *Drosophila melanogaster*. In this thesis various genetic experiments, imaging approaches and behavioural studies were applied to unravel the role of *dCirl* in the fruit fly.

4.1.1 Confirmation of *dCirl*^{KO} as a null mutant

The first aim of this project was to precisely characterise the function of dCIRL in *Drosophila melanogaster*. Therefore we utilised the *dCirl*^{KO} mutant, which was generated within a previous diploma thesis by R. Fischer (2011) via ends-out targeting and homologous recombination according to Huang et al. (2008) and (2009). A 10.7 kb fragment, including the complete *dCirl* open reading frame (ORF), the 5´and 3´ untranslated regions (UTRs) and part of the 5´ intergenic site encoding the putative *dCirl* promoter, was replaced by and *attP* site and a floxable *hsp70-white* selection cassette (Fig. 9). By utilising *hs-hid/UAS-Rpr*-mediated negative selection and PCR-genotyping two recombinant fly strains were recovered. After sequencing across 5´ and 3´ homology arm break points, to confirm precise replacement of the *dCirl* locus, one recombinant fly strain, termed *dCirl*^{KO}, was selected.

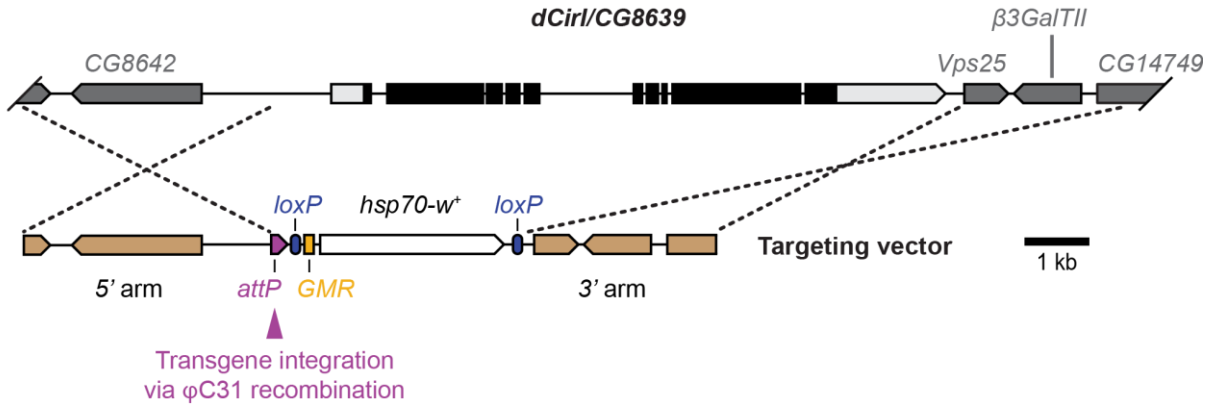

Fig. 9 Schematic showing the *dCirl* locus and null allele construction strategy.

Genomic organisation of the *dCirl/CG8639* locus and ends-out targeting vector for creation of a *dCirl*^{KO} null allele. Using homologous recombination a 10.7 kb fragment encompassing the *dCirl* ORF and both putative UTRs was replaced by a floxable *white* marker and an *attP* site, which subsequently served as integration site for *dCirl* transgenes.

The results from this present thesis verified that *dCirl*^{KO} is a null allele by RT-PCR from *dCirl*^{KO} and control flies using a *dCirl*-specific primer pair. For each genotype total RNA was isolated from adult fly heads, reversely transcribed into cDNA and tested by RT-PCR, as described in 3.1.4. The resulting data revealed that no residual transcript is present in *dCirl*^{KO} homozygous fly heads, while in the heterozygous *dCirl*^{KO}/+ line slight amounts of residual transcript were found as expected (Fig. 10A). *dCirl*^{RFP} samples, a genomic *dCirl* transgene fused in-frame with a monomeric RFP chromophore (described in 4.1.3) also showed *dCirl* transcript.

In addition, we performed western blot analysis using protein extracts from wild-type larvae, larvae homozygous for *dCirl*^{KO} and for *Df(2R)Exel8047*, a deficiency that includes the *dCirl* locus as well as six adjacent genes. A polyclonal antiserum that recognises a peptide which is situated in the extracellular region of dCIRL was used for immunodetection (see 3.1.5). Notably, two specific bands were visible in wild-type extracts, corresponding to the full-length (~ 180 kDa) and autoproteolysed receptor (~ 70 kDa) cleaved at the GPS motif (Fig. 10B). Both bands were absent in *dCirl*^{KO} and *Df(2R)Exel8047* homozygous samples, as shown in Fig. 10B, which confirms that *dCirl*^{KO} is a clean protein null allele.

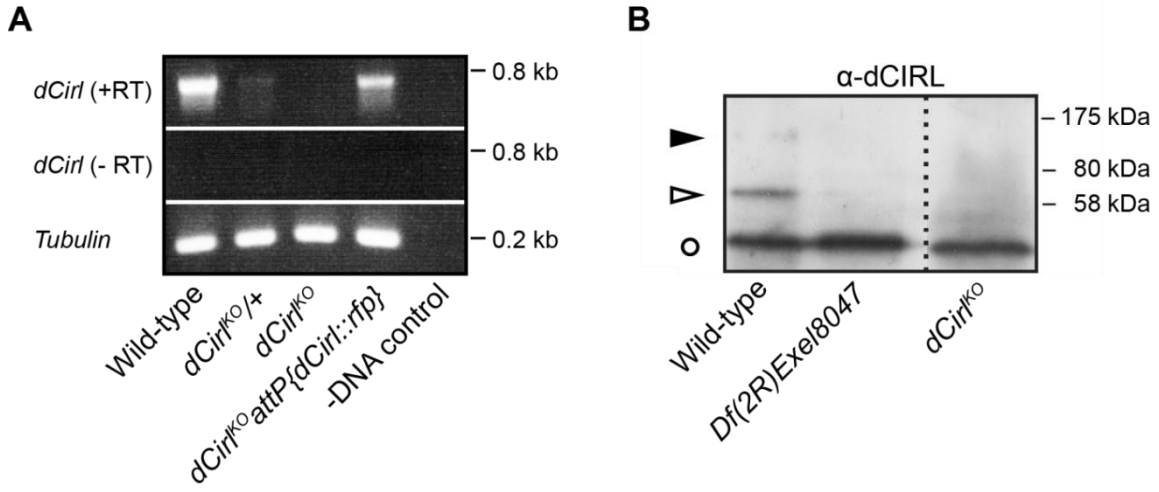

Fig. 10 Confirmation of the *dCirl*^{KO} allele.

RT-PCR of cDNA prepared from adult fly heads shows loss of *dCirl* transcript in *dCirl*^{KO} animals in contrast to WT larvae, heterozygous *dCirl*^{KO} and *dCirl*^{RFP} larvae (A). Western blot analysis using a dCIRL antiserum show no residual protein in *dCirl*^{KO} and *Df(2R)Exel8047* larvae compared to WT, where the full-length (open arrowhead, ~ 180 kDa) and autoproteolysed receptor band (closed arrowhead, ~ 70 kDa) is present at expected size. An unspecific signal detected by the antiserum functioned as loading control (open circle).

4.1.2 Loss of *dCirl* does not influence development in *Drosophila*

Because it is known from *C. elegans* that LAT-1 functions in development and homozygous *lat-1* worms arrest in the first larval stage to nearly a 100% (Langenhan et al., 2009) the survival rate of *dCirl* knockout animals was analysed. We observed no differences in the survival rate of $dCirl^{KO}$ animals crossed over a deficiency (*Df(2R)Exel8047*), to exclude second site hits on the $dCirl^{KO}$ chromosome, in comparison to heterozygous $dCirl^{KO}$ and control samples (Fig. 11: $dCirl^{KO}$*/CyO*: d.p.f. 2: 100 ± 24.58, n = 76, d.p.f. 7: 48.25 ± 4.83, n = 37, d.p.f. 11: 41.67 ± 2.88, n = 32, d.p.f. 16: 39.47 ± 0.76, n = 30; $dCirl^{KO}$*/Df*: d.p.f. 2: 100 ± 13.41, n = 108, d.p.f. 7: 53.56 ± 3.65, n = 58, d.p.f. 11: 47.37 ± 3.75, n = 51, d.p.f. 16: 46.13 ± 3.14, n = 50; *+/CyO*: d.p.f. 2: 100 ± 15.70, n = 102, d.p.f. 7: 47.39 ± 3.12, n = 48, d.p.f. 11: 42.81 ± 2.91, n = 44, d.p.f. 16: 39.22 ± 3.96, n = 40). Thus, these data suggest that *dCirl* does not influence the survival rate and is therefore unlikely to evoke severe developmental defects in *Drosophila*.

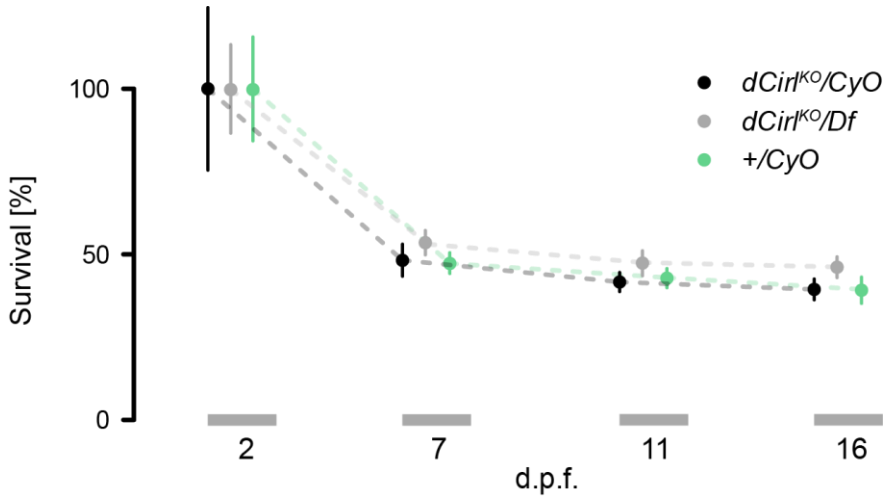

Fig. 11 Survival rate of $dCirl^{KO}$ animals.

$dCirl^{KO}$*/CyO*, $dCirl^{KO}$*/Df* and *+/CyO* animals were counted over a time period of 16 days past fertilization (d.p.f.). No significant difference was observed in the survival rate (indicated in percentage) between sampled genotypes.

4.1.3 Genomic engineering of *dCirl* fusion proteins

Next, we were interested in the localisation of *dCirl* in the fruit fly. Unfortunately, the polyclonal dCIRL antiserum used in western blot analysis did not reveal a specific staining on third-instar larvae in standard immunohistochemistry experiments.

To circumvent this drawback two different tagged genomic *dCirl* fusion proteins, *dCirl*^{Flag} and *dCirl*^{RFP} were created (Fig. 12A, C). The *attB*-flanked genomic *dCirl* wild-type locus, corresponding to that removed by genomic targeting, was fused in-frame with a *Flag* tag in the 3rd intracellular loop of the 7TM domain and with a monomeric *RFP* in the intracellular domain, respectively. The in-frame fused transgenes were integrated via phiC31-mediated recombination into the *dCirl* knock-out line, containing an *attP*-site as indicated in Fig. 9. *Cre* recombinase was applied to remove the *white*$^{+}$ -marker (Huang et al., 2009). The same strategy was applied for generating a genomic rescue strain (*dCirl*^{Rescue}) containing solely the *dCirl* wild-type locus without any tag. Notably this resulted in reconstitution of the *dCirl* locus at single copy rate in order to examine *dCirl* fusion proteins under endogenous genetic control accompanying all *cis*-regulatory elements.

Western blot analysis of protein extracts from *dCirl*^{Flag} and *dCirl*^{RFP} animals confirmed the presence of dCIRL tagged fusion proteins at expected sizes (Fig. 12B, D). Protein extracts from *dCirl*^{Flag} animals showed full-length dCIRL::FLAG fusion protein (open arrowhead), and samples of *dCirl*^{RFP} animals displayed full-length (open arrowhead) as well as cleaved (filled arrowhead) fusion protein. This indicates that autoproteolysis was not disturbed by chromophore insertion. An unspecific band (open circle) detected by the anti-FLAG and anti-RFP antibody, respectively was used as a loading control.

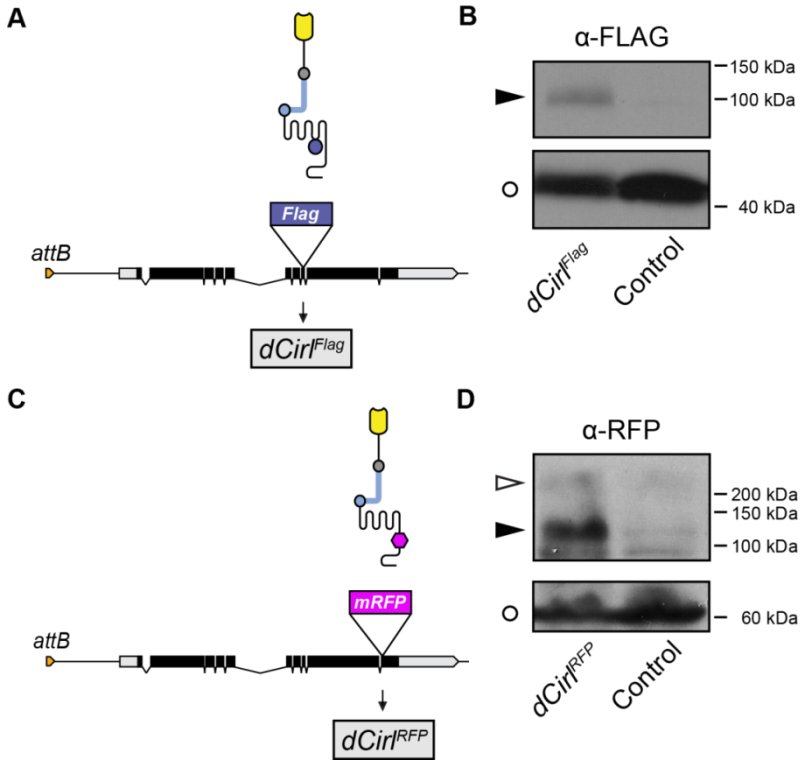

Fig. 12 Genomic engineering strategy of *dCirl* fusion proteins and validation via western blot analysis.

Schematic depiction of *dCirl*^{Flag} (A) and *dCirl*^{RFP} (C) fusion construct, showing a *Flag* tag insertion located in the third loop of the 7TM structure and a *mRFP* chromophore insertion near the C-terminal end of dCIRL, respectively. Western blot analysis using an anti-FLAG and anti-RFP antibody show the presence of dCIRL full-length (open arrowhead) and cleaved (filled arrowhead) fusion protein at expected size (B, D). An unspecific band detected by the antibody served as a loading control (open circle).

4.1.4 dCIRL is expressed in the larval and adult nervous system

Using confocal microscopy we were unable to detect any fluorescent signal of the chromophore fusion dCIRL::RFP, suggesting low endogenous expression levels of dCIRL, similar to LAT-1 in *C.elegans* (Langenhan et al., 2009). However, immunohistochemistry analysis using an antibody directed against the FLAG tag or the monomeric RFP revealed the subcellular localisation of dCIRL::FLAG and dCIRL::RFP, respectively.

Immunofluorescence analysis of *dCirl*^{Flag} larvae revealed that dCIRL is widely expressed in the third instar larval ventral nerve cord (VNC) (Fig. 13A). Higher magnification revealed co-localisation between dCIRL::FLAG and the neuronal membrane marker HRP (Fig. 13B, arrow), which confirms the localisation of dCIRL to the cell membrane of expressing cells. In contrast, control *w*^{1118} larvae lacked the specific anti-FLAG signal (Fig. 13C).

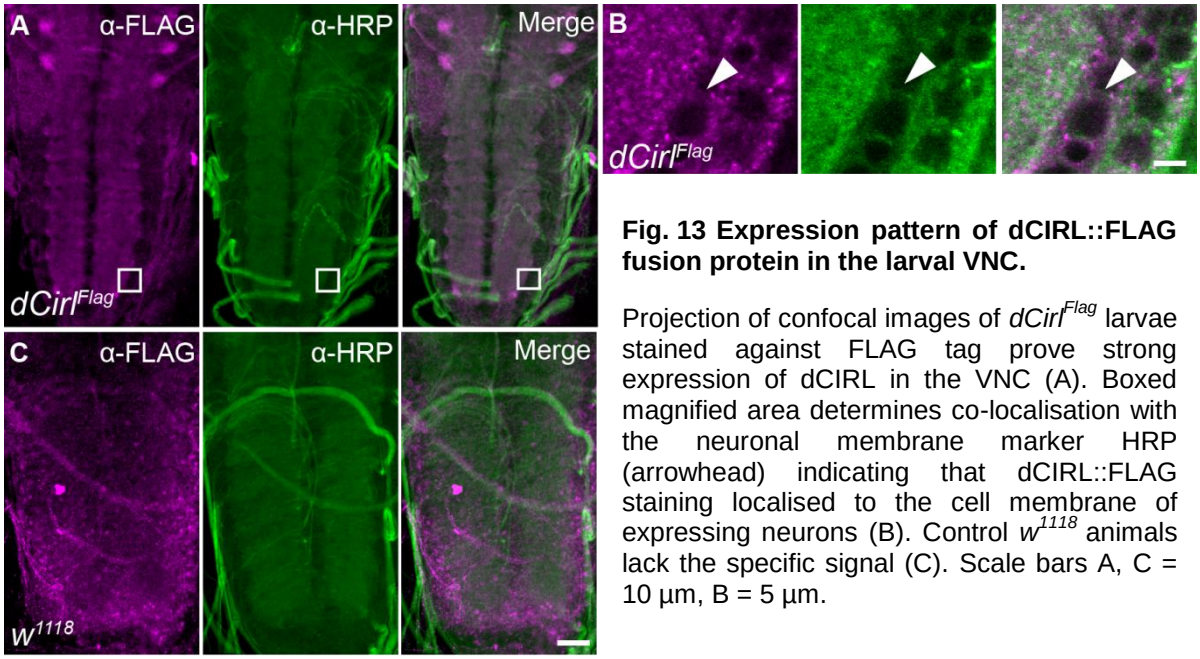

Fig. 13 Expression pattern of dCIRL::FLAG fusion protein in the larval VNC.

Projection of confocal images of *dCirl*^{Flag} larvae stained against FLAG tag prove strong expression of dCIRL in the VNC (A). Boxed magnified area determines co-localisation with the neuronal membrane marker HRP (arrowhead) indicating that dCIRL::FLAG staining localised to the cell membrane of expressing neurons (B). Control *w*^{1118} animals lack the specific signal (C). Scale bars A, C = 10 µm, B = 5 µm.

Anti-RFP immunostainings of *dCirl*^{RFP} larvae also showed strong dCIRL expression in the ventral ganglion, with extent and localisation of dCIRL comparable to *dCirl*^{Flag} animals (Fig. 14A). Co-labeling with the active zone marker BRP (Wagh et al., 2006) exhibited co-localisation between dCIRL and BRP (Fig. 14A), indicating that dCIRL is enriched in the synapse-rich neuropil of the larval CNS. Control *w*^{1118} larvae, devoid of RFP signal, approved the specificity of the anti-RFP staining in *dCirl*^{RFP} animals (Fig. 14B). These results revealed robust expression of dCIRL in the larval nervous system of *Drosophila*.

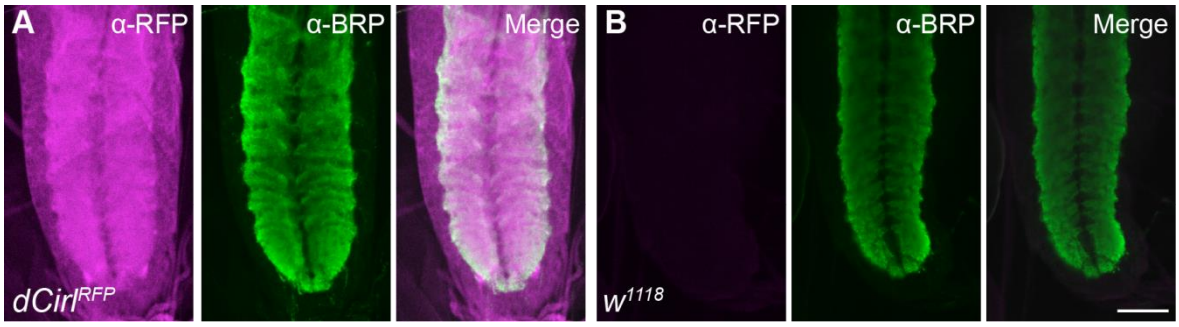

Fig. 14 Expression pattern of dCIRL::RFP fusion protein in the larval VNC.

Immunostainings detecting the RFP-epitope in *dCirl*^{RFP} larvae demonstrate expression of dCIRL in the VNC as indicated by co-localisation with the neuropil marker BRP (A). Control animals lack the RFP signal (B). Scale bar = 50 µm.

Beyond localisation of dCIRL in the larval CNS, studies performed by N. Hartmann exhibited dCIRL::RFP expression also in the adult brain of *Drosophila* (Fig. 15), which was equally observed for *dCirl*^{Flag} animals (data not shown). Whole-mount projections revealed strong labeling of the medulla of the optic system (arrow) and

the lobe of the mushroom body (arrowhead). The latter structure is important for olfactory learning and memory in *Drosophila* (Heisenberg, 1998). Conversely, co-labeling with BRP uncovered no co-localisation with dCIRL::RFP in the adult CNS like in the larval situation. Taken together, these data confirmed that dCIRL is widely expressed in the larval as well as the adult nervous system of the fruit fly.

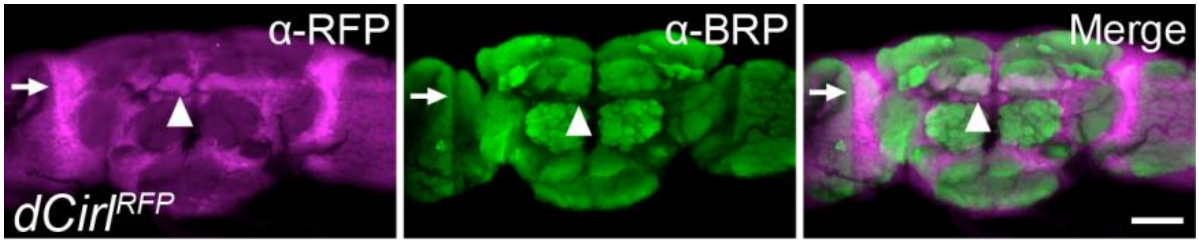

Fig. 15 Expression pattern of dCIRL in the adult CNS.

In the adult brain of *dCirl*^{RFP} animals dCIRL is expressed in distinct neuropil regions indicated by co-localisation with BRP. Prominent expression areas are the lobe of the mushroom body (arrowhead) as well as the optic lobes (arrow). Scale bar = 50 µm.

4.1.5 Diminished wandering behaviour of *dCirl*^{KO} larvae

Next, larval wandering behaviour was exmanied because observing *dCirl*^{KO} larvae it seemed they had difficulties in starting linear locomotion. Foraging larvae have bouts of linear crawling but also show periods of pausing, the so-called decision-making component of locomotion (Wang et al., 1997). However, *dCirl*^{KO} larvae exhibited more frequent turns while crawling as well as increased head swinging than control animals (Fig. 16A). This observation was tested by analysing the total crawling distance of mutant animals for two minutes (see 3.5.2, experiment performed by N. Hartmann). In addition to purely testing *dCirl*^{KO} larvae, all sampled genotypes were crossed over a deficiency (*Df(2R)Exel8047*). Loss of dCIRL seems to influence locomotion behaviour as mutant larvae covered a minor overall distance compared to control larvae (Fig. 16B; w^{1118}/*Df*: 2158 ± 88.12, n = 11; *dCirl*^{KO}/*Df*: 1346 ± 183, n = 14; *dCirl*^{KO}: 1629 ± 80, n = 35). Control larvae exhibited more regular and persistent linear locomotion, with fewer and shorter intervals of decision-making and turning. The reduction in crawling distance can be rescued by knock-in of the genomic *dCirl* wild-type locus (Fig. 16B; *dCirl*^{Rescue}/*Df*: 2220 ± 205, n = 11) and *dCirl*^{Flag} (Fig. 16B; *dCirl*^{Flag} /*Df*: 1836 ± 183, n = 12) in the mutant background which suggests that diminished crawling behaviour results directly from loss of dCIRL. In contrast *dCirl*^{RFP} larvae failed to rescue the diminished crawling behaviour (Fig. 16B; *dCirl*^{RFP} /*Df*: 1514

± 285, n = 11), indicating that intracellular RFP insertion interferes the function of dCIRL.

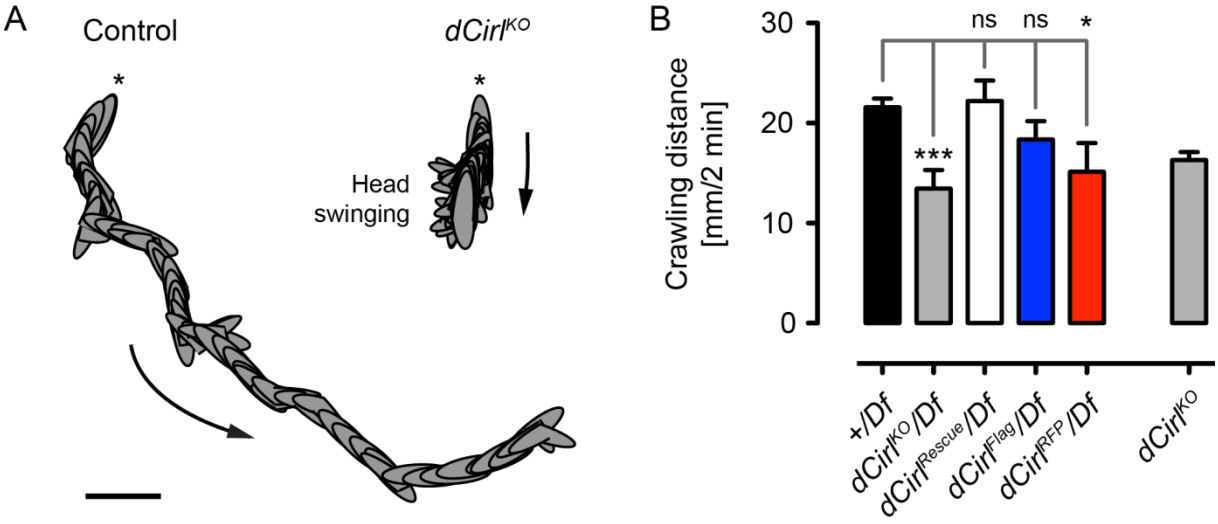

Fig. 16 Diminished wandering behaviour of *dCirl*^{KO} larvae.

Illustration depicting reduced linear locomotion and increased head swing of *dCirl*^{KO} larvae compared to control. Stars indicate starting point and arrow designate crawling direction (A). Shown is the crawling distance in mm/2min with standard deviation bars. In addition to testing *dCirl*^{KO} larvae, all genotypes were crossed over a deficiency (*Df*). Significant differences in mean touch sensitivity indicated by * between *dCirl*^{KO}/Df (p = 0.0003), *dCirl*^{RFP} */Df* (p = 0.0432) and *dCirl*^{KO} (p = 0.0006) compared to *w*^{1118}/Df, respectively. Significant differences were analysed by using an unpaired t-test (B).

4.1.6 Expression pattern of *dCirl*-promoter-driven GFP

Reliable and specific immunostainings at the NMJ of *dCirl*^{Flag} and *dCirl*^{RFP} larvae could not been obtained using an antibody directed against the FLAG tag or the monomeric RFP, respectively. Presumably, this is due to low protein concentration of dCIRL in synaptic terminals in comparison to its expression in the VNC. Therefore, the *dCirl* promoter was fused to cDNA encoding the yeast transcription factor *GAL4* and this *dCirlp*^{GAL4} transgene was utilised to drive the expression of a myristoylated GFP (myr::GFP). Immunostainings against GFP revealed expression of *dCirl*-promoter-driven *myr::GFP* in axons and terminals on several muscles (Fig. 17). *dCirl* gene expression seems to be enriched in synaptic boutons, but is also strongly expressed throughout the axons of peripheral nerves (Fig. 17).

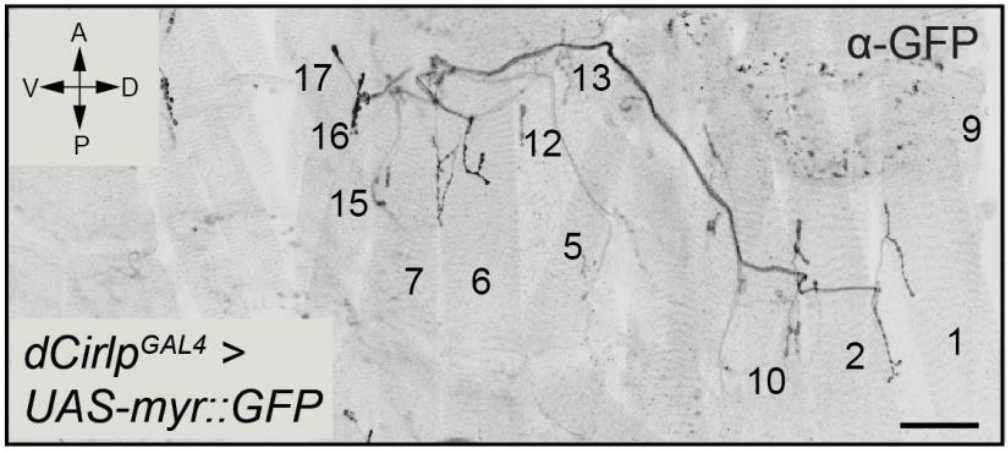

Fig. 17 Larval expression pattern of *dCirl*-promoter-driven *myr::GFP*.

Confocal image of the abdominal hemisegment A3 of a *dCirl*-promoter-driven *myr::GFP* larva stained against GFP shows labelling in axons and terminals on numerous muscles indicated by number. Scale bar = 10 µm.

Moreover, Fig. 18 shows a confocal micrograph of transgenic larvae expressing the combined *dCirl* promoter stained against GFP. Anti-GFP stainings revealed strong transcriptional expression of *dCirl* in the larval CNS (Fig. 18A). Co-staining with anti-MIP (myoinhibitory peptide) antibody, which shows immunoreactivity restricted to peptidergic terminals (Santos et al., 2007; Vomel and Wegener, 2008) revealed co-localisation with *dCirl* at the transcriptional level. We found *dCirl*-promoter-driven *mCD8::GFP* expression in axonal boutons on muscle 12 (Fig. 18B). NMJs on muscle 12 are characterised by four types of innervating axons: type Ib and Is axons, which are purely glutamatergic, type II axons, containing both neuropeptides and glutamate, and type III axons, that contain an insulin-like peptide (Gorczyca et al., 1993; Hoang and Chiba, 2001). Additionally, *dCirl* promoter-driven *myr::GFP* labelling was present in motoneuron endings on muscle pair 6/7, indicated by co-immunostainings with HRP (Fig. 18C). Muscle pair 6/7 is supplied by two motoneurons forming Ib and Is glutamatergic boutons (Hoang and Chiba, 2001). These data provide strong evidence that *dCirl* gene activity occurs in glutamatergic as well as in peptidergic neurons.

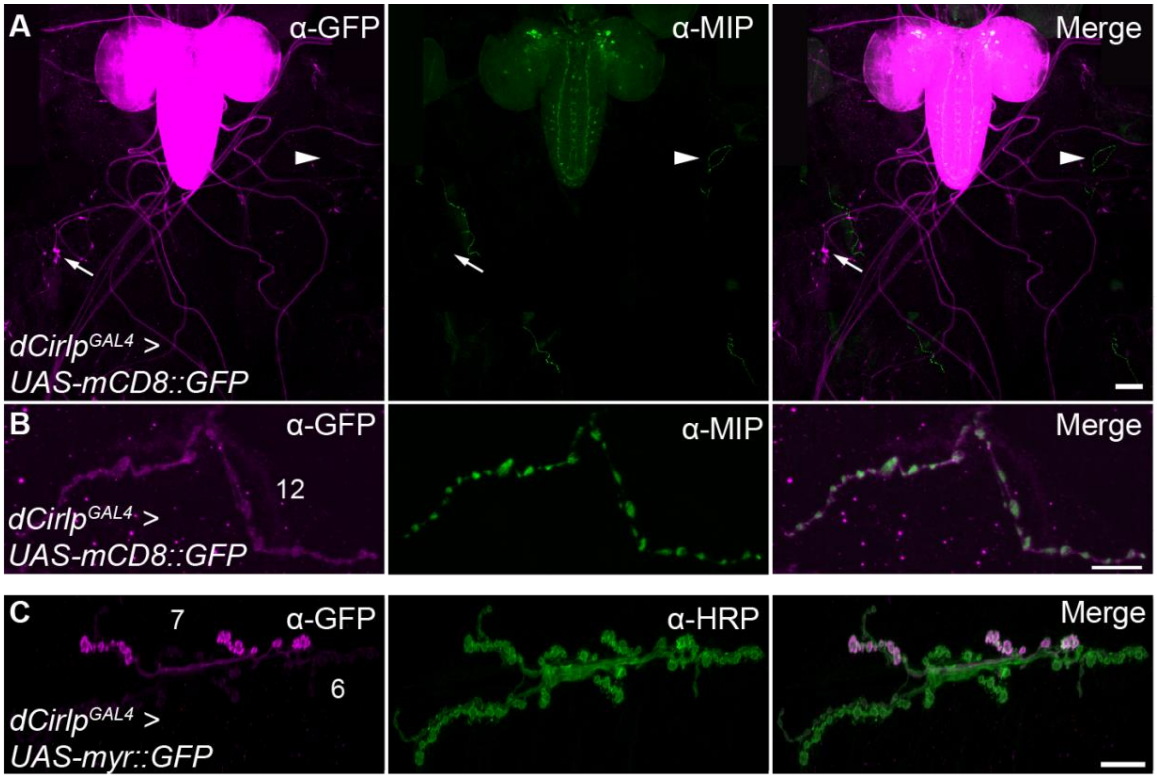

Fig. 18 Expression pattern of *dCirl*-promoter-driven GFP.

Double immunostainings of *dCirl*-promoter-driven m*CD8::GFP* larvae show expression in the VNC and descending motoneurons (A). Arrow indicates sensory organs, arrowhead displays peptidergic neurons (A). Magnification reveals co-labelling with MIP in synaptic boutons at the NMJ of muscle 12 (B). *dCirl* promoter-driven *myr::GFP* displays expression in motoneuron endings on muscle pair 6/7 as indicated by co-labelling with HRP (C). Scale bars A = 5 µm; B, C = 10 µm.

4.1.7 Loss of dCIRL does not affect synaptic transmission of glutamatergic motoneurons

Based on the transcriptional expression pattern of *dCirl* in motoneurons (Fig. 17) as well as the reduction of linear locomotion observed in $dCirl^{KO}$ animals (Fig. 16), we examined the morphology of the NMJ of muscle pair 6/7 in $dCirl^{KO}$ and control larvae. Therefore, we performed morphometric analysis of the NMJ using antibodies against the active zone marker BRP, the postsynaptic glutamate receptor IID (GluRIID) and HRP, the neuronal membrane marker.

Analysis of co-immunostainings of BRP and GluRIID revealed unaltered size (Fig. 19C; Control: 0.05 ± 0.02 µm^2, n = 12; $dCirl^{KO}$: 0.57 ± 0.04 µm^2, n = 10; p = 0.145) and number (Fig. 19C; Control: 544 ± 51, n = 12; $dCirl^{KO}$: 515 ± 67, n = 10; p = 0.735) of presynaptic active zones in $dCirl^{KO}$ animals. Similarly, the GluRIID size (Fig. 19D; Control: 0.81 ± 0.06 µm^2, n = 12; $dCirl^{KO}$: 0.74 ± 0.06 µm^2, n = 10; p = 0.445) and number (Fig. 19D; Control: 441 ± 64, n = 12; $dCirl^{KO}$: 346 ± 47, n = 10; p =

0.261) is unchanged. Stainings against HRP (data not shown) indicated consistent NMJ size between control and *dCirl*^{KO} larvae (Fig. 19E; Control: 624 ± 30, n = 21; *dCirl*^{KO}: 704 ± 43, n = 18; p = 0.128). Thus, we conclude that basal synaptic structure is largely unaffected by loss of *dCirl*.

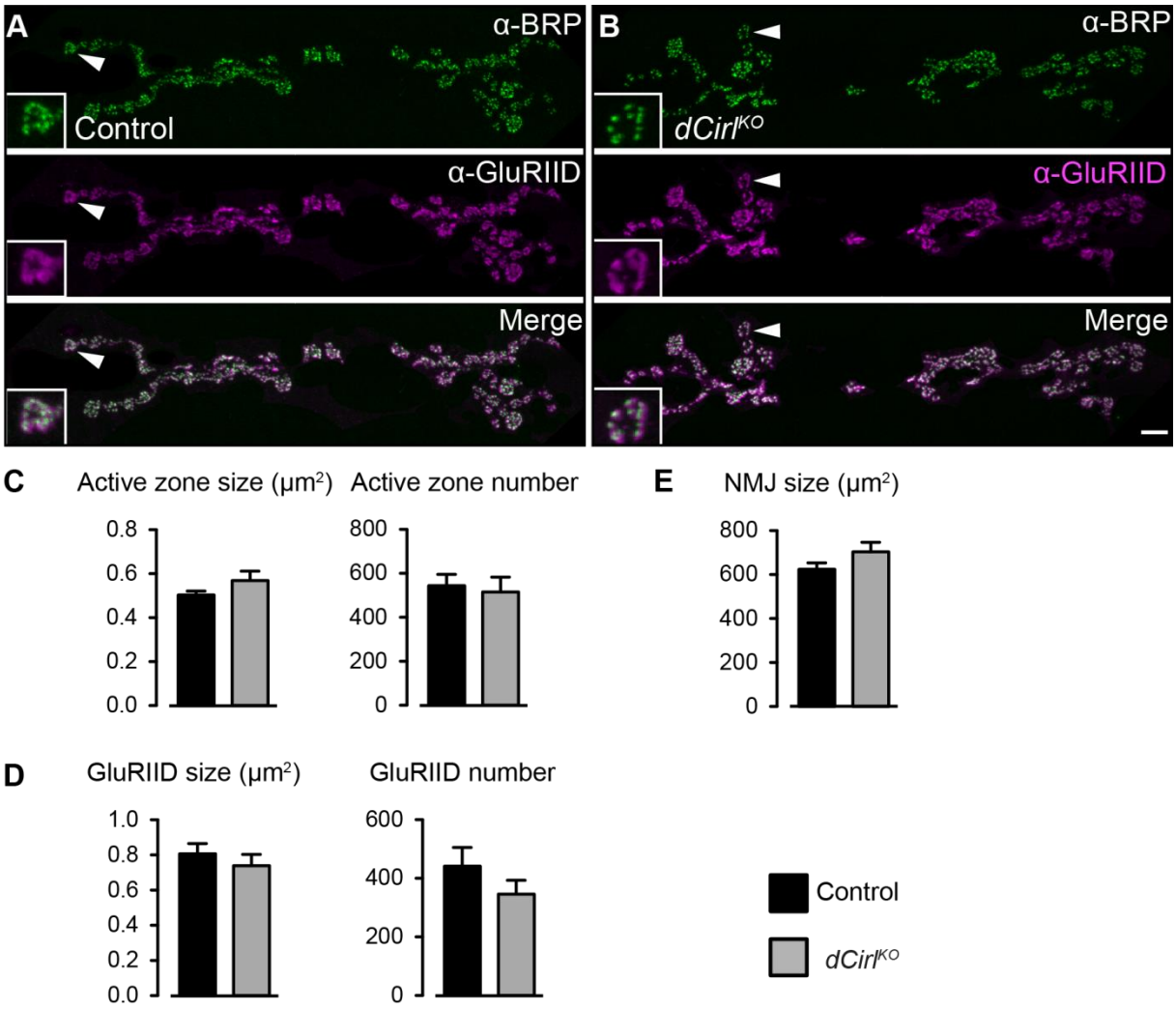

Fig. 19 Unaltered basal NMJ structure of muscle 6/7 boutons in *dCirl*^{KO} animals.

Projection of confocal images of muscle 6/7 NMJs of control (A) and *dCirl*^{KO} larvae (B) stained for presynaptic neuropil marker BRP (green) and postsynaptic receptor subunit GluRIID (magenta). Arrows indicate magnifications of boxed single boutons. Presynaptic active zone parameters (C) as well as size and number of postsynaptic GluRIID receptors (D) and NMJ area (E) are indistinguishable between sampled genotypes. Scale bar = 10 µm.

These results, together with unaltered electrophysiology of muscle pair 6/7 NMJs of *dCirl*^{KO} larvae (work done by D. Ljaschenko, see supplementary Fig S. 1) argue that we can exclude the possibility of basal structural alterations or defects in synaptic transmission resulting in altered locomotion behaviour of animals lacking dCIRL.

4.1.8 Loss of dCIRL increases content of the scaffold protein Discs-large

Next, we examined other synaptic proteins, known to regulate the structure of the NMJ, e.g. Spectrin, Fasciclin, Futsch and Discs-large (DLG) in terms of morphological differences in *dCirl*^{KO} larvae. No differences were found between sampled genotypes except for DLG that seemed highly enriched at the NMJ of muscle 6/7 in some animals lacking dCIRL (Fig. 20A, B; staining by N. Hartmann). DLG is a scaffold protein, located pre- and postsynaptically at the NMJ and supposed to play a central role in structural organisation and downstream signaling of cell adhesion molecules (Thomas et al., 1997). The increase in DLG content present in some mutants missing dCIRL was validated by using Western blot analysis together with densitometric measurements to quantify the intensity of DLG bands and found a significant, almost double rise in DLG intensity in *dCirl*^{KO} mutants compared to controls (Fig. 20C). Thus, we conclude that by loss of dCIRL DLG is upregulated in various animals.

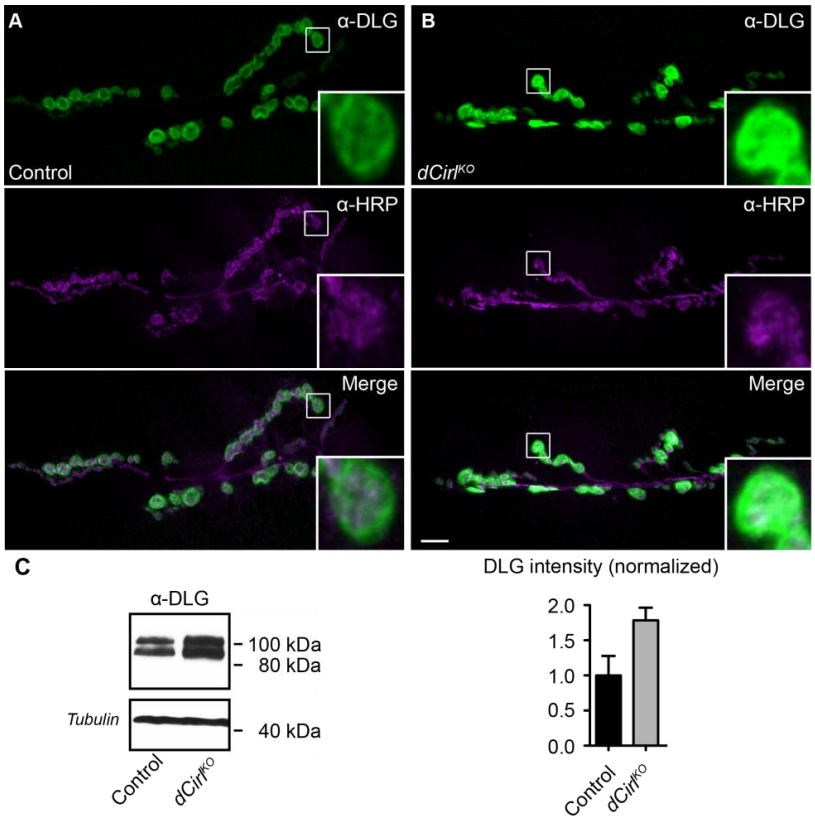

Fig. 20 Increase of synaptic scaffold protein DLG by loss of dCIRL.

Projection of confocal images of muscle 6/7 NMJs of control (A) and *dCirl*^{KO} larvae (B) stained for DLG (green) and HRP (magenta). Insets illustrate magnifications of boxed single boutons highlighting the increase of DLG in *dCirl*^{KO} mutants. Scale bar = 10 µm. Western blot analysis of larval protein extracts depicting the increase in DLG content in larvae lacking *dCirl* (C, left panel). Pooled dataset of densitometric measurements of DLG bands on Western blots from four experiments (five larvae each) indicate the augmentation of DLG content in *dCirl*^{KO} animals.

To analyse the upregulation of DLG and the subcellular structure in larvae missing dCIRL in more detail electron microscopy was utilised (work done by N. Wagner, see supplementary Fig S. 2). These data suggest that enrichment of DLG found in type I boutons of *dCirl*^{KO} larvae is related to severe extension of the subsynaptic reticulum (SSR), a membrane-layered structure surrounding the boutons. Presumably, the enlargement of the SSR could be either a side effect of frequent turns instead of directional locomotion observed in larvae lacking dCIRL (Fig. 16) or some kind of compensation mechanism underlying this behaviour.

4.1.9 Transcriptional expression of *dCirl* in the peripheral nervous system

Taken together, these results suggest that basal synaptic function at the NMJ, the site of motoneuronal muscle innervation, in larvae lacking dCIRL appears largely unaffected. This indicates that either sensory input or central integration of motor behaviour relies on the function of dCIRL. Hence, we analysed the peripheral nervous system (PNS). Within the PNS, sensory neurons transmit impulses from sensory receptors to the CNS.

Strong *dCirl* promoter-driven expression of *mCD8::GFP* was observed in larval and adult peripheral sensory neurons, most prominently in chordotonal organs (chos) of *Drosophila* (Fig. 21). Chos are found in a variety of structures in different species, e.g. thorax, abdomen, legs, wings and antenna, where they adapted to function as auditory organs and thus enable hearing for each organism (Eberl, 1999; Jarman, 2002). There are two major designs of auditory organs: tympanal organs, e.g. in the leg, function as sound pressure detectors and used for “far-field” sound, whereas flagellar organs are particle velocity detectors, useful near the sound source. The latter is found in the Johnston´s organ located in the antenna and used for discriminating species-specific courtship songs at close range (Eberl, 1999). Immunostainings against GFP confirmed the presence of *dCirl*-promoter-driven m*CD8::GFP* in the Johnston´s organ in the antenna as well as in the leg of adult flies (Fig. 21).

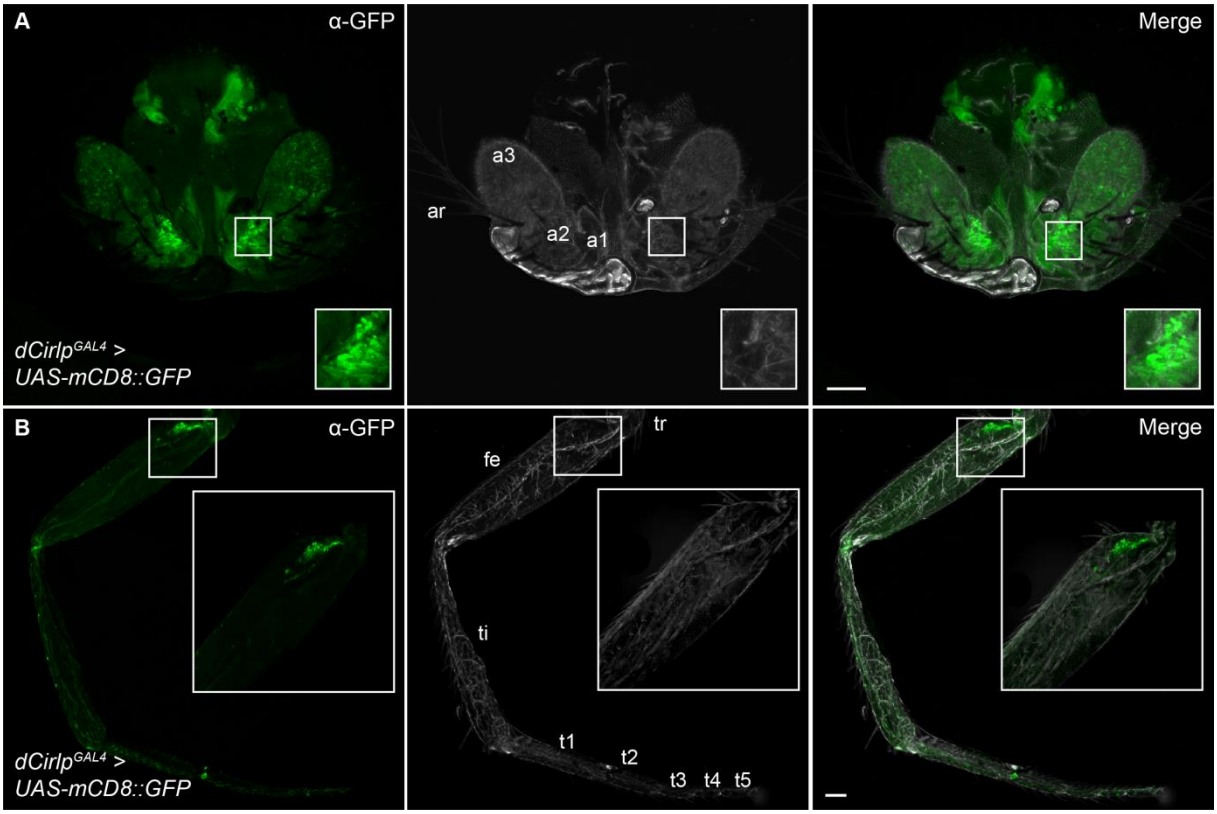

Fig. 21 Transcriptional *dCirl* expression in adult chordotonal organs.

Anti-GFP staining and transmitted light image of *dCirlp*^{GAL4} driven *UAS-mCD8::GFP* adult *Drosophila* antennae (A). In response to sound the arista (ar) vibrates, putting torque on the third antennal segment (a3), which then rotates. The Johnston´s organ, located inside the second antennal segment (a2) processes and transmits auditory information via the antennal nerve through the first antennal segment (a1) to the brain. Anti-GFP staining and transmitted light image of *dCirlp*^{GAL4} *driven UAS-mCD8::GFP* adult *Drosophila* leg (B). Indicated are trochanter (tr), femur (fe), tibia (ti) and first to fifth tarsal segments (t1-t5). Scale bars A, B = 10 µm.

In *Drosophila* larvae chos function as mechanosensory neurons providing feedback to the locomotor central pattern generator networks in the CNS, important for rhythmic movements, such as peristaltic contraction in the larvae (Caldwell et al., 2003). Fig. 22A displays an overview of the third abdominal hemisegment of a *dCirlp*^{GAL4} *driven UAS-mCD8::GFP* larva stained against anti-GFP. Strong *dCirl* gene expression was observed in type II multidendritic (MD) neurons, in external sensory (es) neurons as well as in the lateral pentascolopidial cho (lch5) and likely the lateral monoscolopidial cho (lch1) of the larval abdominal body wall (Fig. 22A). Highlighted in Fig. 22B is the prominent *dCirl*-promoter-driven m*CD8::GFP* signal in the lateral cho composed of five scolopidia (lch5), with robust expression in the sensory neurons (sn). Interestingly, the molecular machinery responsible for mechanotransduction in chordotonal neurons has not yet been satisfactorily identified. Because of the reduced specificity of the dCIRL antibody in

immunostainings we were unable to confirm dCIRL expression in chos at the protein level following our observation at the transcriptional level of *dCirlp*^{GAL4}.

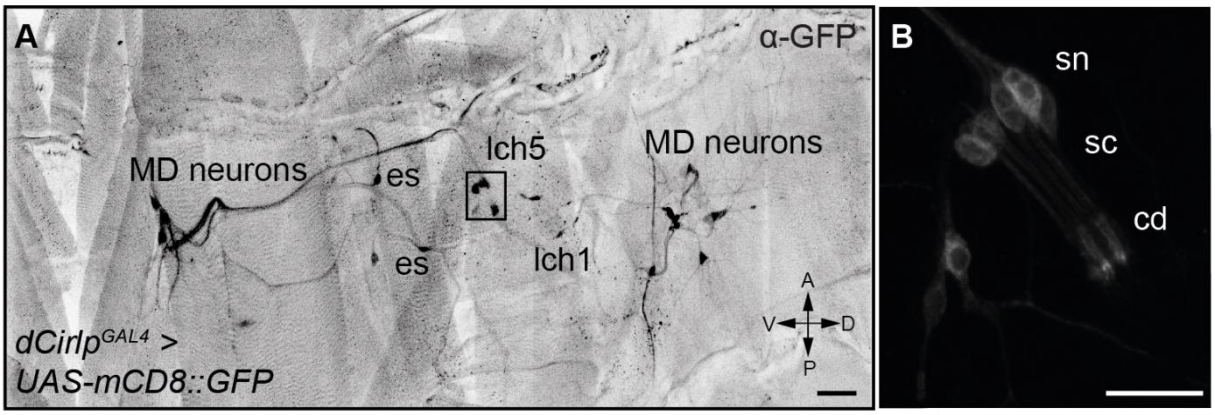

Fig. 22 Transcriptional *dCirl* expression in larval sensory neurons.

Anti-GFP staining of *dCirlp*^{GAL4} driven *UAS-mCD8::GFP* larval sensory neurons. Overview of the third abdominal hemisegment depicting *dCirl* gene expression in type II multidendritic (MD) neurons as well as in type I external sensory neurons (es) and the lateral chordotonal organ lch5 and lch1 (A). Highlighted is the lateral pentascolopidial chordotonal organ (lch5) (B). *dCirl* gene expression is exposed in each scolopidium consisting of a sensory neuron (sn), ciliary dilation (cd) and sensory-ciliae (sc). Scale bars A, B = 10 µm.

4.1.10 Loss of *dCirl* reduces gentle touch sensitivity

Having established that *dCirl* is expressed in chos at the transcriptional level we performed larval behavioural studies as Caldwell et al. (2003) demonstrated that gentle touch sensitivity of *Drosophila* larvae is mediated primarily by the chos. I tested for external gentle touch sensitivity using a method developed by Kernan et al. (1994). Therefore, the anterior end of the larvae was stimulated by a gentle touch using a thin von-Frey filament (0.3 mN) during free locomotion behaviour (see 3.5.3). This stimulus elicits response in any of the presumable peripheral nervous system (PNS) mechanosensory components including chos and external sense organs, allowing to determine to which extent touch sensitivity was affected in dCIRL mutants. All sampled genotypes were crossed over a deficiency (*Df(2R)Exel8047*), uncovering the *dCirl* locus, to exclude effects from second site hits on the *dCirl*^{KO} chromosome. Additionally, we also tested homozygous *dCirl*^{KO} larvae. *dCirl*^{KO}*/Df(2R)Exel8047* as well as *dCirl*^{KO} larvae showed diminished sensitivity to touch (Fig. 23; *dCirl*^{KO}*/Df*: 6.00 ± 0.46, n = 49; *dCirl*^{KO}: 7.22 ± 0.48; n = 18), compared to control *w*^{1118}*/Df* (Fig. 23; +/*Df*: 9.30 ± 0.46, n = 51). In addition, both rescue strains except for *dCirl*^{RFP} (Fig. 23; *dCirl*^{RFP} */Df*: 7.14 ± 0.59, n = 29) show a strong response

to touch (Fig. 23; *dCirl*^{Rescue} */Df*: 8.02 ± 0.46, n = 43; *dCirl*^{Flag} */Df*: 8.25 ± 0.53, n = 32). The reduction of touch sensitivity in mutant animals seems to directly result from loss of dCIRL as the touch insensitive phenotype can be rescued by back-insertion of the genomic *dCirl* wild-type locus in the mutant background in various layouts (*dCirl*^{Rescue} and *dCirl*^{Flag}). In contrast, the *dCirl*^{RFP} genomic transgene failed to rescue the diminished touch sensitivity, equally observed in locomotion studies (see 4.1.5).

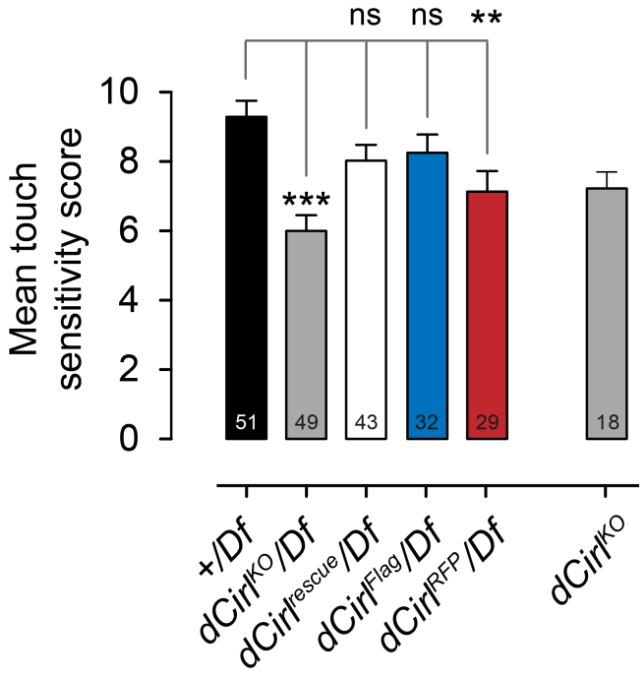

Fig. 23 Gentle touch sensitivity is reduced in *dCirl*^{KO} mutants.

Shown is the mean gentle touch sensitivity histogram with standard deviation bars. In addition to testing *dCirl*^{KO} larvae, all genotypes were crossed over a deficiency (*Df(2R)Exel8047*) covering the *dCirl* locus and six flanking genes. Significant differences in mean gentle touch sensitivity indicated by * between *dCirl*^{KO}/Df (p = 0.0001), *dCirl*^{RFP} */Df* (p = 0.0052) and *dCirl*^{KO} (p = 0.0001) compared to +/ Df, respectively. Date were analysed by using an unpaired t-test.

To differentiate between innocuous (< 10 mN) and noxious (> 30 mN) touch, I also tested for harsh touch sensation in larvae lacking dCIRL. Harsh touch was delivered by stimulating the anterior end of a freely moving larva using a needle instead of a von-Frey filament. As indicated in Fig. 24, *dCirl*^{KO} larvae retain harsh touch responses (Control: 14.92 ± 0.19, n = 12; *dCirl*^{KO}: 15.0 ± 0.20, n = 13; p = 0.78), comparable to control larvae. Therefore, in contrast to gentle touch sensitivity, harsh touch sensation seems largely unaffected in *dCirl*^{KO} mutant animals. However, a suitable positive control, e.g. *painless* mutant larvae that display increased thresholds to thermal and mechanical nociception (Tracey et al., 2003) was not tested in this experiment.

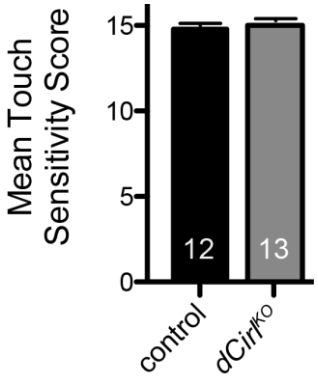

Fig. 24 Harsh touch sensation is unaffected in *dCirl*^{KO} mutants.

Shown is the mean harsh touch sensitivity histogram with standard deviation bars. There are no significant differences in the sensitivity to harsh touch stimuli in larvae lacking dCIRL compared to control animals.

4.1.11 Expression of *dCirl* in chos is required for normal response to gentle touch

We have shown that *dCirl* is expressed in sensory neurons at the transcriptional level and that loss of *dCirl* affects proper response to gentle touch stimuli. To reveal which types of neurons contribute to the touch insensitivity phenotype of mutant animals we used different GAL4 driver lines, expressing a *20xUAS-dCirl*^{Flag} transgene in the *dCirl*^{KO} mutant background in a distinct subset of cells. Following driver lines were used to unravel which neurons depend on the expression of *dCirl* in order to rescue the mutant phenotype:

Driver line	Expression						Reference
	ubiquitous	pan-neuronal	moto-neuronal	type II	type I		
					es	cho	
actin-GAL4	●	●	●	●	●	●	Burn et al. (1989)
elav-GAL4		●	●	●	●	●	Yao and White (1994)
ok6-GAL4			●				Sanyal (2009)
5-40-GAL4				●	●	●	Song et al. (2007)
21-7-GAL4				●		●	Song et al. (2007) and this work (Fig. 25)
iav-GAL4						●	Kwon et al. (2010)

Additionally, I checked the expression pattern of the sensory neuron driver lines *5-40-GAL4*, *21-7-GAL4* and *iav-GAL4* by driving the expression of a *UAS-mCD8::GFP* transgene (Fig. 25). Anti-GFP stainings revealed strong *5-40-GAL4* driven *UAS-mCD8::GFP* pan-sensory neuron expression (Fig. 25A), which was already shown by Song et al. (2007). However, *21-7-GAL4* driven *UAS-mCD8::GFP* expression seemed not only present in type II sensory neurons (Song et al., 2007), but also in chos (Fig. 25B). In accordance to Kwon et al. (2010) anti-GFP stainings displayed

iav-GAL4 driven *UAS-mCD8::GFP* expression solely in chos (Fig. 25C). Taken together, these results suggest that *5-40-GAL4* shows a pan-sensory neuron expression pattern whereas *21-7-GAL4* expression is restricted to type II sensory neurons and chos, thus absent in es neurons. Finally, *iav-GAL4* expression is limited to chos (Fig. 25).

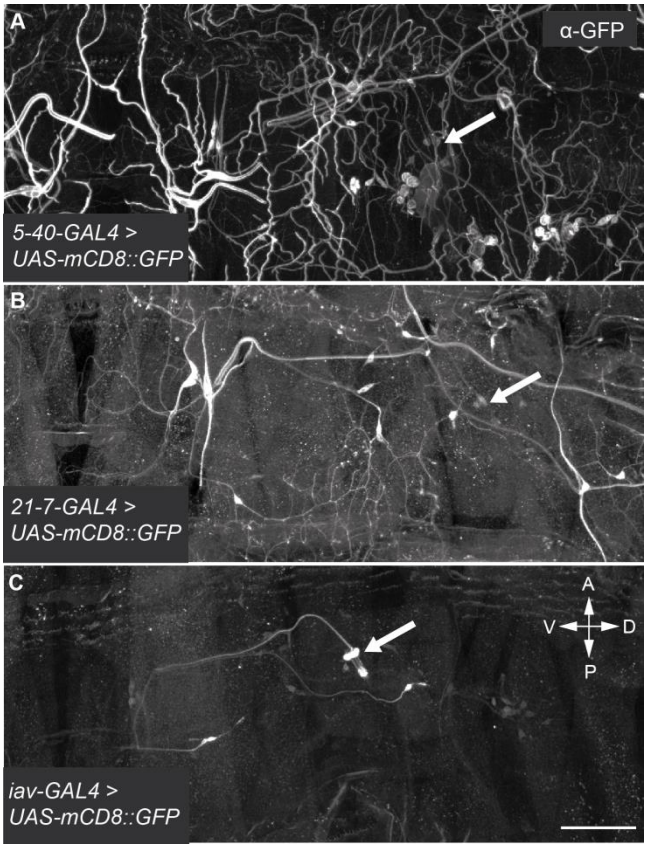

Fig. 25 Expression pattern of sensory neuron driver lines 5-40-GAL4, *21-7-GAL4* and *iav-GAL4.*

Overview of an abdominal hemisegment of *5-40-GAL4* (A), *21-7-GAL4* (B) and *iav-GAL4* (C) driven *UAS-mCD8::GFP* expression. Anti-GFP staining confirms pan-sensory neuron expression of *5-40-GAL4* (A), expression of *21-7-GAL4* in type II sensory neurons and chos (B) and strong *iav-GAL4* expression solely in chos (C). Arrows indicate the pentascolopidial organ (lch5). Scale bar = 100 µm.

Subsequently, I tested larvae containing an *actin-GAL4*, *elav-GAL4*, *ok6-GAL4*, *5-40-GAL4*, *21-7-GAL4* or *iav-GAL4* driver line driving the expression of a *20xUAS-dCirl*^{Flag} transgene in the *dCirl*^{KO} mutant background for gentle touch sensitivity (Fig. 26). Reduced touch sensation is rescued in animals expressing *actin-GAL4* (Control: 6.77 ± 0.86, n = 13; *actin-GAL4*: 12.24 ± 0.62, n = 17; p = 0.0001) and *iav-GAL4* (Control: 9.86 ± 0.46, n = 14; *iav-GAL4*: 11.78 ± 0.50, n = 18; p = 0.0195) driven *20xUAS-dCirl*^{Flag} in the mutant background. Interestingly, *actin*-GAL4 revealed a gain-of-function effect resulting in touch sensation scores highly above wild-type level. In addition, *elav-GAL4 driven 20xUAS-dCirl*^{Flag}, although not significant, tends to rescue the diminished touch sensation of *dCirl*^{KO} larvae (Control: 10.50 ± 0.93, n = 10; *elav-GAL4*: 11.57 ± 0.57, n = 7). In contrast, expression of the *20xUAS-dCirl*^{Flag} transgene driven by *5-40-GAL4* (Control: 9.60 ± 0.72, n = 10; *5-40-GAL4*: 8.80 ± 1.50, n = 10) and *21-7-GAL4* (Control: 12.18 ± 0.69, n = 11; *21-7-GAL4*: 10.54 ±

1.03, n = 13) in the *dCirl*^{KO} mutant background seemed insufficient to rescue the diminished sensitivity to gentle touch. Apparently, *5-40-GAL4* and *21-7-GAL4* driver lines exhibit lower expression levels in chos compared to *iav-GAL4* (Fig. 25). Thus, these results suggest that expression of the genomic *dCirl* wild-type locus in chos rescues the reduced touch sensation of *dCirl*^{KO} mutant animals.

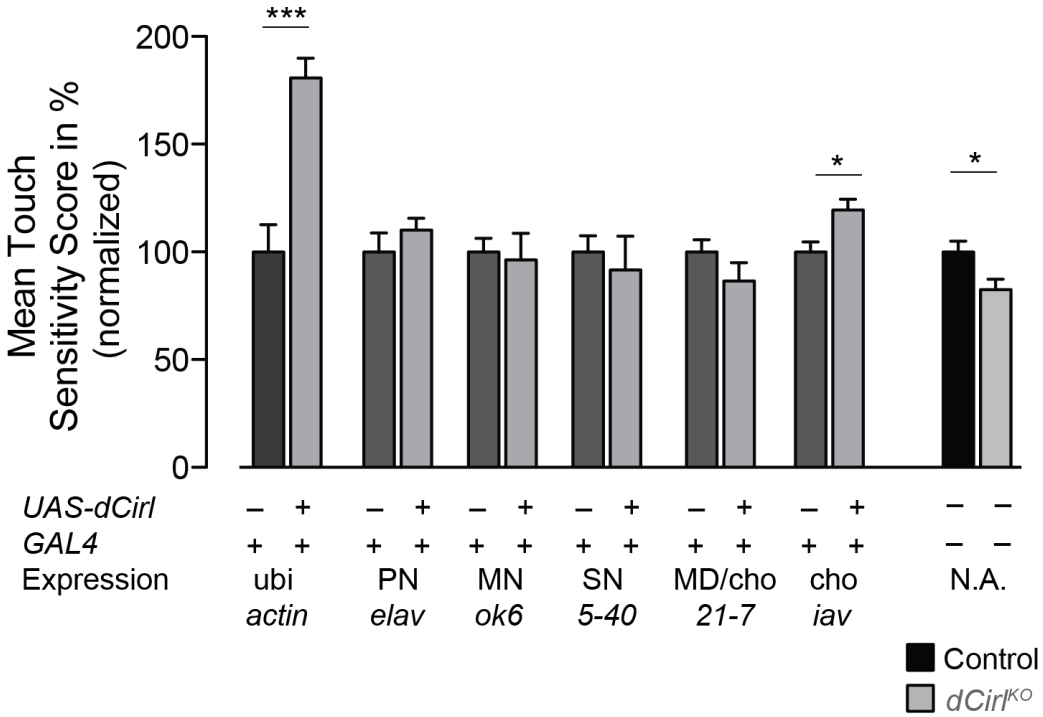

Fig. 26 Rescue of diminished gentle touch sensitivity of *dCirl*^{KO} mutants.

Shown is the difference of mean touch sensitivity in percentage of larvae containing an *actin-GAL4*, *elav-GAL4*, *ok6-GAL4*, *5-40-GAL4*, *21-7-GAL4* or *iav-GAL4*, driving the expression of a *20xUAS-dCirl*^{Flag} transgene in the *dCirl*^{KO} background compared to the *GAL4* control, respectively. Touch insensitivity is rescued in animals expressing *actin-GAL4* (p = 0.0001) and *iav-GAL4* (p = 0.0195) driven *20xUAS-dCirl*^{Flag} in the mutant background. Significant differences in mean gentle touch sensitivity between *dCirl*^{KO} and *w*^{1118} (p = 0.0110) are shown for comparison. Expression pattern of *GAL4* driver lines: ubiquitous (ubi), pan-neuronal (PN), motoneuronal (MN), sensory neurons (SN), multidendritic (MD) and chordotonal neurons (cho).

4.1.12 Cho morphology is largely unaffected in larvae lacking *dCirl*

Anti-GFP stainings of *dCirlp*^{GAL4} driven *UAS-mCD8::GFP Drosophila* sensory neurons revealed that chos are present and specified properly. Thus, defects in larvae lacking dCIRL may be either due to physiological defects that disrupt proper function or morphological defects in the differentiation of the chos. We performed ultrastructural analysis of the larval pentascolopidial organ using the cho-specific driver line *iav-GAL4* (Kwon et al., 2010) driving the expression of a *20xUAS-IVS-CD8::GFP* transgene in the *dCirl*^{KO} mutant background, to analyse lch5 morphology

(Fig. 27). Anti-GFP immunostainings revealed no significant differences regarding missing scolopidia, disruptions of outer dendritic segment (ODS) morphology, lack of ciliary dilation (cd) and relative orientation of the whole lch5 in mutant animals. *dCirl*^{KO} larvae showed a slightly but not significant increase in the number of missing scolopidia within the lch5 cluster (Control: 0.13 ± 0.09, n = 16; *dCirl*^{KO}: 0.19 ± 0.1, n = 16). However, there are less disturbances of the ODS (Control: 0.81 ± 0.21, n = 16; *dCirl*^{KO}: 0.69 ± 0.24, n = 16) as well as fewer cd missing (Control: 0.81 ± 0.19, n = 16; *dCirl*^{KO}: 0.69 ± 0.2, n = 16) in the mutant situation compared to control. Presumptively, this results from disturbances e.g. shear forces during the preparation or staining process of larval filets that might lead to rearrangement of parts of the lch5. In contrast, there are no differences in the change of orientation of the whole pentascolopidial organ (Control: 0.13 ± 0.09, n = 16; *dCirl*^{KO}: 0.13 ± 0.09, n = 16). Thus, *dCirl*^{KO} mutant larvae exhibit no obvious morphological defects of chos that could be detected by using ultrastructural analysis. These data lead to the assumption that instead of morphology, the physiological function of chos is impaired in larvae lacking dCIRL.

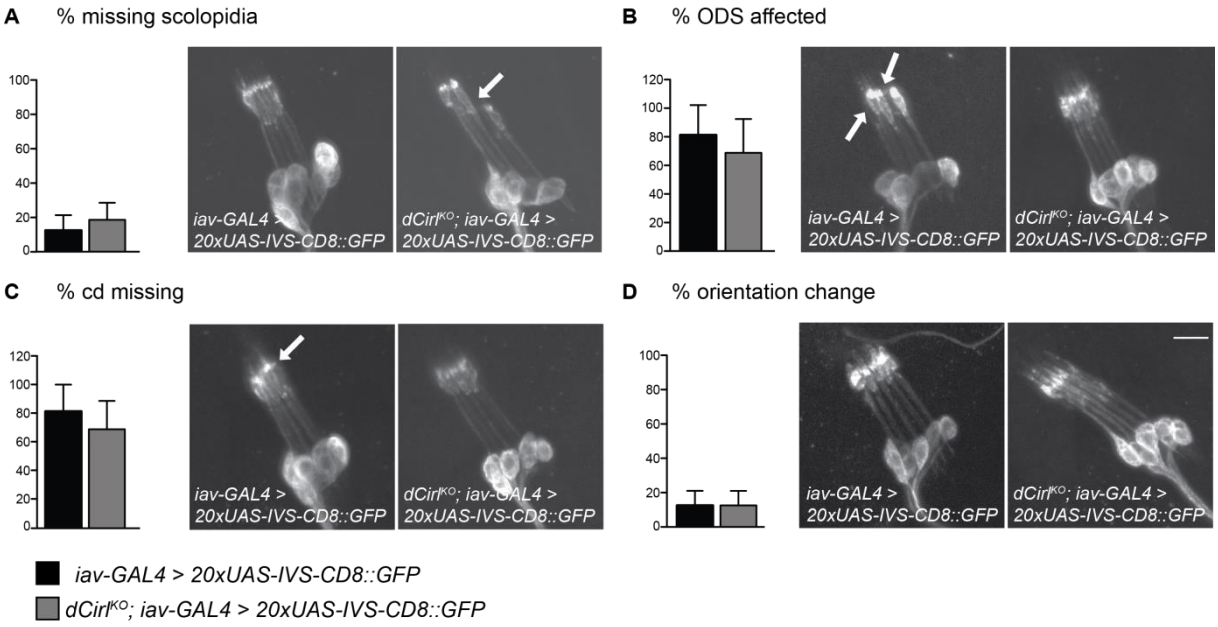

Fig. 27 Ultrastructural analysis of lch5 morphology in *dCirl*^{KO} mutant larvae.

Anti-GFP immunostainings of larvae expressing *iav-GAL4* driven *20xUAS-IVS-CD8::GFP* in the *dCirl*^{KO} mutant background were examined for morphological defects of the lch5 in the abdominal segment A2 and A3. Within the lch5 clusters, individual scolopidia were scored for presence, disruptions of the outer dendritic segment (ODS), and visibility of the ciliary dilation (cd). Whole pentascolopidial organs were scored for relative orientation of the five units. Examples of these effects are shown in confocal images. We observed no significant differences in larvae lacking *dCirl*. Scale bar = 10 µm.

Taken together, the present study confirmed that in *Drosophila dCirl*/Latrophilin is widely expressed in neurons of the larval central nervous system including moto- and sensory neurons. We found that genetic removal of *dCirl* results in locomotion defects while basal synaptic function at the NMJ seems unaffected. This indicates that either sensory input or central integration of motor behaviour relies on the function of dCIRL. While we showed that *dCirl* is expressed in sensory neurons at the transcriptional level, we could not follow our observation at the protein level. However, we established that loss of dCIRL results in diminished sensitivity to gentle touch. This phenotype can be rescued by back-insertion of the genomic *dCirl* wild-type locus in larval chordotonal organs demonstrating that *dCirl* is required for cho function. Having established that the pentascolopidial organ morphology of mutant larvae is unaltered, we assume that the physiological function of chos might be affected in $dCirl^{KO}$ larvae.

4.2 Characterisation of intracellular protein interactions using the split-GFP system

Another approach of thesis was to examine the interactions between several presynaptic proteins during vesicle exocytosis *in vivo* using the split-GFP (spGFP) method established by Hamilton, Regan, Kerppola, Gosh, Chalfie, Shen and Bargmann labs.

Initial experiments showed that full length reporter protein fusions with n-Synaptobrevin (n-Syb), Synaptotagmin (Syt) and Syntaxin (Syx) allow expression in *Drosophila* and confirmed that fusion to either end of each synaptic protein did not impair expression and moreover not influence the viability of transgenic flies. Further, transgenes containing protein fusions of Syx, Syt and n-Syb with spGFP fragments were established in previous studies using the Gateway-recombination cassette (Gehring, 2010). Once brought into an entry vector, this tool enables the recombination of an open reading frame (ORF) of interest into any destination vector via a simple but efficient recombinase reaction. These destination vectors are suited with different spGFP fragments (spGFP1-10 and spGFP11) at either the C-terminus or the N-terminus, thus creating protein fusions with cloned synaptic proteins (Gehring, 2010). Fig. 28 illustrates an overview of expression vectors with spGFP

chromophores created via Gateway cloning in order to analyse essential steps of transmitter release at the AZ in *Drosophila*.

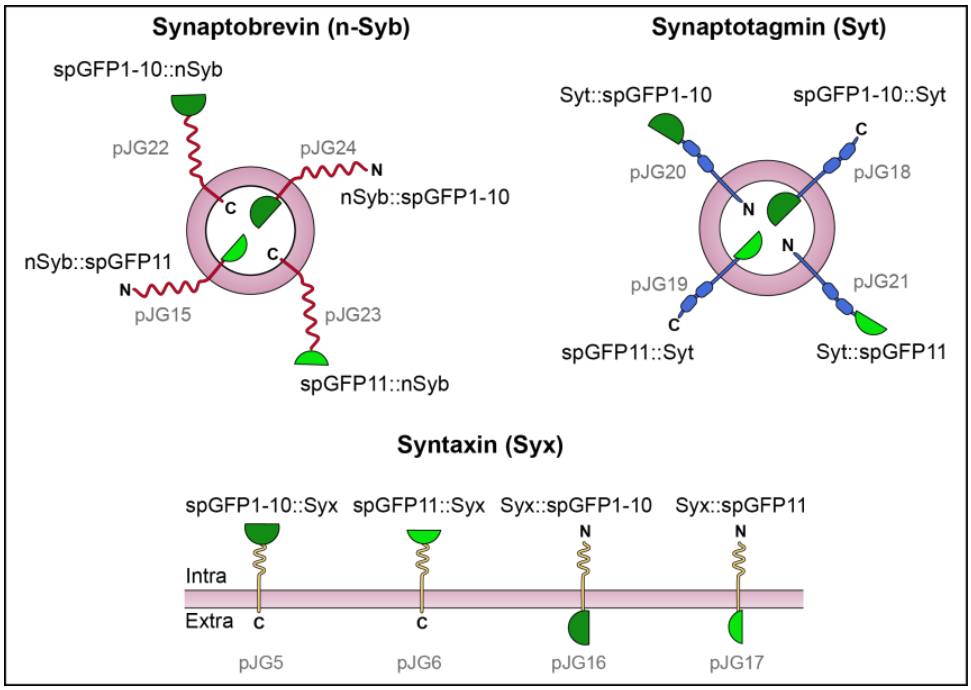

Fig. 28 Overview of split-GFP constructs for expression in *Drosophila*.

Schematic diagram depicting the expression vectors with spGFP chromophores for n-Syb (pJG15 and 22-24), Syt (pJG18-21) and Syx (pJG5-6 and 16-17). The spGFP1-10 chromophore is shown in dark green and the spGFP11 in bright green, for N- and C-terminal sites respectively. The different linkers between the chromophore and the synaptic protein are illustrated in red (n-Syb), blue (Syt) and yellow (Syx). The vesicle membrane (n-Syb and Syt) and the presynaptic membrane (Syx) are pink-coloured.

4.2.1 Expression pattern of spGFP docking and fusion sensors

The attempt described in this work takes advantage of the principle of coincidence detection upon direct protein-protein interactions when protein fusions with different spGFP components encounter each other. In order to characterise different stages of synaptic vesicle turnover at active zones, so called docking and fusion sensor pairs were established (Fig. 29). We hypothesised following protein pairs implicated in docking events based on putative protein interactions described earlier (reviewed for example by Rosenmund (2003) and Sudhof (2004)): N-terminal tagged Syx located in the presynaptic membrane interacts with C-terminal tagged vesicle protein Syt (Fig. 29A, left panel) and N-terminal tagged vesicle protein n-Syb, respectively (Fig. 29A, right panel). Vesicle fusion events on the other hand were analysed using C-terminal tagged Syx which interrelates with Syt, N-terminally tagged (Fig. 29B, left panel) and n-Syb, C-terminally tagged (Fig. 29B, right panel). Each of the synaptic

proteins was endowed with either the spGFP1-10 fragment or the spGFP11 fragment at either end, the very C-terminus or N-terminus.

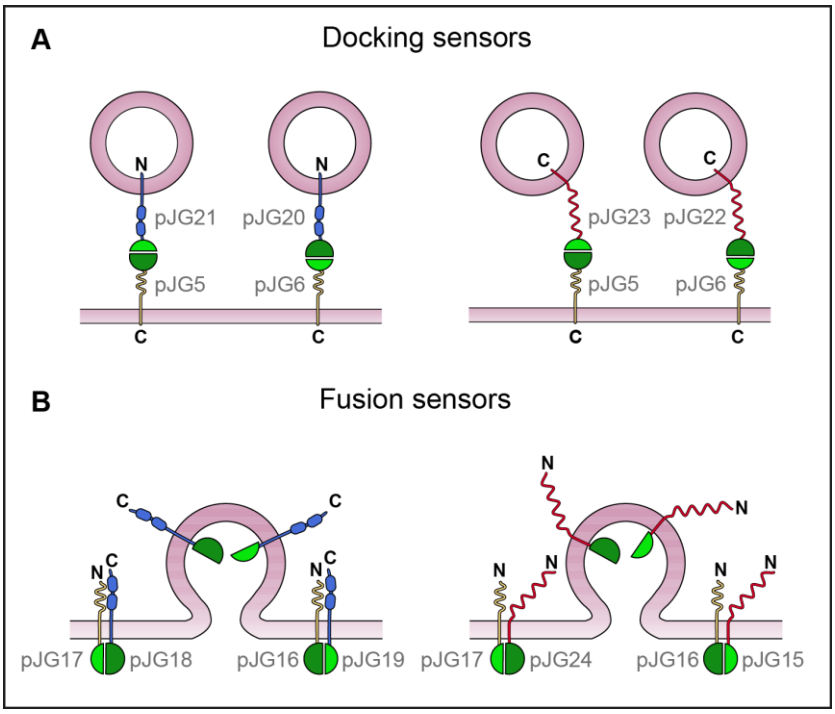

Fig. 29 Docking and fusion sensors for characterisation of synaptic vesicle turnover.

Schematic depiction illustrating docking and fusion sensors with docking sensor pairs Syt-Syx (A, left panel) and n-Syb-Syx (A, right panel) as well as fusion sensor pairs Syt-Syx (B, left panel) and n-Syb-Syx (B, right panel). Dark green illustrates the spGFP1-10, bright green the spGFP11 chromophore and the linkers between the spGFP and the synaptic protein are shown in red (n-Syb), blue (Syt) and yellow (Syx). Depicted in pink are the vesicle membrane (n-Syb and Syt) and the presynaptic membrane (Syx).

In addition to n-Syb, Syt and Syx, we also created expression vectors with spGFP chromophores for Bruchpilot Domain 3 (BRPD3). Several driver-lines were used to overexpress the spGFP tagged proteins in order to visualise their localisation in living animals and fixed samples. First, I utilised the motoneuron/neuron specific driver line *ok6-GAL4 (*Sanyal, 2009) to overexpress the spGFP tagged protein pairs at the NMJ. Fig. 30 shows a projection of confocal sections of larval NMJs indicating synaptic protein interactions between spGFP1-10::Syx + Syt::spGFP11, Syx::spGFP1-10 + spGFP11::Syt and BRPD3::spGFP1-10 + Syt::spGFP11. The upper row illustrates endogenous fluorescence in living larvae, the lower panel shows immunofluorescence analysis of fixed animals, using a monoclonal anti-GFP antibody that exclusively recognizes the fully folded and thus functional GFP chromophore. The endogenous fluorescence *in vivo* seems rather weak compared to the antibody stainings of fixed samples. Notably, visualisation of interactions between

synaptic proteins via reconstituted GFP in immunostainings required methanol fixation. We did not accomplish any reconstituted GFP signal by using standard paraformaldehyde (PFA) fixation procedures. Interaction between spGFP1-10::Syx + Syt::spGFP11, Syx::spGFP1-10 + spGFP11::Syt and BRPD3::spGFP1-10 + Syt::spGFP11 is enriched in synaptic boutons (Fig. 30), but immunostainings revealed also expression of spGFP1-10::Syx + Syt::spGFP11 in the axons of peripheral nerves (Fig. 30A). Bright spots within boutons are indicated by arrows that point towards sites of augmented protein-protein interactions (Fig. 30). Presumably at these sites there is enhanced release of neurotransmitter which requires increased events of vesicle-docking and fusion.

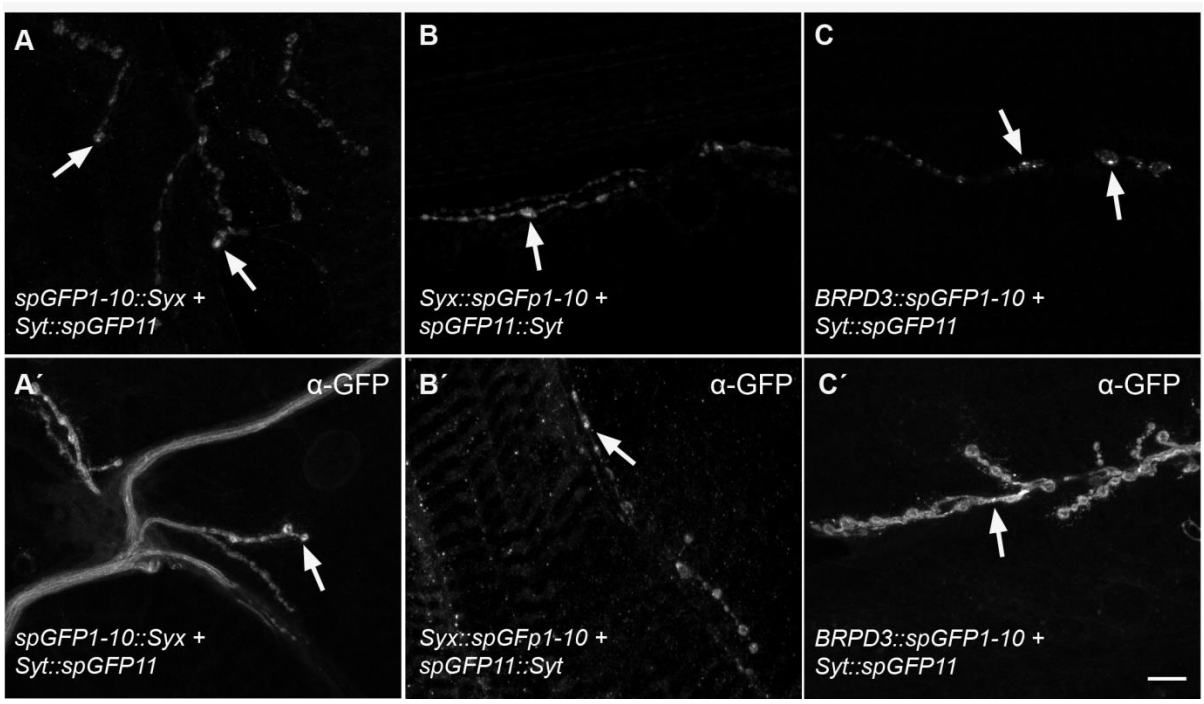

Fig. 30 Split-GFP expression pattern of *ok6-GAL4* driven synaptic protein pairs.

Upper row shows endogenous fluorescence in living animals between spGFP1-10::Syx + Syt::spGFP11 (A), Syx::spGFP1-10 + spGFP11::Syt (B) and BRPD3::spGFP1-10 + Syt::spGFP11 (C). Lower panel (A´-B´) shows confocal projections of immunostainings against the reconstituted GFP in methanol fixed samples. Arrows display bright spots indicating sites of increased protein-protein interaction. Scale bar = 10 µm.

Further, Fig. 31A illustrates a projection of confocal sections of a transgenic *Drosophila* larval VNC expressing *spGFP1-10::Syt + Syx::spGFP11* driven by *actin-GAL4* (ubiquitous expression (Burn et al., 1989)). Immunofluorescence analysis using a monoclonal anti-GFP antibody against the reconstituted GFP revealed protein interactions between vesicle associated Syt and presynaptic membrane protein Syx. The expression pattern of spGFP1-10::Syt + Syx::spGFP11 seems to

correspond to the localisation of glutamatergic motoneurons which are often clustered and located in a segmental manner along the anterior-posterior axis of the VNC (Fig. 31A, arrow) (Landgraf et al., 1997). In addition, protein-protein interaction was also found at the interface between motoneurons and target muscle, the larval NMJ. The expression pattern of *actin-Gal4* driven Syb::spGFP1-10 + Syx::spGFP11 is shown in Fig. 31B. Co-labelling with the neuronal membrane marker HRP suggests that synaptic protein interaction between Syb::spGFP1-10 + Syx::spGFP11 is highly enriched at neuromuscular junction boutons as expected (Fig. 31B, arrowhead).

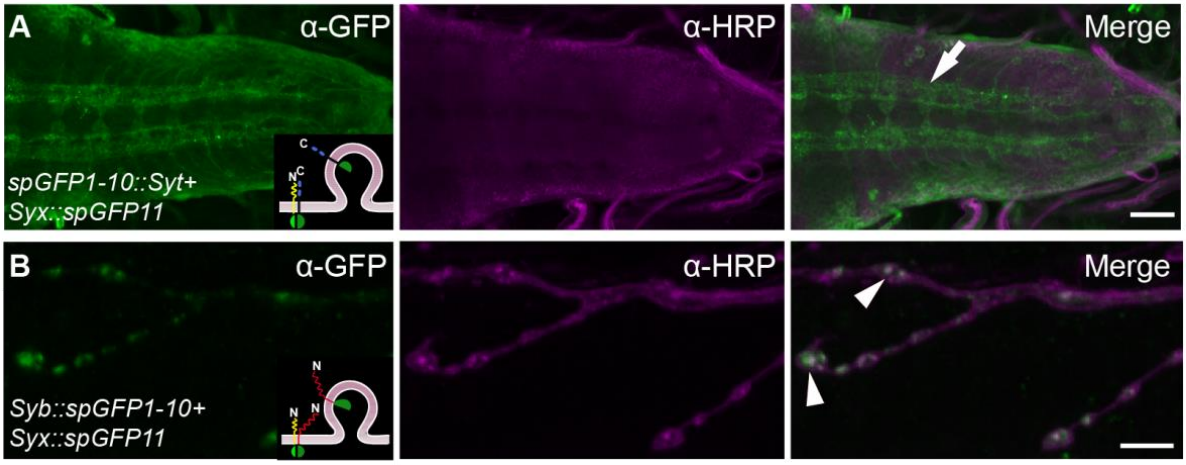

Fig. 31 Split-GFP expression pattern of *actin-GAL4* driven protein pairs.

Projection of confocal images labeled for spGFP1-10::Syt+Syx::spGFP11 and HRP in the larval CNS (A). Arrow indicates possible co-localisation with glutamatergic motoneurons clustered in the VNC (A). Expression pattern of Syb::spGFP1-10+Syx::spGFP11 and HRP at the NMJ (B).The arrowheads indicate co-localisation with HRP designating protein-protein interactions to synaptic boutons (B). Scale bars A = 10 µm, B = 5 µm.

Not all docking and fusion sensor pairs showed a specific signal in confocal laser-scanning microscopy studies. Presumably, this is due to the fact that these specific protein pairs are not in sufficient proximity needed for spGFP chromophore formation or probably various putative protein pairs do not meet at all during synaptic vesicle turnover. The following spGFP tagged synaptic protein pairs yielded reliable GFP expression at the NMJ using a monoclonal anti-GFP antibody exclusively recognizing the functional GFP chromophore:

Strain name	spGFP protein pairs
GR80;GR69	spGFP1-10::Syt+Syx::spGFP11
GR139;GR89	BRPD3::spGFP1-10+Syt::spGFP11

GR48;GR89	spGFP1-10::Syx+Syt::spGFP11
GR68;GR89	Syx::spGFP1-10+ Syt::spGFP11
GR108;GR69	Syb::spGFP1-10+Syx::spGFP11
GR91;GR100	spGFP1-10::Syb+spGFP11::Syb

Next, the extracellular potassium concentration was increased to 90 mM in order to achieve high-intensity stimulation of neurotransmitter release. Consequently the synaptic vesicle turnover rises requiring an increased interaction of synaptic proteins which should result in an enhanced reconstituted spGFP signal at the NMJ. Unfortunately, we could not achieve any enriched GFP signal analysing the functionally proofed spGFP proteins by using extracellular high potassium application.

4.2.2 Analysing the localisation of dCIRL using spGFP fusion proteins

This study also utilised the spGFP approach to gain more detailed information about the subcellular localisation of dCIRL at the NMJ. In previous experiments I could show that vesicle associated n-Syb N-terminally tagged with the yellow fluorescent protein Venus from *Aequorea Victoria* (Venus::n-Syb) (Nagai et al., 2002) is highly enriched at neuromuscular junction boutons (Gehring, 2010). By using either the presynaptic driver-line *VGlut-GAL4*, driving expression only in glutamatergic motoneurons (Daniels et al., 2008) or the muscle-specific driver line *G7-GAL4* (Aravamudan and Broadie, 2003) I confirmed that Venus::n-Syb is expressed both at the pre- and postsynapse (Fig. 32A). Fig. 32B shows the expression pattern of spGFP1-10::n-Syb and spGFP11::n-Syb. Although the reconstituted signal is much weaker, the expression pattern of spGFP1-10::n-Syb + spGFP11::n-Syb shows localisation comparable to Venus::n-Syb at pre- and postsynaptic sites. Control experiments revealed no labeling at the NMJ (Fig. 32C).

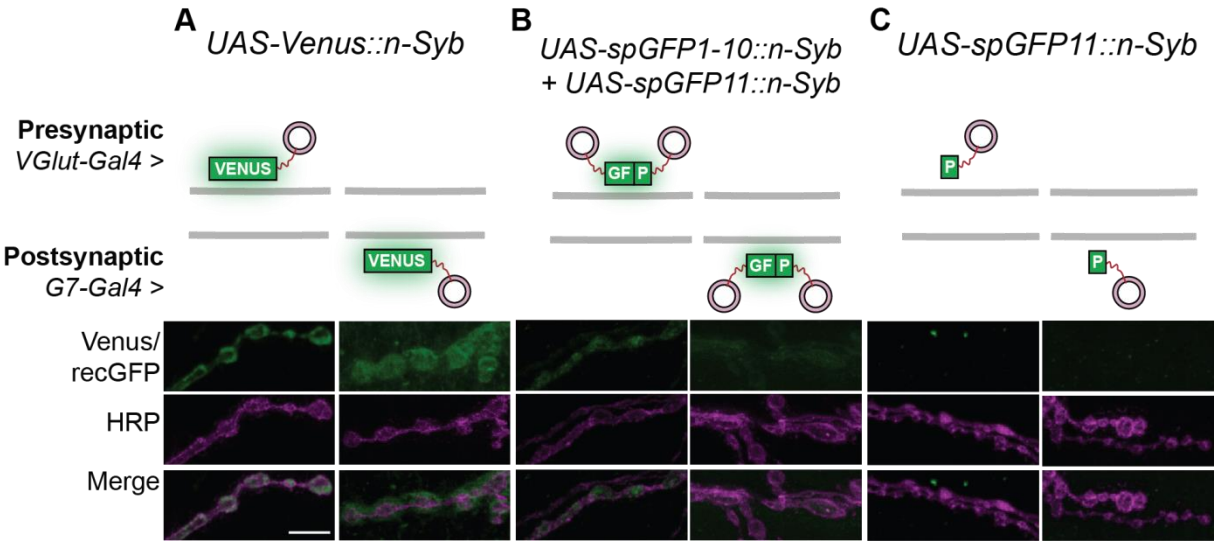

Fig. 32 Pre-and postsynaptic expression pattern of n-Synaptobrevin.

Upper panels schematically illustrate various n-Syb constructs. Lower panels show confocal images of different n-Syb constructs driven either with *VGlut-Gal4* (A-C left) or *G7-Gal4* (A-C right) and stained with anti-GFP antibody: *Venus::n-Syb* (A), *UAS-spGFP1-10::n-Syb* + *UAS-spGFP11::n-Syb* (B) and *UAS-spGFP11::n-Syb* (C). Shown below is a counterstaining against HRP and merged stainings are displayed below. Scale bar = 10 µm.

To address the localisation of dCIRL I designed a genomic *dCirl* fusion protein, dCIRL::spGFP1-10, utilising an in-frame fusion of the *attB*-flanked genomic *dCirl* wild-type locus with the spGFP1-10 fragment. Equally to dCIRL::RFP and dCIRL::FLAG, this reconstituted the *dCirl* locus at single copy rate allowing the examination of dCIRL fusion proteins under endogenous conditions. However, co-expression of endogenously expressed dCIRL::spGFP1-10 and pre- or postsynaptically driven spGFP11::n-Syb revealed no detectable fluorescent signal in immunostainings using a monoclonal anti-GFP antibody.

In addition, a red fluorescent protein (RFP) was N-terminally tagged with the spGFP::11 fragment, termed spGFP11::RFP. This should result in cytoplasmic expression of the spGFP11 fragment instead of an expression restricted to vesicle associated n-Syb at the NMJ. Using the ubiquitously expressing driver-line *actin-GAL4* we could not detect any spGFP complementation between dCIRL::spGFP1-10 and spGFP11::RFP in immunostainings. Presumably, this is due to low endogenous expression levels of dCIRL in *Drosophila*.

Together, these results suggest that in general it is feasible to study protein interactions at larval *Drosophila* active zones using spGFP fusion proteins. However, one must consider that attraction between the fragments is extremely strong and as a

result once complemented the split GFP is irreversible (Cabantous and Waldo, 2006). This results in a fluorescent signal even though the actual synaptic protein interaction has already passed. This reduces the application of the spGFP method in resolving fast and transient protein-protein interactions. Therefore, the spGFP assay seems only partly suitable for resolving fast and transient protein-protein interactions at larval *Drosophila* active zones *in vivo*.

5. Discussion

5.1 Functional analysis of *dCirl*

Despite defining the second largest group of the GPCR superfamily (Fredriksson et al., 2003), adhesion GPCRs (aGPCRs) are only poorly understood regarding their physiological function. The fact that latrophilins are highly conserved across phyla (Nordstrom et al., 2009) makes them an ideal prototype of the aGPCR class. Containing only one latrophilin homolog (*dCirl*) together with its genetic accessibility and well-established transgenic approaches renders the fruit fly a very suitable model organism. In this thesis genetic experiments, imaging approaches and behavioural studies were utilised to unravel the localisation and physiological function of dCIRL in *Drosophila*.

5.1.1 Verification of the *dCirl*^{KO} null allele

One of the major aims of this thesis was to investigate the function of dCIRL in *Drosophila*. Due to the lack of specific RNAi probes targeting *dCirl* transcripts RNA interference (RNAi) experiments (Fire et al., 1998) could not be employed to knock-down *dCirl* gene expression. The main advantage of transgenic RNAi constructs, in addition to its relatively simple design and fast execution time, is that it allows spatial and temporal control of the knock-down construct using different GAL4 driver lines. Nonspecific and off-target effects of RNAi probes, on the other hand, present an inherent limitation to their usefulness in basic research. Therefore, we utilised the *dCirl*^{KO} mutant, which was generated during the diploma studies of R. Fischer (2011) via ends-out targeting and homologous recombination according to Huang et al. (2008) and (2009). Although being labor and cost intensive, one major drawback in the use of knock-out animals is that lethal mutations may prevent the study of developmental effects. However, knock-out experiments entirely eliminate target gene expression instead of post-transcriptionally reducing it, offering a more efficient and reliable alternative to RNAi. Using RT-PCR we established that no residual transcript is present in *dCirl*^{KO} homozygotes. Additionally, western blot analysis using a polyclonal antiserum that recognizes a peptide which is situated in the extracellular region of dCIRL showed two bands corresponding to the full-length (~ 180 kDa) and autoproteolyzed receptor (~ 70 kDa) cleaved at the GPS motif in wild-type samples. Both bands were absent from *dCirl*^{KO} and *Df(2R)Exel8047*, a deficiency that includes

the *dCirl* locus as well as six adjacent genes, protein extracts. Thus, these data confirmed that *dCirl*^{KO} is a protein null allele.

To date the biological function of most aGPCRs is still unknown. However, there are studies demonstrating that mutations in some members of the aGPCR family cause developmental defects in humans like bilateral frontoparietal polymicrogyria (GPR56) (Piao et al., 2004) and Usher Syndrome (VLGR1) (Weston et al., 2004). Interestingly, while the aGPCR GPR126 has been implicated in the myelination of peripheral nerves in zebrafish (Monk et al., 2009), GPR126 has recently been shown to be required for embryonic viability and cardiovascular development in mouse (Patra et al., 2013). Thus, the analysis of GPR126 mutations in Zebrafish does not comply with the essential function in mammalian development. Presumably, the phenotypic differences result from compensation mechanisms by other aGPCR members or different levels of functional redundancy. Other studies using the fruit fly confirmed that the cadherin-like aGPCR *flamingo/starry night* (FMI) and its mammalian homolog (CELSR) has been associated with planar cell polarity in *Drosophila* (Usui et al., 1999; Lawrence et al., 2007) and axonal tract development in mice (Tissir et al., 2005). Recent reports established that *lat-1* functions in development and fertility in *C. elegans* (Langenhan et al., 2009; Promel et al., 2012). In contrast, *lat-2*, the second latrophilin homolog of *C. elegans* displayed no role in development. The distinct phenotypes are consistent with different expression patterns: While in addition to its zygotic expression profile in the embryo, *lat-1* is expressed in the nervous system, the pharynx, the gonad and the vulva, *lat-2* remains restricted to the pharynx and gland cells (Langenhan et al., 2009). To test for developmental lethality of *dCirl*^{KO} animals we initially employed survival studies. Our analysis revealed that the latrophilin homolog *dCirl* is not required for normal development in *Drosophila*, as opposed to *lat-1* in *C. elegans*. This argues against a zygotic expression pattern of *dCirl* in the fruit fly.

5.1.2 Expression of dCIRL in the larval and adult nervous system

To better understand the function of *dCirl* in *Drosophila* it was essential to study its expression profile. Unfortunately, the polyclonal anti-dCIRL antibody, used in western blot analysis, failed to provide specific and reproducible results in immunohistochemistry. This is likely due to low endogenous expression levels of dCIRL or reduced antigenicity of the dCIRL epitope under tested fixation protocols.

To overcome this obstacle, we took advantage of the *attP* site with which the *dCirl* locus was replaced in the *dCirl*^{KO} strain, and genomically engineered two tags in the ORF of *dCirl*. A *Flag* tag sequence was separately inserted in the exon encoding the third intracellular loop of the 7TM domain, and a monomeric *RFP* into the intracellular domain of the *dCirl* gene product. This resulted in two different tagged genomic *dCirl* fusion proteins, *dCirl*^{Flag} and *dCirl*^{RFP}, under endogenous genetic control accompanying all *cis*-regulatory elements. In addition we generated a genomic rescue strain (*dCirl*^{Rescue}) containing exclusively the *dCirl* wild-type locus without any tag. Verification via western blot analysis using an anti-RFP and anti-FLAG antibody showed the presence of dCIRL tagged fusion proteins at expected sizes indicating that the tagging strategy resulted in mRFP- and FLAG tag-labeled dCIRL product.

We used confocal fluorescence microscopy to visualise the location of the chromophore fusion dCIRL::RFP in the nervous systems of third instar larvae, but could not detect any fluorescent signal. This suggests considerably low endogenous expression levels of dCIRL, similar to LAT-1 in *C.elegans* (Langenhan et al., 2009). However, immunohistochemical analysis using an antibody directed against the FLAG tag or the monomeric RFP revealed the subcellular localisation of dCIRL::FLAG and dCIRL::RFP, respectively. Immunostainings of *dCirl*^{Flag} larvae uncovered strong expression in the larval nervous system. Higher magnification views showed co-localisation between dCIRL::FLAG and the neuronal membrane marker HRP indicating localisation of dCIRL to the cell membrane of expressing neurons. Similar results were obtained for animals expressing dCIRL::RFP visualised by immunodetection with an anti-RFP antibody. Co-localisation with the active zone marker BRP (Wagh et al., 2006) indicated expression in the synapse-rich neuropil of the larval CNS. These results suggest that the site of tag insertion had no effect on the cellular and subcellular expression of dCIRL. Similarly, adult brains exhibited marked expression of either dCIRL::FLAG or dCIRL::RFP, with dense labeling in the lobe of the mushroom body and the medulla of the optic system (studies performed by N. Hartmann). Conversely, dCIRL staining was absent from regions of high BRP concentration, suggesting lack of dCIRL in areas with high numbers of presynapses in adult brains. Taken together these data confirmed that dCIRL is widely expressed in the larval and adult nervous system of *Drosophila*.

This result is consistent with findings from other aGPCR expression studies, such as LPHN in mammals. LPHN1 for example is also strongly expressed in brain, although low levels of mRNA are found in most tissues (Sugita et al., 1998). In contrast, LPHN2 is mainly found outside the brain, especially in lung and liver. Transcriptional expression of *LPHN2* was reported in brain at low levels, while protein expression could not be detected. LPHN3 expression, on the other hand, is primarily detectable in brain (Sugita et al., 1998; Ichtchenko et al., 1999). Using northern blot analysis of RNA isolated from rat tissue Matsushita et al. (1999) discovered that *LPHN1* and *LPHN3* are mostly brain-specific, although *LPHN3* is much less abundant. Additionally, *LPHN1* mRNA was also found in very low amounts in kidney, lung and spleen. The founding that *LPHN1* is about 50 fold more abundant in brain than in other tissues suggests a highly specialised function (Matsushita et al., 1999). Moreover, the brain angiogenesis inhibitors (BAI) 1-3 are expressed almost exclusively in the CNS. Mori et al. (2002) confirmed that human *Bai1* is transcriptionally expressed in the fetal as well as the adult brain. Murine *Bai1* and *Bai2* were found to be up-regulated following birth, displaying its highest expression at postnatal day 10 (P10) and a high expression retained until adult stage (Koh et al., 2001; Kee et al., 2002). This indicates that *Bai1* and *Bai2* might be involved in brain angiogenesis. In contrast, *Bai3* was shown to steadily decrease expression levels after having reached its peak expression at P1 (Kee et al., 2004). In addition, McMillan et al. (2002) demonstrated that the very large G protein-coupled receptor-1 (VLGR1) is highly expressed in mouse embryonic central nervous system, beginning at the time of development of the neural groove. The fact that VLGR1 expression declines as neurogenesis is largely completed suggests a role for VLGR1 in the development of the central nervous system. Mutations in the *VLGR1* gene were linked to human Usher syndrome type II, a genetic disorder characterised by congenital hearing loss and progressive retinitis pigmentosa (Weston et al., 2004). Another aGPCR shown to be expressed at high levels in the brain, in addition to thyroid gland and heart, is GPR 56 (Liu et al., 1999). Mutations in *GPR56* cause a rare central nervous condition called bilateral frontoparietal polymicrogyria (BFPP) suggesting that GPR56 is implicated in the development of human cerebral cortex (Piao et al., 2004). Further, the cadherin-like *flamingo/starry night* (FMI) and its vertebrate homologs (CELSR) were shown to be expressed broadly in the neuroepithilium at early developmental stages and exhibit distinct expression patterns

within a range of different tissues in the developing embryo (Shima et al., 2002). It is confirmed that *fmi/Celsr* have essential and conserved functions in the planar cell polarity pathway and in neuronal development (Usui et al., 1999). In fact, expression profiling uncovered that 17 out of 30 members of rodent aGPCRs are expressed in the CNS (Strokes and Piao, 2010). Our data confirmed that the same is true for dCIRL in *Drosophila*.

5.1.3 Loss of *dCirl* results in locomotion defects

During our studies we noted that freely moving $dCirl^{KO}$ mutant larvae exhibited a conspicuous locomotion behaviour. Wang et al. (1997) established that foraging larvae have bouts of linear crawling and periods of pausing, the so-called decision-making component of locomotion. Based on our observation that $dCirl^{KO}$ larvae showed difficulties in starting linear locomotion and exhibited more frequent turns while crawling than control animals the crawling distance within a given time was measured. Covering a minor overall distance, loss of *dCirl* seems to influence larval locomotion behaviour, confirmed by rescue experiments with $dCirl^{Rescue}$ and $dCirl^{Flag}$ larvae. In contrast, $dCirl^{RFP}$ larvae failed to rescue the reduction in crawling behaviour (further explained in 5.1.5). Locomotion in general relies on a dynamic interplay between the central nervous system (CNS), the peripheral nervous system (PNS) and muscles. CNS and PNS neurons are organised in circuits: sensory neurons (afferent) carry nerve impulses from the periphery to the CNS, while motoneurons (efferent) transmit signals from the CNS to effectors. Whereas afferent and efferent neurons carry information over comparatively long distances, interneurons act locally within the CNS to relay signals between sensory and motoneurons. The rhythmic pattern that underlies locomotion is created by central pattern generator circuits located in the CNS, responsible for coordinating the activation of motoneurons that control movement (Marder and Calabrese, 1996). Sensory feedback from the PNS coordinates contraction of body segments providing adjustment to the pattern (Suster and Bate, 2002; Hughes and Thomas, 2007).

In order to comprehend the mechanism causing the abnormal crawling behaviour in $dCirl^{KO}$ mutant animals we initially examined the efferent motor part of the nervous system. We could not obtain reliable and specific immunostainings at the NMJ of $dCirl^{Flag}$ and $dCirl^{RFP}$ larvae using an antibody directed against the FLAG tag or the monomeric RFP, respectively. Presumably, this is due to low protein concentration of

dCIRL in synaptic terminals in comparison to its expression in the VNC. With the notable exception of rhodopsin, most GPCRs are present in native tissues at relatively low levels making the detection extremely difficult (Khorana, 1992). The exposure of GPCRs to agonists often results in a rapid attenuation of receptor responsiveness to avoid continuous signaling, a process termed desensitization. Different mechanisms such as phosphorylation, endocytosis and down-regulation of mRNA and protein synthesis are responsible for desensitization of GPCRs (Ferguson, 2001). However, high ligand affinities and strong amplification of downstream signals guarantee specific and efficient signal transduction. Moreover, the low expression levels further account for minimal background signaling activity. Besides *Drosophila* dCIRL, low protein expression was reported for other GPCRs such as GPR126 in mouse (Waller-Evans et al., 2010), human β_2-adrenergic receptor (Kobilka and Deupi, 2007) and LAT-1 in *C. elegans* (Langenhan et al., 2009). To circumvent the low expression profile of dCIRL at the NMJ we fused the *dCirl* promoter to cDNA encoding the yeast transcription activator *GAL4* and utilised this *dCirlp*^{GAL4} transgene to drive the expression of an *UAS-myr::GFP* and *UAS-mCD8::GFP*. Despite being under control of the same *GAL4* driver this resulted in different expression patterns of *UAS-myr::GFP* and *UAS-mCD8::GFP*. While *dCirlp*^{GAL4} driven *UAS-myr::GFP* revealed gene expression in synaptic boutons, *dCirlp*^{GAL4} driven *UAS-mCD8::GFP* exposed strong expression in peripheral sensory neurons and type III synaptic boutons on muscle 12. Though, type III boutons have a superficial location on the muscle compared to type I or type II boutons (Martinez-Padron and Ferrus, 1997). Obviously, these distinct expression patterns are caused by different features of the GFP anchors. While the myristoylated GFP is attached via a fatty acid to the membrane, the *mCD8::GFP* is anchored via a transmembrane domain. Thus, *myr::GFP* could show enhanced diffusion from the somata of motoneurons located in the CNS, along the axons to synaptic boutons on muscles. This explains the strong transcriptional expression of *dCirl* in synaptic boutons on numerous muscles, as well as throughout the axons of peripheral nerves. In contrast, the transmembrane domain of *mCD8::GFP* requires a shuttle protein or an extremely strong driver line for expression in motoneurons, with the exception of type III synaptic boutons. Unlike *myr::GFP*, *dCirl*-promoter-driven *mCD8::GFP* expression is present in peripheral sensory neurons with their cell bodies situated on the muscles, where they transmit signals from sensory receptors to the CNS. Thus, the

mCD8::GFP construct seems better suited for peripheral expression, whereas the *myr::GFP* construct revealed motoneuronal expression.

Based on the transcriptional activity of *dCirl* in motoneurons and the locomotion phenotype of *dCirl*^{KO} mutants we analysed the morphology of the most prominent muscle pair 6/7. Data of vertebrate latrophilin homologs suggest that LPHNs modulate glutamatergic synaptic function by interaction with different postsynaptic ligands, such as teneurins (Silva et al., 2011) or FLRTs (O'Sullivan et al., 2012). However, co-immunostainings against BRP and GluRIID revealed unaltered size and number of presynaptic active zones and postsynaptic glutamate receptor subunit IID. Further, I showed that the overall NMJ size is unaltered in *dCirl*^{KO} larvae. Similarly, electrophysiological analysis demonstrated that no general functional defect of synaptic transmission is present in *dCirl*^{KO} mutant larvae. These results indicate that basal structure and synaptic transmission of glutamatergic type I boutons are largely unaffected by loss of *dCirl*. Therefore, we exclude the possibility that the abnormal crawling behaviour results from motoneuronal defects.

While investigating glutamatergic motoneurons, we discovered an increase of DLG in several *dCirl*^{KO} larvae, indicating that *dCirl* might be involved in regulating the abundance of DLG at the NMJ. Western blot analysis confirmed that the amount of DLG was almost doubled in larvae lacking *dCirl*. Though, the distinct enrichment of DLG was only present in some mutants analysed by immunohistochemistry. Postsynaptically, DLG is localised at the SSR, an elaborated membrane structure mainly surrounding glutamatergic type I boutons (Lahey et al., 1994). *dlg* loss-of-function mutants display a strongly reduced SSR, whereas overexpression of *dlg* results in an increase of SSR size and complexity (Budnik et al., 1996). Therefore, we reasoned that upon upregulation of DLG the SSR structure is altered in *dCirl*^{KO} animals. Indeed electron micrographs of *dCirl*^{KO} type I boutons displayed an enlargement of the SSR as measured by its thickness and surface area occupied. These data suggest that *dCirl* is part of a pathway, which controls the structural layout of the NMJ of type I boutons, but which does not greatly effect responsiveness and activity of the neuromuscular synapse.

5.1.4 Diminished touch sensation of *dCirl*^{KO} larvae

According to our morphological and electrophysiological results, basal synaptic structure and function at the NMJ in larvae lacking *dCirl* seems intact. Hence, either

sensory input or central integration of motor behaviour relies on the function of dCIRL.

Having established that sensory neurons display transcriptional activity of the *dCirl* locus via an *UAS-mCD8::GFP* construct, I analysed peripheral sensory neurons transmitting impulses from sensory receptors to the CNS. Utilising the *dCirlp*^{GAL4} transgene to drive the expression of *UAS-mCD8::GFP* robust expression was noticed in larval and adult peripheral sensory neurons, most obviously in chordotonal organs (chos). Immunostainings against GFP confirmed the presence of *dCirl*-promoter-driven *mCD8::GFP* in the Johnston´s organ in the antenna as well as in the leg of adult flies. Containing 227 scolopidia in the second antennal segment, the Johnston´s organ is the largest cho in *Drosophila* (Kamikouchi et al., 2006). Electrophysiological analysis by Eberl et al. (2000) demonstrated that the Johnston´s organ mediates hearing in the fly. With the help of Christian Spalthoff from Martin Göpfert's lab in Göttingen, we tested the hearing abilities of adult *dCirl*^{KO} flies and found no evidence for acustosensory deficits in these animals compared to controls, but this needs further investigation.

In addition to the Johnston´s organ, *dCirl*-promoter-driven *mCD8::GFP* was also present in the adult leg, where chos function as sound pressure detectors used for "far-field" sound (Eberl, 1999). Moreover, strong transcriptional expression of *dCirl* was found in the larval abdominal body wall, especially in type II multidendritic (MD) neurons, as well as type I monodendritic external sensory (es) neurons and the pentascolopidial organ (lch5). The larval lch5 consists of five scolopidial units, with each scolopidium containing four cells: a neuron, a scolopale cell, a ligament cell and a cap cell, that derive from a single sense organ precursor (SOP) (Eberl and Boekhoff-Falk, 2007). Anti-GFP stainings revealed strong transcriptional *dCirl* expression in the five sensory neurons of each scolopidial cell. While es neurons and chos are associated with support cells, this seems not true for MD neurons (Brewster and Bodmer, 1995). Based on their morphology MD neurons are further subdivided into three major classes: neurons that give rise to elaborate dendritic arborisations (da), neurons containing bipolar dendrites (bd) and neurons extending their dendrites along tracheal branches (td) neurons (Bodmer and Jan, 1987). However, anti-GFP stainings from *dCirl*-promoter-driven *mCD8::GFP* larvae do not allow differentiating between da, bd and td neurons. Because of the reduced specificity of the dCIRL

antibody in immunostainings we were unable to confirm dCIRL expression in chos at the protein level following our observation at the transcriptional level of *dCirlp*^{GAL4}. In addition, neither dCIRL::Flag nor dCIRL::RFP fusion proteins could be visualised in sensory neuron somata using immunohistochemical analysis.

Findings by Caldwell et al. (2003) suggest that chos provide major feedback to locomotor central pattern generator networks in the CNS, generating rhythmic peristalsis and thus mediate touch sensitivity in *Drosophila* larvae. Therefore, I tested for external touch sensitivity by gently touching *dCirl*^{KO} larvae during free locomotion behaviour. *dCirl*^{KO} (and similarly *dCirl*^{KO}*/Df*) larvae showed diminished sensitivity to touch. This reduced touch sensitivity phenotype is rescuable by back-insertion of the genomic *dCirl* wild-type locus in *dCirl*^{Rescue} and *dCirl*^{Flag} layouts. In contrast, *dCirl*^{RFP} larvae failed to rescue the diminished touch sensation similarly observed in larval crawling studies (explained further in 5.1.5). Taken together, our results suggest that *dCirl* is expressed in sensory neurons at least at the transcriptional level and that loss of *dCirl* affects normal response to light touch as well as loss of linear locomotion behaviour together with increased head swings, indicating that dCIRL protein is also present in neurons mediating this behaviour.

To determine which types of neurons are responsible for the touch insensitivity phenotype of mutant animals we used different GAL4 driver lines, expressing a *20xUAS-dCirl*^{Flag} transgene in the *dCirl*^{KO} mutant background. This allowed us to determine in which cells *dCirl* is required for the rescue of the loss-of-function phenotype, hence, where *dCirl* function is physiologically necessary. In addition to *actin-GAL4* (ubiquitous expression (Burn et al., 1989)), *elav-GAL4* (pan-neuronal expression (Yao and White, 1994)) and *ok6-GAL4* (motoneuronal-specific (Sanyal, 2009)), we utilised the sensory neuron specific driver lines *5-40-GAL4* (pan-sensory neurons (Song et al., 2007)), *21-7-GAL4* (type II neuron-specific (Song et al., 2007)) and *iav-GAL4* (cho-specific (Kwon et al., 2010)). Characterisation of these sensory specific driver lines using an *UAS-mCD8::GFP* transgene confirmed published expression patterns except for *21-7-GAL4* expression that was not restricted to type II neurons in our studies but was also found weakly expressed in chos, at least in the pentascolopidial organ (lch5). We then observed that diminished touch sensation was rescued in animals expressing *dCirl* ubiquitously (*actin-GAL4*) or exclusively in chos (*iav-GAL4*). In contrast, expression of *dCirl* in type I and type II neurons (*5-40-*

GAL4) as well as in type II and cho (*21-7-GAL4*) seemed insufficient to rescue the diminished sensitivity to gentle touch. Likely, this is due to the observation that *5-40-GAL4* as well as *21-7-GAL4*, although driving expression in chos, revealed considerably weaker expression levels in lch5 compared to *iav-GAL4*. Panneuronal expression of *dCirl* using the *elav-GAL4* driver line showed a tendency towards rescue. However it is known from several immunohistochemical studies, that *elav-GAL4* inserted in the third chromosome drives weaker expression than *elav-GAL4* located on the first chromosome (unpublished results by N. Hartmann), which might be responsible for the lack of rescue in our experiment. Interestingly, rescue of diminished touch sensation of $dCirl^{KO}$ mutants using the *actin-GAL4* line resulted in a gain-of-function phenotype exhibiting touch sensitivity values higher than wild-type standard. This suggests that dCIRL expression levels are highly upregulated by the strong and ubiquitously expressing driver line *actin-GAL4*. Therefore, chos may be more sensitive to gentle touch stimulation resulting in touch sensitivity scores highly above wild-type levels. The fact that *dCirl* is not absolutely required for cho function like the transient receptor channels NANCHUNG and INACTIVE (Kim et al., 2003; Gong et al., 2004) suggests rather a modulatory function of *dCirl* in these neurons. A possible model is that *dCirl* modulates the gain of cho activity via e.g. modulation of transient receptor channels such as NOMPC, NANCHUNG, and INACTIVE that mediate the receptor potential of chos (Zhang et al., 2013). Taken together, our studies indicate that expression of the genomic *dCirl* wild-type locus in chos rescues the reduced touch sensation of $dCirl^{KO}$ animals. These results resemble findings from Caldwell et al. (2003) demonstrating that cho mutants are touch-insensitive. Furthermore, it is known that the duration of linear locomotion is reduced in cho mutants (Caldwell et al., 2003) and in animals, in which cho function was genetically obliterated by expression of a $UAS\text{-}shi^{ts}$ transgene (Hughes and Thomas, 2007), an effect that we also observed in $dCirl^{KO}$ mutant animals. Future studies need to unravel if dysfunctions in linear locomotion can also be rescued by using *actin-GAL4* or *iav-GAL4* driven $20xUAS\text{-}dCirl^{Flag}$ in the $dCirl^{KO}$ mutant background.

Besides innocuous (gentle < 10 mN) touch, I also tested for noxious (harsh > 30 mN) touch sensation in larvae lacking dCIRL by utilising a needle instead of a von-Frey filament. Conversely, harsh touch sensation seems largely unaffected in $dCirl^{KO}$ mutant animals. Though, a suitable positive control, e.g. *painless* mutant larvae, showing increased thresholds to thermal and mechanical nociception (Tracey et al.,

2003) was not tested in this setup. It was shown that the *painless* gene product is strongly expressed in MD type II neurons, while being absent from type I sensory neurons, thus being impaired in strong touch response but showing a normal behavioural response to light touch stimuli (Tracey, 2007). This indicates that harsh touch sensation seems primarily mediated by MD neurons. Our results show, that besides es neurons and chos, MD neurons display transcriptional activity of the *dCirl* locus. As harsh touch response seems unaffected in $dCirl^{KO}$ mutants and as we could not rescue the touch sensation defect by cell-specific expression in MD neurons via the *21-7-GAL4* driver, we conclude that MD neuron function is not impaired, by loss of *dCirl*.

Finally, using structural analysis we confirmed that mutant animals exhibited no obvious morphological defects of the pentascolopidial organ regarding missing scolopidia, disruptions of outer dendritic segment (ODS) morphology, lack of ciliary dilation (cd) and relative orientation of the whole lch5. This leads to the assumption that, instead of their morphology, the physiological function of chos might be impaired in larvae lacking dCIRL.

5.1.5 Molecular mechanism of dCIRL signalling

Consisting of 7TM spanning domains GPCRs transduce extracellular received signals across the cell-membrane activating signal transduction pathways inside the cell via intracellular heterotrimeric G proteins ($G_{\alpha\beta\gamma}$). Following nucleotide exchange of GDP for GTP, the tightly associated G_{α} and $G_{\beta\gamma}$ subunits dissociate and regulate several down-stream signalling effector molecules, including adenylylcyclases, phosphodiesterases, phospholipases, tyrosine kinases and ion channels (Oldham and Hamm, 2008). Interestingly, our results indicate that intracellular RFP insertion impairs the function of dCIRL. We confirmed that $dCirl^{RFP}$ failed to rescue both the reduction in crawling behaviour and the diminished sensation to gentle touch, pointing towards functional disturbance of dCIRL by an intracellular RFP insertion. This might be due to the fact that the C-terminal fragment of LPHN has a typical GPCR structure binding to the $G\alpha_o$ (Lelianova et al., 1997) and $G\alpha_q$ (Rahman et al., 1999) and is therefore involved in the upregulation of IP_3 and mobilisation of intracellular Ca^{2+} by activating Phospholipase C (PLC). Presumably, the activation of second messengers could be perturbed by chromophore insertions close to the C-

terminus, interfering proper function of dCIRL. Furthermore, the cytoplasmic site of the C-terminal fragment of LPHN harbours several potential phosphorylation sites (Silva and Ushkaryov, 2010) that might be disturbed by an intracellular insertion of RFP. Despite great efforts the intracellular pathway of LPHN as well as the endogenous ligand for most aGPCRs and consequently the molecular aGPCR activation still remains undetermined. However, it is speculated that receptor activation results from cell-cell or cell-matrix contact via the extracellular adhesion domains (Hamann et al., 1996; Stacey et al., 2003).

Several models from different studies exist for aGPCR activation and signalling. First, aGPCR can form distinct multicomponent signaling complexes with other transmembrane molecules in *cis* and in *trans* across a single cell, which has been shown for the cadherin-like aGPCR CELSR/Flamingo (FMI) of *Drosophila* (Usui et al., 1999; Chen et al., 2008). Moreover, interaction of a second ligand with the hormone receptor motif (HRM), a domain conserved in many but not all aGPCR, in addition to ligand binding at the N-terminal adhesion domains is required for signaling (Shima et al., 2004; Kimura et al., 2006). Finally, the so called “split-personality”-receptor model suggests the liberation of N-termini from their 7TM domain post-transcriptionally via cleavage at the GPS. The ectodomain fragment is then free to recombine with 7TM modules of other aGPCRs (Silva et al., 2009). Autoproteolysis results in two separate polypeptide chains, NTF and CTF (N- and C-terminal fragments), that might re-associate via the broken GAIN domain into a heterodimer and apparently reconstitute the nascent receptor structure (Promel et al., 2013). While some analyses suggest that self-cleavage at the GAIN domain is essential for membrane targeting (Lin et al., 2004), other studies claim that aGPCR fragment separation and reconstitution are important steps of the signaling cascade (Volynski et al., 2004). Previous investigations have established biochemical properties of aGPCR heterodimerization, but direct evidence of naturally formed aGPCR chimeras remains elusive. Future experiments might allow to directly monitor NTF and CTF of dCIRL at the scale of single molecules by means of genetically encoded chromophores and tags. An alternative approach pursues super-resolution microscopy such as STimulated Emission Depletion (STED) (Hell, 2003; Kittel et al., 2006) and *direct* STochastic Optical Reconstruction Microscopy (*d*STORM) (Heilemann et al., 2008; van de Linde et al., 2011) in the nervous system of *Drosophila* to test whether transgenically encoded and differently tagged dCIRL

fragments can be monitored in their native environment at sub-diffraction resolution. This will enable a direct visualisation of dCIRL autoproteolysis products and fragment re-association of an aGPCR in a physiological environment for the first time. Moreover, recent findings by Zhang et al. (2013) combining *in vivo* recordings and behavioural assays confirmed that sensory neurons are accessible for patch-clamp analysis. Thus, future experiments combining super-resolution microscopy with electrophysiological recordings of sensory neurons enables us to enlight the physiological relevance of *dCirl* at *Drosophila* chos.

In summary, our data showed that in *Drosophila dCirl*/Latrophilin is widely expressed in the larval central nervous system including moto- and sensory neurons. We found that loss of *dCirl* results in locomotion defects while basal synaptic function at the neuromuscular junction, the site of motoneuronal muscle innervation, is unaffected. Consequently, either sensory input or central integration of motor behaviour relies on the function of dCIRL. We showed that *dCirl* is expressed in neurons of the peripheral nervous system at the transcriptional level, but could not confirm expression of dCIRL at the protein level in sensory neurons likely due to low endogenous expression. However, we established that $dCirl^{KO}$ mutant larvae exhibited diminished sensitivity to gentle touch. This loss-of-function phenotype is rescuable by expression of *dCirl* in larval chordotonal organs demonstrating that *dCirl* is required for cho function. Since we could not detect morphological defects in the pentascolopidial organ of mutant animals, it is likely that dCIRL physiological function of chos is impaired. Although this work could contribute to the characterisation of dCIRL in *Drosophila*, both main topics localisation and function of the latrophilin homolog require further investigations. It will be crucial to verify the expression pattern of dCIRL at the protein level in order to gain closer insights into the *in vivo* function of latrophilin.

5.2 Optical sensors for protein-protein interactions

In another approach of this thesis we investigated the interactions between several presynaptic proteins during vesicle exocytosis *in vivo*. In order to comprehend the entire interplay of complex neuronal networks it is of fundamental interest to understand the molecular architecture of synaptic contacts as well as the interaction of synaptic proteins. These interactions are a central mechanism for neurotransmitter

exocytosis and consequently for the communication between cells. By utilising the split-GFP (spGFP) method developed by Hamilton, Regan, Kerppola, Gosh, Chalfie, Shen and Bargmann labs, we took advantage of the principle of coincidence detection upon direct protein-protein interactions when protein fusions with different spGFP components (spGFP1-10 and spGFP11) encounter each other. Having shown that full-length reporter fusions with n-Synaptobrevin (n-Syb), Synaptotagmin (Syt), Syntaxin (Syx) and Bruchpilot Domain 3 (BRPD3) seem fully functional and allow expression in *Drosophila*, we next created transgenes containing protein fusions of Syx, Syt, n-Syb and BRPD3 with spGFP fragments via Gateway cloning (Gehring, 2010).

According to putative protein-protein interactions, described for example by Rosenmund (2003) and Sudhof (2004), we established so called docking and fusion sensor pairs in order to characterise specific steps in synaptic vesicle turnover at active zones. By utilising the motoneuron/neuron specific driver line *ok6-GAL4 (*Sanyal, 2009) we overexpressed the spGFP tagged protein pairs at the NMJ in living animals as well as fixed samples. Not surprisingly endogenous fluorescence *in vivo* is rather weak. In contrast, immunostainings of methanol-fixed larvae using a monoclonal anti-GFP antibody that exclusively recognized the fully folded and hence functional GFP chromophore, revealed robust staining. Besides expression of spGFP1-10::Syx + Syt::spGFP11 in the axon, we confirmed that the interaction between spGFP1-10::Syx + Syt::spGFP11, Syx::spGFP1-10 + spGFP11::Syt and BRPD3::spGFP1-10 + Syt::spGFP11 is enriched at the NMJ. Striking expression was observed at several spots within the bouton, suggesting sites of increased protein-protein interactions at active zones, where upon vesicle docking and fusion neurotransmitter is released into the synaptic cleft.

Additionally, by utilising the ubiquitously expressing driver line *actin-GAL4* (Burn et al., 1989) we revealed protein interaction between vesicle associated Syt and presynaptic membrane protein Syx in the VNC. In accordance with findings from Landgraf et al. (1997) the expression pattern of spGFP1-10::Syt + Syx::spGFP11 seems to resemble the localisation of glutamatergic motoneurons which are often clustered and located in a segmental manner along the anterior-posterior axis of the VNC. Further, *actin-Gal4* driven Syb::spGFP1-10 + Syx::spGFP11 expression was observed at the NMJ. However, only few docking (spGFP1-10::Syx + spGFP11::Syt and

Syb::spGFP1-10 + Syx::spGFP11) and fusion (spGFP1-10::Syt + Syx::spGFP11 and Syx::spGFP1-10 + Syt::spGFP11) sensor pairs yielded fluorescence in confocal laser-scanning microscopy analysis. One obvious explanation is that the proteins do not interact under the conditions tested. It is also possible that various putative protein sensor pairs will not get in contact at all during synaptic vesicle turnover or that steric arrangement of fluorescent protein fragments does not enable their association. We tried high-intensity stimulation of neurotransmitter release by increasing the extracellular potassium concentration to 90 mM. However, we did not achieve augmented interaction of synaptic proteins resulting in an increased reconstituted spGFP signal.

In a third combined approach we made use of the spGFP method to determine the subcellular localisation of dCIRL at the NMJ. Therefore, the *attB*-flanked genomic *dCirl* wild-type locus, corresponding to that removed by genomic targeting, was fused in-frame with a *spGFP1-10*. This resulted in a genomic *dCirl* fusion protein, dCIRL::spGFP1-10, under endogenous genetic control accompanying all *cis*-regulatory elements. Having established that Venus::n-Syb is expressed both at the pre- and postsynapse by using specific the driver-line *VGlut-GAL4* (glutamatergic motoneurons (Daniels et al., 2008)) or the muscle-specific driver line *G7-GAL4* (Aravamudan and Broadie, 2003), respectively, we also confirmed the presence of spGFP1-10::n-Syb + spGFP11::n-Syb at both sites. The expression pattern of Venus::n-Syb corresponds to that seen in n-Syb spGFP fusion experiments at the pre- and postsynapse. Though, the endogenously expressed dCIRL::spGFP1-10 fusion protein and pre- or postsynaptically driven spGP11::n-Syb revealed no fluorescent signal in immunostainings using a monoclonal anti-GFP antibody. In addition, to overcome the restricted vesicular expression pattern of n-Syb at the synapse, we created a cytoplasmic expressed spGFP11::RFP. Similarly, using the ubiquitously expressing driver-line *actin-GAL4* we could not detect spGFP complementation between dCIRL::spGFP1-10 and spGFP11::RFP in living animals and fixed samples. These results resemble the low endogenous expression level of dCIRL in *Drosophila* and demonstrate the limitations of the spGFP system.

Indeed, we found that the spGFP complementation assay is applicable for the visualisation of protein-protein interactions *in vivo*, making it a valuable tool for determining subcellular locations of various protein interactions which can provide

insight into functions of recently discovered protein complexes. However, there are limitations, e.g. the fact that once complemented the split GFP complex is irreversible (Cabantous and Waldo, 2006). Loss of dissociation of the fusion proteins prevents the application of the spGFP method from resolving fast and transient protein-protein interactions at the active zone. Finally, fluorescent protein fragments tend to associate with each other even though there exists no interaction between proteins fused to the fragments (Kerppola, 2006b). Nevertheless, one advantage of the spGFP system is the fact that association between fragments of fluorescent proteins produces a complex with intrinsic fluorescence, eliminating the need for immunostainings and thus enabling direct detection of protein complexes.

6. Supplementary

6.1 Appendices

6.1.1 Supplement figures

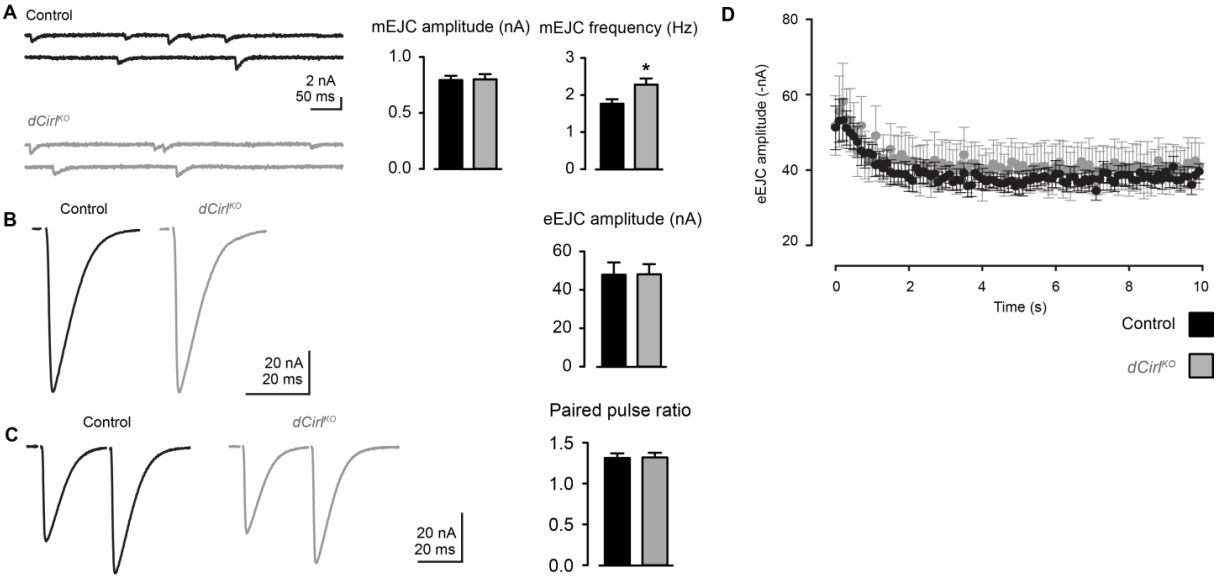

Fig S. 1 Electrophysiological analysis of *dCirl*^{KO} larvae.

Representative recordings of spontaneous single-vesicle fusion (mEJC) at pre- and postsynaptic sites of control and *dCirl*^{KO} larvae (A). mEJC amplitude seems unaltered, but the mEJC frequency is increased in *dCirl*^{KO} animals (A). Representative two-electrode voltage clamp (TEVC) recordings of eEJCs (B) as well as paired pulse analyses (C) revealed no difference between *dCirl*^{KO} and control animals. Normalized amplitudes at a 10-Hz stimulation for 10 s (D), both, control and mutant showed no difference in depression kinetics (work by D. Ljaschenko).

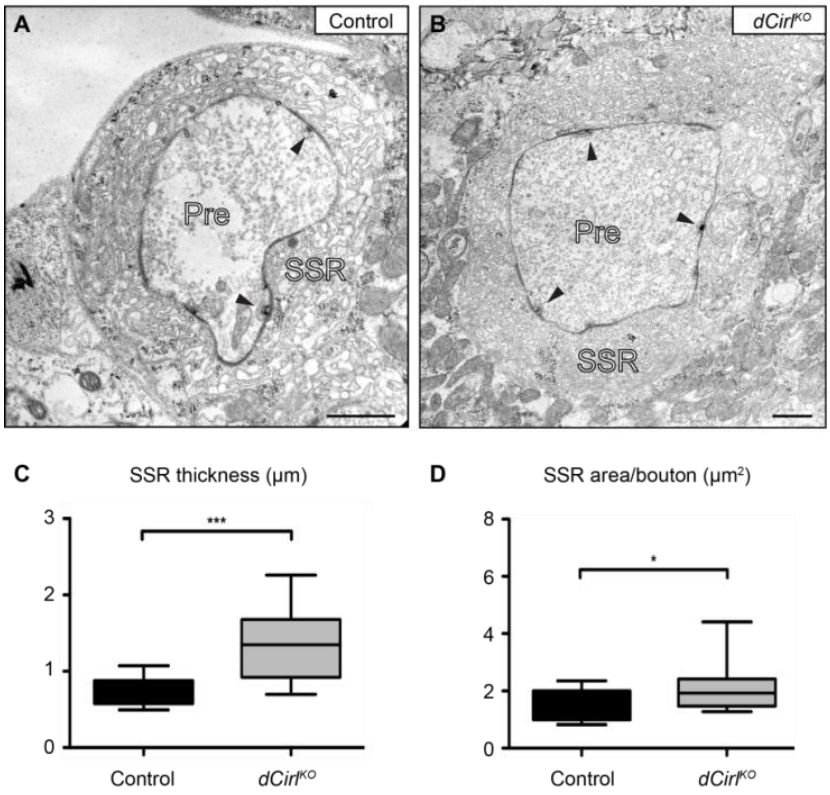

Fig S. 2 Electron microscopy characterisation of *dCirl*^{KO} larvae.

Electron microscopy cross-sections show boutons of control (A) and *dCirl*^{KO} larvae (B). Indicated are the presynaptic bouton (Pre) and the subsynaptic reticulum (SSR) surrounding the bouton and seems enlarged in *dCirl*^{KO} animals (B). Arrows indicate electron-dense T-bars, sites of elevated transmitter release. Statistical analysis of SRR thickness (C) and SSR area/bouton (D) reveal that the SSR of *dCirl*^{KO} larvae is significantly increased compared to control (work by N. Wagner).

6.1.2 Table of figures

6.1.3 Abbreviations

attB	attachment bacteria
attP	attachment plasmid
AZ	active zone
BiFC	bimolecular fluorescence complementation
bp	base pair
BRP	Bruchpilot
CAST	cytomatrix at the active zone-associated structural protein
cd	ciliary dilations
cDNA	complementary DNA
cho	chordotonal organ
Cirl	Ca^{2+}-independent receptor for α-latrotoxin
CNS	central nervous system
da	dendritic arborization
DLG	Discs-large
DNA	deoxyribonucleic acid
eEJC	evoked excitatory junctional current
EM	electron microscope
ERC	ELKS/Rab6-interacting protein/CAST
FasII	Fascilin II
FLRT	fibronectin leucin-rich repeat transmembrane
FMI	Flamingo/starry night
FRET	fluorescence resonance energy transfer
GAIN	GPCR autoproteolsyis inducing
GFP	green fluorescent protein
GluRIID	glutamate receptor IID
GPCR	G-protein coupled receptor
GPS	G-protein coupled receptor proteolytic site
GRASP	GFP reconstitution across synaptic partners
HEPES	4-(2-hydroxyethyl)-1-piperazineethanesulfonic acid
HL-3	hemolymph-like saline solution
HRM	hormone-binding motif
HRP	horseradish peroxidase
kb	kilo base

kDa	kilo Dalton
LPHN	latrophilin
MD	multidendtritic
MIP	myoinhibitory peptide
mM	millimolar
mRFP	monomeric red fluorescent protein
NCAMs	neuronal cell adhesion molecules
NMJ	neuromuscular junction
n-Syb	neuronal Synaptobrevin
OLF	olfactomedin
ORF	open reading frame
PBS	phosphate buffered saline
PCR	polymerase chain reaction
PFA	paraformaldehyde
PKD	polycystic kidney disease
PLC	Phospholipase C
PNS	peripheral nervous system
PSD	postsynaptic density
RBL	rhamnose-binding lectin
sc	sensory-ciliae
sn	sensory neurons
SNAP	soluble N-ethylmaleimide-sensitive factor attachment protein
SNARE	SNAP receptor
spGFP	split-GFP
SSR	subsynaptic reticulum
Syt	Synaptotagmin
Syt	Synaptotagmin
Syx	Syntaxin
Syx	Syntaxin
td	tracheal dendrite
TM	transmembrane
TRPV	transient receptor potential vanilloid
t-SNARE	target-SNARE
UAS	upstream activating sequence

UTR	untranslated region
VNC	ventral nerve cord
v-SNARE	vesicle-SNARE

6.1.4 Strain list

Listed are all strains that I have generated throughout my diploma and doctoral thesis

Strain	Genotype
LAT	
LAT53	*w^{1118}; $Cirl^{108/3A.2}${attP+ loxP+}$^{w-}$ att{Cirl::RFP $^{w+}$}[41] P{GD14785 w^{+}}v29969/CyOGFP w^{-}; +*
LAT56	*w^{1118}; $Cirl^{108/3A.2}${attP+ loxP+}$^{w-}$ att{Cirl::RFP $^{w+}$}[41]; +*
LAT72	*w^{1118}; $Cirl^{108/3A.2}${attP+ loxP+}$^{w-}$G7-Gal4/CyO GFP^{w-};MKRS,Sb/+orTM2*
LAT78	*w^{1118}; phiC31{KK108383}v100749/Cirl::FLAG $^{w+}$; Actin5Gal4/TM6b, Tb, Sb}*
LAT84	*w^{1118}; $Cirl^{108/3A.2}${attP+ loxP+}$^{w-}$ att{Gal4.2::p65d::dCirl $^{w+}$}; CyOGFPw-; MKRS,Sb/TM2*
LAT89	*w^{1118}; $Cirl^{108/3A.2}${attP+ loxP+}$^{w-}$, P{GD14785 w+}v29969/CyOGFP w-; MKRS,Sb/+*
LAT56	*w^{1118}; $Cirl^{108/3A.2}${attP+ loxP+}$^{w-}$ att{Cirl::RFP $^{w+}$}[41]; +*
LAT109	*w^{1118}; $dCirl^{KO}$/CyoGFPw^{-};Act-5C-GAL4w^{+}/TM6B, Tb*
LAT110	*w^{1118}; $dCirl^{KO}$/CyoGFPw^{-};elav-GAL4w^{+}/TM6B, Tb*
LAT111	*w^{1118}; $dCirl^{KO}$/CyoGFPw^{-}; 20xUAS-dCirl::Flag w^{+}/TM6B, Tb*
LAT113	*w^{1118};$dCirl^{KO}$/CyOGFPw^{-};P{y$^{+t7.7}$w^{+mC}=20XUAS-IVS-mCD8::GFP}attP2/TM6B, Tb*
LAT114	*w^{1118};$dCirl^{KO}$21-7-GAL4/CyOGFPw^{-};+*
LAT116	*w^{1118};$dCirl^{KO}$/CyOGFPw^{-}; iav- GAL4w^{+}/TM6B, Tb*
LAT117	*w^{1118} 5-40-GAL4; $dCirl^{KO}$/CyOGFPw^{-};+*
spGFP	
GR01	*w^{1118}; +; P{UAS::Venus::nSyb w+}/TM3(Sb)*
GR03	*w^{1118}; P{UAS::Venus::nSyb w+}/CyO; +*
GR09	*w^{1118}; +; P{UAS::Venus::Syx w+}/TM3(Sb)*
GR11	*w^{1118}; P{UAS::Venus::Syx w+}/CyO; +*
GR15	*w^{1118}; P{UAS::Venus::Syx w+}/FM7i; +; +*

GR16 *w^{1118}; +; P{UAS::Syx::RFP w+}/TM3(Sb)*

GR20 *w^{1118}; P{UAS::Syx::RFP w+}/CyO; +*

GR25 *w^{1118}; +; P{UAS::Venus::Syt w+}/TM3(Sb)*

GR27 *w^{1118}; P{UAS::Venus::Syt w+}/CyO; +*

GR35 *w^{1118}; P{UAS::Syt::RFP w+}/CyO; +*

GR38 *w^{1118}; +; P{UAS::Syt::RFP w+}/TM3(Sb)*

GR42 *w^{1118}; P{UAS::nSyb::RFP w+}/CyO; +*

GR44 *w^{1118}; +; P{UAS::nSyb::RFP w+}/TM3 (Sb)*

GR47 *w^{1118}; P{UAS::nSyb::RFP w+}/CyO; +*

GR48 *w^{1118}; P{UAS::spGFP1-10::Syx w+}/CyO; +*

GR49 *w^{1118}; +; P{UAS::spGFP1-10::Syx w+}/TM3 (Sb)*

GR50 *w^{1118}; P{UAS::spGFP1-10::Syx w+}/CyO; +*

GR51 *w^{1118}; P{UAS::spGFP1-10::Syx w+}/CyO; +*

GR54 *w^{1118}; +; P{UAS::spGFP1-10::Syx w+}/TM3 (Sb)*

GR55 *w^{1118}; P{UAS::spGFP11::Syx w+}/CyO*

GR57 *w^{1118}; P{UAS::spGFP11::Syx w+}/CyO*

GR59 *w^{1118}; +; P{UAS::spGFP11::Syx w+}/TM3(Sb)*

GR60 *w^{1118}; +; P{UAS::nSyb::spGFP11 w+}/TM3(Sb)*

GR61 *w^{1118}; +; P{UAS::nSyb::spGFP11 w+}/TM3(Sb)*

GR63 *w^{1118}; P{UAS::nSyb::spGFP11 w+}/CyO; +*

GR64 *w^{1118}; P{UAS::nSyb::spGFP11 w+}/CyO; +*

GR65 *w^{1118}; +; P{UAS::Syx::spGFP1-10 w+}/TM3(Sb)*

GR66 *w^{1118}; +; P{UAS::Syx::spGFP1-10 w+}/TM3(Sb)*

GR67 *w^{1118}; +; P{UAS::Syx::spGFP1-10 w+}/TM3(Sb)*

GR68 *w^{1118}; P{UAS::Syx::spGFP1-10 w+}/CyO; +*

GR69 *w^{1118}; +; P{UAS::Syx::spGFP11 w+}/TM3(Sb)*

GR73 *w^{1118}; P{UAS::Syx::spGFP11 w+}/CyO; +*

GR74 *w^{1118}; +; P{UAS::Syx::spGFP11 w+}/TM3 (Sb)*

GR75 *w^{1118}; P{UAS::Syx::spGFP11 w+}/CyO; +*

GR78 *w^{1118}; +; P{UAS::spGFP1-10::Syt w+}/TM3 (Sb)*

GR80 *w^{1118}; P{UAS::spGFP1-10::Syt w+}/CyO; +*

GR82 *w^{1118}; P{UAS::spGFP11::Syt w+}/CyO; +*

GR83 *w^{1118}; +; P{UAS::spGFP11::Syt w+}/TM3 (Sb)*

GR84 *w^{1118}; +; P{UAS::Syt::spGFP1-10 w+}/TM3 (Sb)*

GR85 *w^{1118}; +; P{UAS::Syt::spGFP1-10 w+}/TM3 (Sb)*

GR87 *w^{1118}; +; P{UAS::Syt::spGFP1-10 w+}/TM3 (Sb)*

GR88 *w^{1118}; P{UAS::Syt::spGFP1-10 w+}/CyO; +*

GR89 *w^{1118}; +; P{UAS::Syt::spGFP11 w+}/TM3 (Sb)*

GR91 *w^{1118}; P{UAS::spGFP1-10::Syb w+}/CyO; +*

GR92 *w^{1118}; +; P{UAS::spGFP1-10::Syb w+}/TM3 (Sb)*

GR94 *w^{1118}; +; P{UAS::spGFP1-10::Syb w+}/TM3 (Sb)*

GR96 *w^{1118}; +; P{UAS::spGFP1-10::Syb w+}/TM3 (Sb)*

GR99 *w^{1118}; +; P{UAS::spGFP11::Syb w+}/TM3 (Sb)*

GR100 *w^{1118}; +; P{UAS::spGFP11::Syb w+}/TM3 (Sb)*

GR102 *w^{1118}; P{UAS::spGFP11::Syb w+}/CyO; +*

GR103 *w^{1118}; P{UAS::spGFP11::Syb w+}/CyO; +*

GR104 *w^{1118}; +; P{UAS::spGFP11::Syb w+}/TM3 (Sb)*

GR108 *w^{1118}; P{UAS::Syb::spGFP1-10 w+}/CyO; +*

GR109 *w^{1118}; P{UAS::Syb::spGFP1-10 w+}/CyO; +*

GR110 *w^{1118}; +; P{UAS::Syb::spGFP1-10 w+}/TM3 (Sb)*

GR112 *w^{1118}; P{UAS::Syb::spGFP1-10 w+}/FM7i; +; +*

GR113 *w^{1118}; P{UAS::Syb::spGFP1-10 w+}/CyO; +*

GR114 *w^{1118}; +; P{UAS::Syb::spGFP1-10 w+}/TM3 (Sb)*

GR115 *w^{1118}; P{UAS::Syx-5xA-RFP w+}/CyO;+*

GR116 *w^{1118}; +; P{UAS::Syx-5xA-RFP w+}/TM3 (Sb)*

GR117 *w^{1118}; +; P{UAS::Syx-5xA-RFP w+}/TM3 (sb)*

GR118 *w^{1118}; P{UAS::Syx-5xA-RFP w+}/CyO;+*

GR119 *w^{1118}; +; P{UAS::Syx-5xA-RFP w+}/TM3 (sb)*

GR122 *w^{1118}; P{UAS::Syx-5xA-RFP w+}/CyO;+*

GR123 *w^{1118}; +; P{UAS::Syx-5xA-RFP w+}/TM3 (sb)*

GR124 *w^{1118}; P{UAS::Syx-5xA-RFP w+}/CyO;+*

GR129 *w^{1118}; +; P{UAS::Syt::spGFP11 w+}/TM3(Sb)*

GR130 *w^{1118}; +; P{UAS::Syt::spGFP11 w+}/TM3(Sb)*

GR131 *$y^{-}w^{-}$; In(2LR)Gla/CyO; lexAop-rCD2::GFP w^{+}*

GR132 *w^{1118}; +; P{UAS::Syt::spGFP11 w+}/TM3(Sb)*

GR133 *w^{1118}; +; P{UAS::spGFP1-10::BrpD3 w+}/TM3(Sb)*

GR134 *w^{1118}; P{UAS::spGFP1-10::BrpD3 w+}/CyO; +*

GR135 *w^{1118}; P{UAS::spGFP1-10::BrpD3 w+}/FM7i; +; +*

GR136 *w^{1118}; P{UAS::spGFP11::BrpD3 w+}/CyO; +*

GR137 *w^{1118}; +; P{UAS::spGFP11::BrpD3 w+}/TM3(Sb)*

GR138 *w^{1118}; P{UAS::BrpD3::spGFP1-10 w+}/CyO; +*

GR139 *w^{1118}; +; P{UAS::BrpD3::spGFP1-10 w+}/TM3(Sb)*

GR140 *w^{1118}; P{UAS::BrpD3::spGFP11w+}/CyO; +*

GR141 *w^{1118}; P{UAS::BrpD3::spGFP11w+}/CyO; +*

GR142 *w^{1118}; P{UAS::BrpD3::spGFP11w+}/CyO; +*

GR143 *w^{1118}; +; P{UAS::Venus::BrpD3 w+}/TM3(Sb)*

GR144 *w^{1118}; +; P{UAS::BrpD3::mRFP w+}/TM3(Sb)*

GR145 *w^{1118}; +; P{UAS::spGFP11::RFP w+}/TM3(Sb)*

GR146 *w^{1118}; +; P{UAS::spGFP11::RFP w+}/TM3(Sb)*

GR147 *w^{1118}; +; P{UAS::spGFP11::RFP w+}/TM3(Sb)*

GR148 *w^{1118}; +; P{UAS::spGFP11::RFP w+}/TM3(Sb)*

GR144 *w^{1118}; +; P{UAS::BrpD3::mRFP w+}/TM3(Sb)*

GR145 *w^{1118}; +; P{UAS::spGFP11::RFP w+}/TM3(Sb)*

GR146 *w^{1118}; +; P{UAS::spGFP11::RFP w+}/TM3(Sb)*

GR147 *w^{1118}; +; P{UAS::spGFP11::RFP w+}/TM3(Sb)*

GR148 *w^{1118}; +; P{UAS::spGFP11::RFP w+}/TM3(Sb)*

6.1.5 Plasmid list

Listed are all plasmids that I have engineered throughout my diploma and doctoral thesis

Plasmid	Description	Vector backbone
pJG2	Subcloning of *AgeI/SphI* fragment from pTWV into pMCS5	pMCS5
pJG3	PCR fragment using tl_42F-43R from pTL123 and cloned in pTVW using *AgeI/KpnI*	pTVW
pJG4	PCR fragment using tl_44F-41R from pTL124 and cloned in pTVW using *AgeI/KpnI*	pTVW
pJG5	LR reaction pTL141 and pJG3: N'-spGFP1-10-4xGGS-Syx-C'	pJG3
pJG6	LR reaction pTL141 and pJG4: N'-spGFP11-4xGGS-Syx-C'	pJG4
pJG7	Subcloning of PCR fragment using tl_38F-39R from pTL123 into pJG2 using *AgeI/SacI*	pJG2
pJG8	Subcloning of PCR fragment using tl_44F-41R from pTL124 into pJG2 using *AgeI/SacI*	pJG2
pJG9	Insertion of W(spGFP1-10) fragment from pJG7 into pTWV via *AgeI/SphI*	pTWV
pJG10	*Cast1* from rat was recombined into pDONR221.	pDONR221
pJG11	Subcloning of PCR fragment using tl_40F-41R from pTL124 into pJG2 using *AgeI/SacI*	pJG2
pJG12	Subcloning of PCR fragment using tl_40F-41R from pTL124 into pJG2 using *AgeI/SacI*	pJG2
pJG14	Insertion of W(spGFP11) fragment from pJG11 into pTWV via *AgeI/SphI*	pTWV
pJG15	LR reaction pTL140 and pJG14: N´-nSyb-(A)5-spGFP11-C´	pJG14
pJG16	LR reaction pTL144 and pJG9: N'-Syx-4xEAAAK-spGFP1-10-C'	pJG9
pJG17	LR reaction pTL144 and pJG14: N'-Syx-4xEAAAK-spGFP11-C'	pJG14
pJG18	LR-Reaction pTL143 and pJG3: N'-spGFP1-10-4xSGG-Syt-C'	pJG3

pJG19	LR reaction pTL143 and pJG4: N'-spGFP11-4xSGG-Syt-C'	pJG4
pJG20	LR reaction pTL142 and pJG9: N'-Syt-5xA-spGFP1-10-C'	pJG9
pJG21	LR reaction pTL142 and pJG14: N'-Syt-5xA-spGFP11-C'	pJG14
pJG22	LR reaction pTL137 and pJG3: N'-spGFP1-10-5xA-nSyb-C'	pJG3
pJG23	LR reaction pTL137 and pJG4: N'-spGFP11-5xA-nSyb-C'	pJG4
pJG24	LR reaction pTL40 and pJG9: N'-nSyb-5xA-spGFP1-10-C'	pJG9
pJG25	LR reaction pTL206 and pTWR	pTWR
pJG26	Destination vector with mammalian *synapsin* promoter and Gateway cassette	pSyn_Chopt_Dimer
pJG27	LR reaction pTL142 and pJG26: N'-Syt-5xA-pSynapsin-W2-C'	pSynapsin-W2
pJG28	Insertion of W(spGFP11) fragment from pJG14 into pSyn-W via *NotI/AgeI*	pJG26
pJG29	Insertion of W(spGFP1-10) fragment from pJG9 into pSyn-W via *NotI/AgeI*	pJG26
pJG30	Subcloning of PCR fragment using tl_138F and tl_139R from pJG3 and insertion into pJG26 via *NheI/NotI*	pJG26
pJG31	Subcloning of PCR fragment using tl_140F and tl_139R from pJG4 and insertion into pJG26 via *NheI/NotI*	pJG26
pJG32	LR reaction between pJG10 and pJG30	pJG30
pJG33	LR reaction between pJG10 and pJG31	pJG31
pJG34	LR reaction between pTL226 and pJG3	pJG3
pJG35	LR reaction between pTL226 and pJG4	pJG4
pJG36	LR reaction between pTL226 and pJG9	pJG9
pJG37	LR reaction between pTL226 and pJG14	pJG14
pJG38	LR reaction between pTL226 and TVW	TVW
pJG39	LR reaction between pTL226 and TWR	TWR
pJG40	Subcloning of PCR fragment using jg_12F and jg_13R from pTL220 and insertion into pEntry via *DraI/XhoI*	pEntry1ad
pJG41	Subcloning of PCR fragment using jg_14F and jg_15R from pTL220 and insertion into pEntry via *DraI/XhoI*	pEntry1ad
pJG42	Entry clone for RIM splice variant 1	pEntry1ad
pJG43	PAT3-removal from pJG4	pTVW
pJG44	LR reaction pJG43xpTL137: N'-spGFP11-5xA-nSyb-C'	pJG43

pJG45	LR reaction pJG43xpTL141: N'-spGFP11-4xGGS-Syx-C'	pJG43
pJG46	LR reaction pJG43xpTL143: N'-spGFP11-4xSGG-Syt-C'	pJG43
pJG47	Entry vector containing *dCirl* cDNA from *D. melanogaster*	pEntry1ad
pJG48	LR reaction pJG47 and AVW	AVW
pJG49	Entry clone for L172A/E173A open syx mutation of pTL148 using jg_37F and jg_38R - Cloning of Open Syx into pEntry using *DraI/XhoI*	pEntry1ad
pJG50	LR reaction pJG49 and pTWF - Stop codon	pTWF
pJG51	LR reaction pTWV and pJG49 - Stop codon	pTWV
pJG52	Cloning of Open Syx from pJG51 into pTL206 via *EcoRI/NdeI*	pTL206
pJG53	LR reaction pJG52 and pTWV	pTWV
pJG54	LR reaction pJG52 and pTWF	pTWF
pJG55	Subcloning of PCR fragment using jg_45F and jg_46R from pTL149 and insertion into pTW-attB via *EcoRI/NheI*	pTWattB

6.2 Acknowledgements

First and foremost, I would like to thank my supervisor Dr. Tobias Langenhan for giving me the opportunity to conduct these studies in his research group and for sharing his scientific experience and advising me on my project.

I extend my gratitude to Prof. Dr. Manfred Heckmann for the opportunity to stay in his laboratory for the PhD and for being the first referee of this thesis. I also would like to thank Dr. Robert Kittel for sharing his expertise and Prof. Dr. Christian Stigloher for being the second referee of this thesis.

I am grateful to the staff and all members of the Institute of Physiology for any kind of academic, technical and administrative support, especially to Maria Oppmann, Brigitte Trost, Uta Maas and Claudia Wirth.

Moreover, I would like to thank my present and former colleagues, particularly Nici, Nadine, Dimi and Martin for their friendship and support, for having a good time – not only in the laboratory.

Finally, I would like to take this opportunity to express my gratefulness to my parents and grandparents for their unconditional support and for keeping me grounded. Last, but by no means least: thank you *Herzl*.

6.3 Curriculum vitae

Personal information:

Name: Jennifer Gehring
Date of birth: 1985/11/06
Place of birth: Würzburg
Nationality: German

Scientific Education:

2010-2014 PhD study at the University of Würzburg, Institute of Physiology, Department of Neurophysiology

2013 Poster presentation at the 92th Annual meeting of the Deutsche Physiologische Gesellschaft (DPG) in Heidelberg

2012 Co-organizer of the 6th Adhesion-GPCR workshop at the Institute of Physiology, Department of Neurophysiology

2012 Poster presentation at the 91th Annual meeting of the Deutsche Physiologische Gesellschaft (DPG) in Dresden

2010 Diploma thesis at the University of Würzburg, Institute of Physiology, Department of Neurophysiology: “Development of optical sensors for vesicle-membrane interactions”

2004-2010 Study of Biology at the University of Würzburg

6.4 Bibliography

Adams MD et al. (2000) The genome sequence of Drosophila melanogaster. Science 287:2185-2195.

Arac D, Boucard AA, Bolliger MF, Nguyen J, Soltis SM, Sudhof TC, Brunger AT (2012) A novel evolutionarily conserved domain of cell-adhesion GPCRs mediates autoproteolysis. The EMBO journal 31:1364-1378.

Aravamudan B, Broadie K (2003) Synaptic Drosophila UNC-13 is regulated by antagonistic G-protein pathways via a proteasome-dependent degradation mechanism. Journal of neurobiology 54:417-438.

Atwood HL (2006) Neuroscience. Gatekeeper at the synapse. Science 312:1008-1009.

Atwood HL, Govind CK, Wu CF (1993) Differential ultrastructure of synaptic terminals on ventral longitudinal abdominal muscles in Drosophila larvae. Journal of neurobiology 24:1008-1024.

Aust G (2010) Adhesion-GPCRS in tumorigenesis. Advances in experimental medicine and biology 706:109-120.

Bate M, Landgraf M, Ruiz Gomez Bate M (1999) Development of larval body wall muscles. International review of neurobiology 43:25-44.

Bjarnadottir TK, Fredriksson R, Hoglund PJ, Gloriam DE, Lagerstrom MC, Schioth HB (2004) The human and mouse repertoire of the adhesion family of G-protein-coupled receptors. Genomics 84:23-33.

Bockaert J, Pin JP (1999) Molecular tinkering of G protein-coupled receptors: an evolutionary success. The EMBO journal 18:1723-1729.

Bodmer, Jan (1987) Morphological differentiation of the embryonic peripheral neurons in Drosophila. Developmental biology 196:69-77.

Boucard AA, Ko J, Sudhof TC (2012) High affinity neurexin binding to cell adhesion G-protein-coupled receptor CIRL1/latrophilin-1 produces an intercellular adhesion complex. The Journal of biological chemistry 287:9399-9413.

Brand AH, Perrimon N (1993) Targeted gene expression as a means of altering cell fates and generating dominant phenotypes. Development 118:401-415.

Brewster R, Bodmer R (1995) Origin and specification of type II sensory neurons in Drosophila. Development 121:2923-2936.

Budnik V, Koh YH, Guan B, Hartmann B, Hough C, Woods D, Gorczyca M (1996) Regulation of synapse structure and function by the Drosophila tumor suppressor gene dlg. Neuron 17:627-640.

Burn TC, Vigoreaux JO, Tobin SL (1989) Alternative 5C actin transcripts are localized in different patterns during Drosophila embryogenesis. Developmental biology 131:345-355.

Cabantous S, Waldo GS (2006) In vivo and in vitro protein solubility assays using split GFP. Nature methods 3:845-854.

Cabantous S, Terwilliger TC, Waldo GS (2005) Protein tagging and detection with engineered self-assembling fragments of green fluorescent protein. Nature biotechnology 23:102-107.

Caldwell JC, Miller MM, Wing S, Soll DR, Eberl DF (2003) Dynamic analysis of larval locomotion in Drosophila chordotonal organ mutants. Proceedings of the National Academy of Sciences of the United States of America 100:16053-16058.

Capogna M, Volynski KE, Emptage NJ, Ushkaryov YA (2003) The alpha-latrotoxin mutant LTXN4C enhances spontaneous and evoked transmitter release in

CA3 pyramidal neurons. The Journal of neuroscience : the official journal of the Society for Neuroscience 23:4044-4053.
Chen WS, Antic D, Matis M, Logan CY, Povelones M, Anderson GA, Nusse R, Axelrod JD (2008) Asymmetric homotypic interactions of the atypical cadherin flamingo mediate intercellular polarity signaling. Cell 133:1093-1105.
Clegg RM (1995) Fluorescence resonance energy transfer. Curr Opin Biotechnol 6:103-110.
Daniels RW, Gelfand MV, Collins CA, DiAntonio A (2008) Visualizing glutamatergic cell bodies and synapses in Drosophila larval and adult CNS. The Journal of comparative neurology 508:131-152.
Davletov BA, Shamotienko OG, Lelianova VG, Grishin EV, Ushkaryov YA (1996) Isolation and biochemical characterization of a Ca2+-independent alpha-latrotoxin-binding protein. The Journal of biological chemistry 271:23239-23245.
Eberl DF (1999) Feeling the vibes: chordotonal mechanisms in insect hearing. Curr Opin Neurobiol 9:389-393.
Eberl DF, Boekhoff-Falk G (2007) Development of Johnston's organ in Drosophila. The International journal of developmental biology 51:679-687.
Eberl DF, Hardy RW, Kernan MJ (2000) Genetically similar transduction mechanisms for touch and hearing in Drosophila. The Journal of neuroscience : the official journal of the Society for Neuroscience 20:5981-5988.
Fan JY, Cui ZQ, Wei HP, Zhang ZP, Zhou YF, Wang YP, Zhang XE (2008) Split mCherry as a new red bimolecular fluorescence complementation system for visualizing protein-protein interactions in living cells. Biochemical and biophysical research communications 367:47-53.
Feinberg EH, Vanhoven MK, Bendesky A, Wang G, Fetter RD, Shen K, Bargmann CI (2008) GFP Reconstitution Across Synaptic Partners (GRASP) defines cell contacts and synapses in living nervous systems. Neuron 57:353-363.
Ferguson SS (2001) Evolving concepts in G protein-coupled receptor endocytosis: the role in receptor desensitization and signaling. Pharmacological reviews 53:1-24.
Fire A, Xu S, Montgomery MK, Kostas SA, Driver SE, Mello CC (1998) Potent and specific genetic interference by double-stranded RNA in Caenorhabditis elegans. Nature 391:806-811.
Fischer R (2011) Location and function of the latrophilin homolog *dCirl* in *Drosophila melanogaster*.1-90.
Flower DR (1999) Modelling G-protein-coupled receptors for drug design. Biochimica et biophysica acta 1422:207-234.
Fouquet W, Owald D, Wichmann C, Mertel S, Depner H, Dyba M, Hallermann S, Kittel RJ, Eimer S, Sigrist SJ (2009) Maturation of active zone assembly by Drosophila Bruchpilot. The Journal of cell biology 186:129-145.
Fredriksson R, Lagerstrom MC, Lundin LG, Schioth HB (2003) The G-protein-coupled receptors in the human genome form five main families. Phylogenetic analysis, paralogon groups, and fingerprints. Molecular pharmacology 63:1256-1272.
Gehring J (2010) Development of optical sensors for synaptic vesicle-membrane interactions in *Drosophila melanogaster*. In.
Gong Z, Liu J, Guo C, Zhou Y, Teng Y, Liu L (2010) Two pairs of neurons in the central brain control Drosophila innate light preference. Science 330:499-502.
Gong Z, Son W, Chung YD, Kim J, Shin DW, McClung CA, Lee Y, Lee HW, Chang DJ, Kaang BK, Cho H, Oh U, Hirsh J, Kernan MJ, Kim C (2004) Two

interdependent TRPV channel subunits, inactive and Nanchung, mediate hearing in Drosophila. The Journal of neuroscience : the official journal of the Society for Neuroscience 24:9059-9066.

Gorczyca M, Augart C, Budnik V (1993) Insulin-like receptor and insulin-like peptide are localized at neuromuscular junctions in Drosophila. The Journal of neuroscience : the official journal of the Society for Neuroscience 13:3692-3704.

Gordon MD, Scott K (2009) Motor control in a Drosophila taste circuit. Neuron 61:373-384.

Groth AC, Fish M, Nusse R, Calos MP (2004) Construction of transgenic Drosophila by using the site-specific integrase from phage phiC31. Genetics 166:1775-1782.

Hadjantonakis AK, Formstone CJ, Little PF (1998) mCelsr1 is an evolutionarily conserved seven-pass transmembrane receptor and is expressed during mouse embryonic development. Mechanisms of development 78:91-95.

Hamann J, Vogel B, van Schijndel GM, van Lier RA (1996) The seven-span transmembrane receptor CD97 has a cellular ligand (CD55, DAF). The Journal of experimental medicine 184:1185-1189.

Heilemann M, van de Linde S, Schuttpelz M, Kasper R, Seefeldt B, Mukherjee A, Tinnefeld P, Sauer M (2008) Subdiffraction-resolution fluorescence imaging with conventional fluorescent probes. Angewandte Chemie 47:6172-6176.

Heisenberg M (1998) What do the mushroom bodies do for the insect brain? an introduction. Learning & memory 5:1-10.

Hell SW (2003) Toward fluorescence nanoscopy. Nature biotechnology 21:1347-1355.

Hoang B, Chiba A (2001) Single-cell analysis of Drosophila larval neuromuscular synapses. Developmental biology 229:55-70.

Hu CD, Grinberg AV, Kerppola TK (2006) Visualization of protein interactions in living cells using bimolecular fluorescence complementation (BiFC) analysis. Curr Protoc Cell Biol Chapter 21:Unit 21 23.

Huang J, Zhou W, Watson AM, Jan YN, Hong Y (2008) Efficient ends-out gene targeting in Drosophila. Genetics 180:703-707.

Huang J, Zhou W, Dong W, Watson AM, Hong Y (2009) From the Cover: Directed, efficient, and versatile modifications of the Drosophila genome by genomic engineering. Proceedings of the National Academy of Sciences of the United States of America 106:8284-8289.

Hughes CL, Thomas JB (2007) A sensory feedback circuit coordinates muscle activity in Drosophila. Molecular and cellular neurosciences 35:383-396.

Hughes J, Ward CJ, Aspinwall R, Butler R, Harris PC (1999) Identification of a human homologue of the sea urchin receptor for egg jelly: a polycystic kidney disease-like protein. Human molecular genetics 8:543-549.

Ichtchenko K, Khvotchev M, Kiyatkin N, Simpson L, Sugita S, Sudhof TC (1998) alpha-latrotoxin action probed with recombinant toxin: receptors recruit alpha-latrotoxin but do not transduce an exocytotic signal. The EMBO journal 17:6188-6199.

Ichtchenko K, Bittner MA, Krasnoperov V, Little AR, Chepurny O, Holz RW, Petrenko AG (1999) A novel ubiquitously expressed alpha-latrotoxin receptor is a member of the CIRL family of G-protein-coupled receptors. The Journal of biological chemistry 274:5491-5498.

Jarman AP (2002) Studies of mechanosensation using the fly. Human molecular genetics 11:1215-1218.

Jarman AP, Grau Y, Jan LY, Jan YN (1993) atonal is a proneural gene that directs chordotonal organ formation in the Drosophila peripheral nervous system. Cell 73:1307-1321.

Jia XX, Gorczyca M, Budnik V (1993) Ultrastructure of neuromuscular junctions in Drosophila: comparison of wild type and mutants with increased excitability. Journal of neurobiology 24:1025-1044.

Johansen J, Halpern ME, Johansen KM, Keshishian H (1989) Stereotypic morphology of glutamatergic synapses on identified muscle cells of Drosophila larvae. The Journal of neuroscience : the official journal of the Society for Neuroscience 9:710-725.

Kamikouchi A, Shimada T, Ito K (2006) Comprehensive classification of the auditory sensory projections in the brain of the fruit fly Drosophila melanogaster. The Journal of comparative neurology 499:317-356.

Kee HJ, Koh JT, Kim MY, Ahn KY, Kim JK, Bae CS, Park SS, Kim KK (2002) Expression of brain-specific angiogenesis inhibitor 2 (BAI2) in normal and ischemic brain: involvement of BAI2 in the ischemia-induced brain angiogenesis. Journal of cerebral blood flow and metabolism : official journal of the International Society of Cerebral Blood Flow and Metabolism 22:1054-1067.

Kee HJ, Ahn KY, Choi KC, Won Song J, Heo T, Jung S, Kim JK, Bae CS, Kim KK (2004) Expression of brain-specific angiogenesis inhibitor 3 (BAI3) in normal brain and implications for BAI3 in ischemia-induced brain angiogenesis and malignant glioma. FEBS letters 569:307-316.

Keil TA (1997) Functional morphology of insect mechanoreceptors. Microscopy research and technique 39:506-531.

Kernan M, Cowan D, Zuker C (1994) Genetic dissection of mechanosensory transduction: mechanoreception-defective mutations of Drosophila. Neuron 12:1195-1206.

Kerppola TK (2006a) Complementary methods for studies of protein interactions in living cells. Nature methods 3:969-971.

Kerppola TK (2006b) Design and implementation of bimolecular fluorescence complementation (BiFC) assays for the visualization of protein interactions in living cells. Nature protocols 1:1278-1286.

Khorana HG (1992) Rhodopsin, photoreceptor of the rod cell. An emerging pattern for structure and function. The Journal of biological chemistry 267:1-4.

Kim J, Chung YD, Park DY, Choi S, Shin DW, Soh H, Lee HW, Son W, Yim J, Park CS, Kernan MJ, Kim C (2003) A TRPV family ion channel required for hearing in Drosophila. Nature 424:81-84.

Kittel RJ, Wichmann C, Rasse TM, Fouquet W, Schmidt M, Schmid A, Wagh DA, Pawlu C, Kellner RR, Willig KI, Hell SW, Buchner E, Heckmann M, Sigrist SJ (2006) Bruchpilot promotes active zone assembly, Ca2+ channel clustering, and vesicle release. Science 312:1051-1054.

Kobilka BK, Deupi X (2007) Conformational complexity of G-protein-coupled receptors. Trends in pharmacological sciences 28:397-406.

Koh JT, Lee ZH, Ahn KY, Kim JK, Bae CS, Kim HH, Kee HJ, Kim KK (2001) Characterization of mouse brain-specific angiogenesis inhibitor 1 (BAI1) and phytanoyl-CoA alpha-hydroxylase-associated protein 1, a novel BAI1-binding protein. Brain research Molecular brain research 87:223-237.

Krasnoperov V, Lu Y, Buryanovsky L, Neubert TA, Ichtchenko K, Petrenko AG (2002) Post-translational proteolytic processing of the calcium-independent receptor of alpha-latrotoxin (CIRL), a natural chimera of the cell adhesion

protein and the G protein-coupled receptor. Role of the G protein-coupled receptor proteolysis site (GPS) motif. The Journal of biological chemistry 277:46518-46526.

Krasnoperov VG, Beavis R, Chepurny OG, Little AR, Plotnikov AN, Petrenko AG (1996) The calcium-independent receptor of alpha-latrotoxin is not a neurexin. Biochemical and biophysical research communications 227:868-875.

Krasnoperov VG, Bittner MA, Beavis R, Kuang Y, Salnikow KV, Chepurny OG, Little AR, Plotnikov AN, Wu D, Holz RW, Petrenko AG (1997) alpha-Latrotoxin stimulates exocytosis by the interaction with a neuronal G-protein-coupled receptor. Neuron 18:925-937.

Kwon Y, Shen WL, Shim HS, Montell C (2010) Fine thermotactic discrimination between the optimal and slightly cooler temperatures via a TRPV channel in chordotonal neurons. The Journal of neuroscience : the official journal of the Society for Neuroscience 30:10465-10471.

Lagerstrom MC, Schioth HB (2008) Structural diversity of G protein-coupled receptors and significance for drug discovery. Nature reviews Drug discovery 7:339-357.

Lahey T, Gorczyca M, Jia XX, Budnik V (1994) The Drosophila tumor suppressor gene dlg is required for normal synaptic bouton structure. Neuron 13:823-835.

Landgraf M, Thor S (2006) Development of Drosophila motoneurons: specification and morphology. Seminars in cell & developmental biology 17:3-11.

Landgraf M, Bossing T, Technau GM, Bate M (1997) The origin, location, and projections of the embryonic abdominal motorneurons of Drosophila. The Journal of neuroscience : the official journal of the Society for Neuroscience 17:9642-9655.

Lang J, Ushkaryov Y, Grasso A, Wollheim CB (1998) Ca2+-independent insulin exocytosis induced by alpha-latrotoxin requires latrophilin, a G protein-coupled receptor. The EMBO journal 17:648-657.

Lange M, Norton W, Coolen M, Chaminade M, Merker S, Proft F, Schmitt A, Vernier P, Lesch KP, Bally-Cuif L (2012) The ADHD-susceptibility gene lphn3.1 modulates dopaminergic neuron formation and locomotor activity during zebrafish development. Molecular psychiatry 17:946-954.

Langenhan T, Promel S, Mestek L, Esmaeili B, Waller-Evans H, Hennig C, Kohara Y, Avery L, Vakonakis I, Schnabel R, Russ AP (2009) Latrophilin signaling links anterior-posterior tissue polarity and oriented cell divisions in the C. elegans embryo. Developmental cell 17:494-504.

Lawrence PA, Struhl G, Casal J (2007) Planar cell polarity: one or two pathways? Nature reviews Genetics 8:555-563.

Lelianova VG, Davletov BA, Sterling A, Rahman MA, Grishin EV, Totty NF, Ushkaryov YA (1997) Alpha-latrotoxin receptor, latrophilin, is a novel member of the secretin family of G protein-coupled receptors. The Journal of biological chemistry 272:21504-21508.

Li A, Tian X, Sung SW, Somlo S (2003) Identification of two novel polycystic kidney disease-1-like genes in human and mouse genomes. Genomics 81:596-608.

Lin HH, Chang GW, Davies JQ, Stacey M, Harris J, Gordon S (2004) Autocatalytic cleavage of the EMR2 receptor occurs at a conserved G protein-coupled receptor proteolytic site motif. The Journal of biological chemistry 279:31823-31832.

Liu M, Parker RM, Darby K, Eyre HJ, Copeland NG, Crawford J, Gilbert DJ, Sutherland GR, Jenkins NA, Herzog H (1999) GPR56, a novel secretin-like human G-protein-coupled receptor gene. Genomics 55:296-305.

Martinez-Padron M, Ferrus A (1997) Presynaptic recordings from Drosophila: correlation of macroscopic and single-channel K+ currents. The Journal of neuroscience : the official journal of the Society for Neuroscience 17:3412-3424.

Matsushita H, Lelianova VG, Ushkaryov YA (1999) The latrophilin family: multiply spliced G protein-coupled receptors with differential tissue distribution. FEBS letters 443:348-352.

McMillan DR, Kayes-Wandover KM, Richardson JA, White PC (2002) Very large G protein-coupled receptor-1, the largest known cell surface protein, is highly expressed in the developing central nervous system. The Journal of biological chemistry 277:785-792.

Mee CJ, Tomlinson SR, Perestenko PV, De Pomerai D, Duce IR, Usherwood PN, Bell DR (2004) Latrophilin is required for toxicity of black widow spider venom in Caenorhabditis elegans. The Biochemical journal 378:185-191.

Monastirioti M, Gorczyca M, Rapus J, Eckert M, White K, Budnik V (1995) Octopamine immunoreactivity in the fruit fly Drosophila melanogaster. The Journal of comparative neurology 356:275-287.

Monk KR, Naylor SG, Glenn TD, Mercurio S, Perlin JR, Dominguez C, Moens CB, Talbot WS (2009) A G protein-coupled receptor is essential for Schwann cells to initiate myelination. Science 325:1402-1405.

Mori K, Kanemura Y, Fujikawa H, Nakano A, Ikemoto H, Ozaki I, Matsumoto T, Tamura K, Yokota M, Arita N (2002) Brain-specific angiogenesis inhibitor 1 (BAI1) is expressed in human cerebral neuronal cells. Neuroscience research 43:69-74.

Nagai T, Ibata K, Park ES, Kubota M, Mikoshiba K, Miyawaki A (2002) A variant of yellow fluorescent protein with fast and efficient maturation for cell-biological applications. Nature biotechnology 20:87-90.

Nordstrom KJ, Lagerstrom MC, Waller LM, Fredriksson R, Schioth HB (2009) The Secretin GPCRs descended from the family of Adhesion GPCRs. Molecular biology and evolution 26:71-84.

O'Sullivan ML, de Wit J, Savas JN, Comoletti D, Otto-Hitt S, Yates JR, 3rd, Ghosh A (2012) FLRT proteins are endogenous latrophilin ligands and regulate excitatory synapse development. Neuron 73:903-910.

Oldham WM, Hamm HE (2008) Heterotrimeric G protein activation by G-protein-coupled receptors. Nature reviews Molecular cell biology 9:60-71.

Oohashi T, Zhou XH, Feng K, Richter B, Morgelin M, Perez MT, Su WD, Chiquet-Ehrismann R, Rauch U, Fassler R (1999) Mouse ten-m/Odz is a new family of dimeric type II transmembrane proteins expressed in many tissues. The Journal of cell biology 145:563-577.

Patra C, van Amerongen MJ, Ghosh S, Ricciardi F, Sajjad A, Novoyatleva T, Mogha A, Monk KR, Muhlfeld C, Engel FB (2013) Organ-specific function of adhesion G protein-coupled receptor GPR126 is domain-dependent. Proceedings of the National Academy of Sciences of the United States of America 110:16898-16903.

Piao X, Hill RS, Bodell A, Chang BS, Basel-Vanagaite L, Straussberg R, Dobyns WB, Qasrawi B, Winter RM, Innes AM, Voit T, Ross ME, Michaud JL, Descarie JC, Barkovich AJ, Walsh CA (2004) G protein-coupled receptor-dependent development of human frontal cortex. Science 303:2033-2036.

Pierce KL, Premont RT, Lefkowitz RJ (2002) Seven-transmembrane receptors. Nature reviews Molecular cell biology 3:639-650.

Ponting CP, Hofmann K, Bork P (1999) A latrophilin/CL-1-like GPS domain in polycystin-1. Current biology : CB 9:R585-588.

Prokop A, Meinertzhagen IA (2006) Development and structure of synaptic contacts in Drosophila. Seminars in cell & developmental biology 17:20-30.

Promel S, Langenhan T, Arac D (2013) Matching structure with function: the GAIN domain of Adhesion-GPCR and PKD1-like proteins. Trends in pharmacological sciences 34:470-478.

Promel S, Frickenhaus M, Hughes S, Mestek L, Staunton D, Woollard A, Vakonakis I, Schoneberg T, Schnabel R, Russ AP, Langenhan T (2012) The GPS motif is a molecular switch for bimodal activities of adhesion class G protein-coupled receptors. Cell reports 2:321-331.

Qin G, Schwarz T, Kittel RJ, Schmid A, Rasse TM, Kappei D, Ponimaskin E, Heckmann M, Sigrist SJ (2005) Four different subunits are essential for expressing the synaptic glutamate receptor at neuromuscular junctions of Drosophila. The Journal of neuroscience : the official journal of the Society for Neuroscience 25:3209-3218.

Rahman MA, Ashton AC, Meunier FA, Davletov BA, Dolly JO, Ushkaryov YA (1999) Norepinephrine exocytosis stimulated by alpha-latrotoxin requires both external and stored Ca2+ and is mediated by latrophilin, G proteins and phospholipase C. Philosophical transactions of the Royal Society of London Series B, Biological sciences 354:379-386.

Richmond JE, Broadie KS (2002) The synaptic vesicle cycle: exocytosis and endocytosis in Drosophila and C. elegans. Curr Opin Neurobiol 12:499-507.

Richmond JE, Davis WS, Jorgensen EM (1999) UNC-13 is required for synaptic vesicle fusion in C. elegans. Nature neuroscience 2:959-964.

Rohrbough J, Broadie K (2005) Lipid regulation of the synaptic vesicle cycle. Nature reviews Neuroscience 6:139-150.

Rosenmund C (2003) Molecular mechanisms of active zone function. Current Opinion in Neurobiology 13:509-519.

Rubin GM, Spradling AC (1983) Vectors for P element-mediated gene transfer in Drosophila. Nucleic Acids Res 11:6341-6351.

Santos JG, Vomel M, Struck R, Homberg U, Nassel DR, Wegener C (2007) Neuroarchitecture of peptidergic systems in the larval ventral ganglion of Drosophila melanogaster. PloS one 2:e695.

Sanyal S (2009) Genomic mapping and expression patterns of C380, OK6 and D42 enhancer trap lines in the larval nervous system of Drosophila. Gene Expr Patterns 9:371-380.

Schuster CM, Davis GW, Fetter RD, Goodman CS (1996) Genetic dissection of structural and functional components of synaptic plasticity. II. Fasciclin II controls presynaptic structural plasticity. Neuron 17:655-667.

Shima Y, Copeland NG, Gilbert DJ, Jenkins NA, Chisaka O, Takeichi M, Uemura T (2002) Differential expression of the seven-pass transmembrane cadherin genes Celsr1-3 and distribution of the Celsr2 protein during mouse development. Developmental dynamics : an official publication of the American Association of Anatomists 223:321-332.

Silva JP, Ushkaryov YA (2010) The latrophilins, "split-personality" receptors. Advances in experimental medicine and biology 706:59-75.

Silva JP, Lelianova V, Hopkins C, Volynski KE, Ushkaryov Y (2009) Functional cross-interaction of the fragments produced by the cleavage of distinct adhesion G-protein-coupled receptors. The Journal of biological chemistry 284:6495-6506.

Silva JP, Lelianova VG, Ermolyuk YS, Vysokov N, Hitchen PG, Berninghausen O, Rahman MA, Zangrandi A, Fidalgo S, Tonevitsky AG, Dell A, Volynski KE, Ushkaryov YA (2011) Latrophilin 1 and its endogenous ligand Lasso/teneurin-2 form a high-affinity transsynaptic receptor pair with signaling capabilities. Proceedings of the National Academy of Sciences of the United States of America 108:12113-12118.

Sollner T, Bennett MK, Whiteheart SW, Scheller RH, Rothman JE (1993) A protein assembly-disassembly pathway in vitro that may correspond to sequential steps of synaptic vesicle docking, activation, and fusion. Cell 75:409-418.

Song W, Onishi M, Jan LY, Jan YN (2007) Peripheral multidendritic sensory neurons are necessary for rhythmic locomotion behavior in Drosophila larvae. Proceedings of the National Academy of Sciences of the United States of America 104:5199-5204.

Stacey M, Chang GW, Davies JQ, Kwakkenbos MJ, Sanderson RD, Hamann J, Gordon S, Lin HH (2003) The epidermal growth factor-like domains of the human EMR2 receptor mediate cell attachment through chondroitin sulfate glycosaminoglycans. Blood 102:2916-2924.

Strokes N, Piao X (2010) Adhesion-GPCRs in the CNS. Advances in experimental medicine and biology 706:87-97.

Sudhof TC (2001) alpha-Latrotoxin and its receptors: neurexins and CIRL/latrophilins. Annual review of neuroscience 24:933-962.

Sudhof TC (2004) The synaptic vesicle cycle. Annual review of neuroscience 27:509-547.

Sugita S, Ichtchenko K, Khvotchev M, Sudhof TC (1998) alpha-Latrotoxin receptor CIRL/latrophilin 1 (CL1) defines an unusual family of ubiquitous G-protein-linked receptors. G-protein coupling not required for triggering exocytosis. The Journal of biological chemistry 273:32715-32724.

Suster ML, Bate M (2002) Embryonic assembly of a central pattern generator without sensory input. Nature 416:174-178.

Thomas U, Kim E, Kuhlendahl S, Koh YH, Gundelfinger ED, Sheng M, Garner CC, Budnik V (1997) Synaptic clustering of the cell adhesion molecule fasciclin II by discs-large and its role in the regulation of presynaptic structure. Neuron 19:787-799.

Tissir F, Bar I, Jossin Y, De Backer O, Goffinet AM (2005) Protocadherin Celsr3 is crucial in axonal tract development. Nature neuroscience 8:451-457.

Tobaben S, Sudhof TC, Stahl B (2002) Genetic analysis of alpha-latrotoxin receptors reveals functional interdependence of CIRL/latrophilin 1 and neurexin 1 alpha. The Journal of biological chemistry 277:6359-6365.

Tomarev SI, Nakaya N (2009) Olfactomedin domain-containing proteins: possible mechanisms of action and functions in normal development and pathology. Molecular neurobiology 40:122-138.

Tracey WD, Jr. (2007) Genetics Can Be Painless: Molecular Genetic Analysis of Nociception in Drosophila. In: TRP Ion Channel Function in Sensory Transduction and Cellular Signaling Cascades (Liedtke WB, Heller S, eds). Boca Raton (FL).

Tracey WD, Jr., Wilson RI, Laurent G, Benzer S (2003) painless, a Drosophila gene essential for nociception. Cell 113:261-273.

Tucker RP, Kenzelmann D, Trzebiatowska A, Chiquet-Ehrismann R (2007) Teneurins: transmembrane proteins with fundamental roles in development. The international journal of biochemistry & cell biology 39:292-297.

Tymiak AA, Norman JA, Bolgar M, DiDonato GC, Lee H, Parker WL, Lo LC, Berova N, Nakanishi K, Haber E, et al. (1993) Physicochemical characterization of a ouabain isomer isolated from bovine hypothalamus. Proceedings of the National Academy of Sciences of the United States of America 90:8189-8193.

Ushkaryov YA, Petrenko AG, Geppert M, Sudhof TC (1992) Neurexins: synaptic cell surface proteins related to the alpha-latrotoxin receptor and laminin. Science 257:50-56.

Usui T, Shima Y, Shimada Y, Hirano S, Burgess RW, Schwarz TL, Takeichi M, Uemura T (1999) Flamingo, a seven-pass transmembrane cadherin, regulates planar cell polarity under the control of Frizzled. Cell 98:585-595.

Vakonakis I, Langenhan T, Promel S, Russ A, Campbell ID (2008) Solution structure and sugar-binding mechanism of mouse latrophilin-1 RBL: a 7TM receptor-attached lectin-like domain. Structure 16:944-953.

van de Linde S, Loschberger A, Klein T, Heidbreder M, Wolter S, Heilemann M, Sauer M (2011) Direct stochastic optical reconstruction microscopy with standard fluorescent probes. Nature protocols 6:991-1009.

Volynski KE, Silva JP, Lelianova VG, Atiqur Rahman M, Hopkins C, Ushkaryov YA (2004) Latrophilin fragments behave as independent proteins that associate and signal on binding of LTX(N4C). The EMBO journal 23:4423-4433.

Volynski KE, Capogna M, Ashton AC, Thomson D, Orlova EV, Manser CF, Ribchester RR, Ushkaryov YA (2003) Mutant alpha-latrotoxin (LTXN4C) does not form pores and causes secretion by receptor stimulation: this action does not require neurexins. The Journal of biological chemistry 278:31058-31066.

Vomel M, Wegener C (2008) Neuroarchitecture of aminergic systems in the larval ventral ganglion of Drosophila melanogaster. PloS one 3:e1848.

Wagh DA, Rasse TM, Asan E, Hofbauer A, Schwenkert I, Durrbeck H, Buchner S, Dabauvalle MC, Schmidt M, Qin G, Wichmann C, Kittel R, Sigrist SJ, Buchner E (2006) Bruchpilot, a protein with homology to ELKS/CAST, is required for structural integrity and function of synaptic active zones in Drosophila. Neuron 49:833-844.

Waller-Evans H, Promel S, Langenhan T, Dixon J, Zahn D, Colledge WH, Doran J, Carlton MB, Davies B, Aparicio SA, Grosse J, Russ AP (2010) The orphan adhesion-GPCR GPR126 is required for embryonic development in the mouse. PloS one 5:e14047.

Wang JW, Sylwester AW, Reed D, Wu DA, Soll DR, Wu CF (1997) Morphometric description of the wandering behavior in Drosophila larvae: aberrant locomotion in Na+ and K+ channel mutants revealed by computer-assisted motion analysis. Journal of neurogenetics 11:231-254.

Weber T, Zemelman BV, McNew JA, Westermann B, Gmachl M, Parlati F, Sollner TH, Rothman JE (1998) SNAREpins: minimal machinery for membrane fusion. Cell 92:759-772.

Weigmann K, Klapper R, Strasser T, Rickert C, Technau G, Jackle H, Janning W, Klambt C (2003) FlyMove--a new way to look at development of Drosophila. Trends Genet 19:310-311.

Weston MD, Luijendijk MW, Humphrey KD, Moller C, Kimberling WJ (2004) Mutations in the VLGR1 gene implicate G-protein signaling in the pathogenesis of Usher syndrome type II. American journal of human genetics 74:357-366.

Willson J, Amliwala K, Davis A, Cook A, Cuttle MF, Kriek N, Hopper NA, O'Connor V, Harder A, Walker RJ, Holden-Dye L (2004) Latrotoxin receptor signaling

engages the UNC-13-dependent vesicle-priming pathway in C. elegans. Current biology : CB 14:1374-1379.

Yao KM, White K (1994) Neural specificity of elav expression: defining a Drosophila promoter for directing expression to the nervous system. Journal of neurochemistry 63:41-51.

Zhai RG, Bellen HJ (2004) The architecture of the active zone in the presynaptic nerve terminal. Physiology (Bethesda) 19:262-270.

Zhang W, Yan Z, Jan LY, Jan YN (2013) Sound response mediated by the TRP channels NOMPC, NANCHUNG, and INACTIVE in chordotonal organs of Drosophila larvae. Proceedings of the National Academy of Sciences of the United States of America 110:13612-13617.